~~CONFIDENTIAL~~

DEVELOPMENT AND TESTING OF SUPERIOR NOZZLE MATERIALS

(Title Unclassified)

Final Report

Prepared For

National Aeronautics and Space Administration

Contract No. - NASw-67

APRIL, 1961

Prepared by: Heinz A. Jaffe
Heinz A. Jaffe
Project Engineer

Approved by: H. Moak
H. Moak
Chief Engineer

ARDE-PORTLAND, INC.
Paramus, N.J.

~~CONFIDENTIAL~~

TABLE OF CONTENTS

LIST OF FIGURES

LIST OF FIGURES - APPENDIX

1. INTRODUCTION

Uncooled rocket nozzles require throat inserts which can withstand for about one minute, without significant erosion, decomposition or structural failure, the abrasive, high temperature, reactive gases generated by high performance solid propellants. The best materials available are only marginal in todays applications. As the demand for higher performance pushes propellant temperatures upward, the throat insert materials become the limiting item.

The materials which offer the greatest potential for successful application are the high melting point refractory carbides. The performance of these materials may be further improved by impregnation with a gas generating or vaporizing substance which will act as a coolant.

The major problem in using refractory carbides is the lack of adequate facilities and processes for producing materials of a quality and with structural properties suitable for fabrication into throat inserts. New fabrication techniques are still in the early stages of development and a limited number of sources are available which can supply materials of the size and quality required.

Under National Aeronautics and Space Administration's contract NASw-67, Arde-Portland has conducted a materials evaluation and test program with the following basic objectives:

1.1 To investigate systematically the performance of various refractory materials.

1.2 To investigate the effects of adding a vaporizing material to the refractory carbide showing the best erosion resistance.

The program was initially based on evaluating materials made by a new proprietary process developed by Electro-Thermal Industries of Pearl River, New York. This process was claimed to produce materials, by rapid reaction at temperatures of 7000°F and pressures of 3,000,000 psi, that would achieve densities close to theoretical and approach more closely the structure and strength of cast materials.

Electro-Thermal Industries had successfully produced small samples of refractory carbides, but unfortunately the scale-up problems in going from these small samples to a size required

for inserts having a throat diameter from 1/2" to 3/4" proved to be insurmountable. Electro-Thermal did provide material for one insert, but was unable to produce any others and the program was therefore revised to include materials available from other sources.

2. SUMMARY

A search for materials with melting points exceeding 6000°F disclosed the following eight materials:

Materials	Melting Point
Hafnium carbide	6984°F
Columbium carbide	6332°F
Tantalum carbide	6984°F
Zirconium carbide	6386°F
Tungsten	6157°F
Carbon (Graphite)	6600°F
80% Tantalum carbide + 20% Hafnium carbide	7124°F
80% Tantalum carbide + 20% Zirconium carbide	7106°F

Tungsten and graphite were eliminated from this program by direction of the contracting agency because of the work already sponsored for these materials.

The final choice of materials to be procured and tested was based on availability, delivery, and cost. These materials and their suppliers are listed below:

2.1 Tantalum carbide - Electro-Thermal Industries
2.2 Pyrolytic graphite - Raytheon Company
2.3 Sintered columbium carbide in a tungsten honeycomb - Avco Corp.
2.4 Sintered columbium carbide - Firth Sterling, Inc.
2.5 Sintered tantalum carbide - Firth Sterling, Inc.
2.6 Sintered tantalum carbide filled with aluminum - Firth Sterling, Inc.

Three of the six pyrolytic graphite nozzle inserts procured were made available to this program at no cost through the courtesy of the Director, Special Projects, Bureau of Naval Weapons, Department of the Navy.

The materials chosen for investigation are by no means the only ones that could be expected to perform well, but they were considered logical choices on the basis of cost and availability.

Seventeen nozzle inserts were tested. The tests were conducted at the Hercules Powder Company in Kenvil, New Jersey using their CLW propellant which has a calculated flame temperature of 6536°F at 1000 psi. Pressures of 500, 750, and 1000 psi and

firing durations of 30 and 60 seconds were used. Nozzle throat diameters ranged from approximately 1/2" to 3/4".

Results of these tests are presented in Figure 1.

A theoretical analysis was performed to determine the feasibility of converting presently available low melting point materials to new forms exhibiting high melting points by the application of ultra-high pressures.

3. CONCLUSIONS

On the basis of the limited number of tests performed under this program, the following general conclusions are drawn. More detailed conclusions pertaining to each material investigated are listed in Section 9, Results and Discussion.

3.1 The impregnation of a refractory carbide nozzle insert with a relatively low boiling point material having a high heat of vaporization reduces the erosion rate appreciably.

3.2 All of the materials investigated appear to have erosion rates low enough to make them suitable for a nozzle application where the pressure does not exceed 500 psi.

3.3 All of the materials investigated were sensitive to increases in pressure, i.e., the erosion rate increased with pressure.

3.4 With the exception of the tantalum carbide filled with aluminum, pyrolytic graphite showed the lowest erosion rate at both 500 psi and 750 psi.

The theoretical analysis made to study the conversion of low melting point materials to new forms exhibiting high melting points by the application of ultra high pressures concludes that this conversion is feasible.

4. RECOMMENDATIONS

The following recommendations are made to further improve nozzle insert materials capable of performing successfully with high performance solid propellants.

4.1 Further investigation of refractory carbides filled with vaporizing materials should be carried out to determine the following:

4.1.1 The optimum refractory carbide matrix in terms of maximum performance and minimum weight.

4.1.2 The effect of various vaporizing materials on the performance of the insert.

4.1.3 The optimum amount of vaporizing material.

4.2 Investigate manufacturing processes and bonding characteristics to improve the reliability of pyrolytic graphite.

4.3 Investigate the production of new high melting point materials by the application of ultra-high pressures.

5. SELECTION OF MATERIALS

The selection of materials to be evaluated in this program was limited to those exhibiting high melting points. A search for materials with melting points exceeding 6000°F disclosed the following eight materials:

Materials	Melting Point
Hafnium carbide	6984°F
Columbium carbide	6332°F
Tantalum carbide	6984°F
Zirconium carbide	6386°F
Tungsten	6157°F
Carbon (Graphite)	6600°F
80% Tantalum carbide + 20% Hafnium carbide	7124°F
80% Tantalum carbide + 20% Zirconium carbide	7106°F

Tungsten and graphite were eliminated from this program by direction of the contracting agency because of the work already sponsored for these materials. Hafnium carbide was discarded because the limited availability of hafnium rules it out as a practical nozzle material at this time. This, therefore, left the carbides of columbium, tantalum and zirconium, and any combinations thereof to be investigated.

Initially, an order for several of these materials was placed with Electro-Thermal Industries of Pearl River, New York. This company had developed a proprietary process for producing samples of refractory carbides with close to theoretical densities. Their process differs from the more usual sintering process in that there is a relatively short time reaction between the refractory metal powder and carbon. This reaction was claimed to result in pressures of about 3,000,000 psi and temperatures of 7000°F. It was therefore believed that materials produced by this method, instead of the usual sintering methods, would approach more closely the structure and strength of cast materials.

The projected program was based solely on evaluating materials furnished under this contract by Electro-Thermal Industries. Initially, Zirconium carbide, columbium carbide, tantalum carbide and zirconium carbide bonded with graphite were ordered. Subsequently, the best of the above materials were to be impregnated with a relatively low melting point, high heat capacity material such as aluminum to evaluate whether the addition of such a material could materially improve the perfor-

mance of the basic material.

Electro-Thermal Industries unfortunately was unable to furnish these materials as initially expected. The scale-up problems in going from the small sample piece which they were capable of providing to the size required for nozzle inserts having throat diameters of 1/2" to 3/4" proved to be insurmountable. With the exception of two pieces of tantalum carbide, Electo-Thermal Industries was either unable to make deliveries or the pieces delivered were full of cracks and disintegrated during machining operations. The two pieces that were delivered, because of their small size, were made into a single nozzle insert and tested. Electro-Thermal Industries also supplied a piece of titanium carbide bonded with graphite. This insert was not expected to perform well and was used only to check out test setups and reliability of instrumentation for future tests.

Since Electro-Thermal Industries could not provide the materials required, the program was revised to include materials from other sources. The final choice as to the materials to be procured was based on suitability, delivery and cost.

The following table lists all of the materials evaluated and their source:

Material	Vendor
Titanium carbide bonded with graphite	Electro-Thermal Industries
Tantalum carbide	Electro-Thermal Industries
Pyrolytic Graphite	Raytheon Company
Sintered columbium carbide in a tungsten honeycomb	Arco Corporation
Sintered columbium carbide	Firth Sterling, Inc.
Sintered tantalum carbide	Firth Sterling, Inc.
Sintered tantalum carbide filled with aluminum	Firth Sterling, Inc.

5.1 Titanium Carbide Bonded with Graphite

This insert was produced by the proprietary process developed by Electro-Thermal Industries which is described above. It was procured only because of its availability and was used to check out the test set up.

5.2 Tantalum Carbide

Two pieces of tantalum carbide made by the Electro-Thermal Industries' process were combined into a single nozzle insert to permit evaluation of this material.

5.3 Pyrolytic Graphite

These inserts were made by coating a graphite substrate with pyrolytic graphite in thicknesses varying from 0.040" to 0.050" depending on the throat diameter of the insert. This variation in thickness was recommended by Raytheon in order to keep the ratio of coating thickness to throat I.D. within limits that they had found to be successful.

Pyrolytic graphite is an unusual form of graphite exhibiting a high degree of preferred orientation and a wide range of anisotropy in thermal and electrical properties. It is a polycrystalline graphite formed by high temperature pyrolysis of a carbon bearing material.

The material is produced by the deposition of carbon from a vapor phase onto a substrate which is maintained at elevated temperatures. This results in growth of a material which has a metallic type of behavior in the plane of the material and a ceramic type of behavior normal to this plane. These properties of pyrolytic graphite result in the material having excellent heat transfer characteristics in the plane of the material, good insulating properties across the plane, and much better erosion resistance than ordinary graphite. Detailed properties of the material will be found in Appendix D.

5.4 Sintered Columbium Carbide in a Tungsten Honeycomb

The inserts procured from the Avco Corporation were made by a proprietory process. Basically they consist of a tungsten honeycomb structure, the cells of which have been filled with columbium carbide and then sintered. The theory of this type of structure is that the rather brittle carbide is subject to thermal shock failure and therefore the addition of the tungsten tends to distribute the temperature more quickly due to its higher thermal conductivity and also adds structural strength and mechanical bonding.

5.5 Sintered Tantalum Carbide and Columbium Carbide

The several materials procured from Firth Sterling Inc. were made by a conventional sintering and pressing process of the refractory metal powders and graphite. The tantalum carbide and the columbium carbide inserts were made by this method and then ground to the proper shape. This process resulted in densities of approximately 80% of the theoretical value for tantalum carbide, and 90% of the theoretical value for columbium carbide.

5.6 Sintered Tantalum Carbide Filled with Aluminum

The tantalum carbide insert filled with aluminum was produced by the same method except that the insert was immersed in molten aluminum and with the help of a suction pump impregnated with as much aluminum as possible.(16% by vol.) Properties of these materials are also listed in Appendix D.

The materials investigated in this program are by no means the only ones that could be expected to perform well under the test conditions, but they were considered logical choices on the basis of cost and availability.

Another approach to developing materials capable of withstanding the temperatures and pressures expected in future applications is to produce new materials not available today. A theoretical analysis was made of the possible conversion of presently available low melting materials to new forms exhibiting high melting points. While no definite answer was obtained, several interesting possibilities were investigated, the most promising of which is the generation of diamond-type structures from a wide variety of chemical compounds by the application of ultra high pressures. This work was carried out for Arde-Portland by Dr. Irving B. Cadoff, Associate Professor of Metallurgy at New York University and is reported in Appendix F.

6. TEST EQUIPMENT AND FACILITIES

6.1 Test Nozzle Design

The nozzle for testing of the insert materials was designed for structural and thermal reliability, ease of assembly, and low cost. A schematic of the nozzle is shown in Figure 2, and Figures 3 and 4 show views of the inlet and exit side. The nozzle essentially consists of the following five components:

6.1.1 Casing
6.1.2 Shear plate and tungsten ring
6.1.3 Insulation
6.1.4 Graphite
6.1.5 Nozzle throat insert

6.1.1 Casing

The casing was fabricated of mild steel and is essentially the primary structural member of the nozzle assembly. The inlet end of the casing was threaded to allow fastening to the motor case, a schematic of which is shown in Figure 5. The three brackets shown on Figure 3 were used to support thermocouples. Pressure taps are also visible in Figure 3.

6.1.2 Shear Plate and Tungsten Ring

The shear plate was designed to serve two functions. It served as a blowout ring in the event of a pressure build-up in the nozzle due to exit plugging, thereby protecting the casing against rupture. It also served as an axial restraining ring for the components in the throat region during normal operation. Although originally designed to shear at 1200 psi, 20% above the expected propellant pressure, pressure excursions encountered during tests due to apparent irregularities in the propellant dictated a redesign to 1500 psi. The shear plate was protected on its upstream side by a tungsten ring to prevent direct impingment of the hot flame upon it. A ceramic coating as shown in Figure 3 served to protect the shear plate against the "wiping" effect of the exit gases.

6.1.3 Insulation

The insulating material used in this nozzle is a grade A asbestos phenolic plastic. A 5/8" thick ring protected the metal in the region of the throat and a 1/4" thick ring protected the inside of the casing. These thicknesses were chosen to keep the steel casing temperature at a safe value.

6.1.4 Graphite

Graphite was used both as a heat sink and as an erosion resistant material in the subsonic section of the nozzle. National Carbide Co., Grade ATJ graphite was used. This graphite is an extremely fine grained, essentially flaw free, high strength premier quality molded graphite which can be machined to very close limits and finishes. In addition to these characteristics, its resistance to thermal shock and its ability to withstand the anticipated high temperatures made this graphite a logical selection for this application.

6.1.5 Nozzle Throat Insert

A detailed discussion of the throat insert materials is found in section 5 and the properties of the materials are listed in Appendix D. A sketch of a typical refractory carbide insert is shown in Figure 6 and that of a pyrolytic graphite insert in Figure 7.

The geometry of the throat insert and the thickness of the graphite heat sink behind it were determined by a heat transfer analysis to meet the objectives of the nozzle design. These objectives were to reach an inner wall temperature of about 5000°F and uniform conditions along the length of the throat.

6.2 Test Facilities

The facilities of the Hercules Powder Company's Kenvil Works were used for all tests in this program. Testing was conducted in an open end, windowless concrete bay in which a large concrete reaction block and a motor support rig were located. The motor and test nozzle assembly was cradled on rollers and clamped to prevent movement during firing. Figure 8 is a view of a motor and test nozzle

assembly mounted on the test stand. Since access to the test cell was prohibited during firing, observation of the test was made by camera. Pretest calibration of instruments was conducted through an inter-communication system between the test cell and the control room.

6.2.1 Test Stand Instrumentation

The following equipment furnished by the Hercules Powder Company was used for this series of tests:

Description	Manufacturer	Model	No. of Channels
Pressure Transducers	Taber	176	2
Transducer Power Supply	Video Instruments	SR-200	4
Balance - Calibrator units	Allegany Instruments	B-8	4
D.C. Amplifiers	Allegany Instruments	512-A	4
Voltage-to-Frequency Converters	Allegany Instruments	303-C	4
Totalizer-Counters	Allegany Instruments	703	4
Oscillograph	Hathaway	S-25	14
Thermocouple Calibrator	Allegany Instruments	MV-60	1
Millivolt Potentiometer	Leed & Northrup	-	1
Time Standard	Allegany Instruments	402-A	1

The pressure transducers were capable of measuring pressures from 10 psi to 50,000 psi. The range of temperature measurements depended on the type of thermocouple used.

6.2.2 Calibration of Instruments

The pressure transducers were calibrated with instruments which are guaranteed to be accurate within 0.1% of the indicated pressure. A model 470 Amthor Dead Weight Calibrator was used for pressure calibrations. Normally, calibrations are performed weekly for transducers which are in daily use. All calibrations are designed to follow the "hysteresis loop" of the transducer. At least four weight steps are used in both ascending and descending weight application.

Thermocouples were calibrated by application of a known millivolt source whose accuracy is within 1% of the true value.

7. PROPELLANT

All testing under this contract was performed with a propellant developed by the Hercules Powder Co. and designated CLW. A description of the propellant is given in Tables C-1, C-2 and C-3 of Appendix C.

According to the Hercules Powder Co., the CLW propellant has a calculated flame temperature of 6536°F at 1000 psi using the shifting equilibrium method of calculation. At a pressure of 250 psi the flame temperature is reduced to 6204°F. Experimental specific impulse values of 247 to 248 seconds, corrected to 1000 psi chamber pressure and full expansion to sea level pressure, have been obtained with this propellant using a 15° expansion cone.

The ratio of specific heats for the products of combustion of this propellant is 1.16 and the characteristic velocity is 5280 ft. per sec. Burning rates of the propellant have been established as follows:

0.8" per second at 1000 psi and 80°F.
0.7" per second at 750 psi and 80°F.
0.6" per second at 500 psi and 80°F.

The actual performance of this propellant tended to vary appreciably between tests. An examination of several different pressure traces clearly indicates this variation. Figures 9, 10, and 11 show three of these traces. The trace for test number 15, Figure 9, is representative of the expected performance of the propellant while the traces of test 6, Figure 10, and test 9, Figure 11 indicate the large variation experienced during this program.

Attempts by both Hercules Powder Co. and Arde-Portland to determine the cause of these high pressure peaks were not successful. Suspected causes such as cracks or voids in the propellant grain or the lack of bonding between the propellant and the inhibitor could not be substantiated by a review of x-ray pictures taken of the grain before loading into motors. The possibility of blockage of the nozzle throat by pieces of propellant or of the nozzle being ejected during the test was also considered, but no evidence could be found to sustain this theory.

A tentative conclusion reached was that long time storage of the propellant may have affected its performance.

8. NOZZLE INSTRUMENTATION

The basic parameters recorded were chamber pressure and wall temperatures of the materials tested. Facilities were available to measure and record thrust but these were not used for two reasons: (1) thrust data was of little interest in this program, and (2) measurement of thrust required some minute motion of the motor case and nozzle which would have prevented the proper focusing of the optical pyrometer used in attempting to measure temperature.

8.1 Pressure

Pressures were sensed by means of two pressure transducers, (Section 6) located 180° apart on the motor. In general, all pressure data recorded were reliable.

8.2 Temperature

8.2.1 Thermocouples

One of the objectives of this program was to test the selected materials at as high a surface temperature as could be achieved. In order to verify the calculated surface temperature, three thermocouples were imbedded at various distances from the inner wall of the nozzles. The distances from this inner wall were approximately 0.1", 0.18" and 0.3" as shown in Figure 12. In all cases, with the exception of the pyrolytic graphite nozzles, the thermocouples were imbedded in, and made contact with, the test material. Due to thinness of the pyrolytic graphite coating, the thermocouples in these tests were imbedded in the graphite substrate.

In general, two types of thermocouples were used. Conventional types of Iron-Constantan or Chromel-Alumel were used in the pyrolytic graphite tests where the temperature level was expected to be low. Special high temperature thermocouples were used in all other tests in which the expected temperature level was beyond the useful range of conventional thermocouples.

The performance of the Iron-Constantan and Chromel-Alumel thermocouples was entirely satisfactory for

the pyrolytic graphite tests. Temperature data was as expected and was useful in determining the actual time of failure of the pyrolytic graphite where such failure occurred. This is shown in Figures 13 and 14.

Measurements of high temperatures in the other inserts tested proved to be much more difficult and much less reliable. In one of the early tests, thermocouples made of platinum - 20% rhodium and platinum - 40% rhodium were used. Since the upper limit of these thermocouples is only about 3200°F and their millivolt output is exceedingly low, both low temperature accuracy and high temperature range was lacking. These thermocouples were later replaced by a different type of thermocouple capable of measuring higher temperatures. This thermocouple consisted of tungsten and tungsten - 25% rhenium with a reported useful life up to 5000°F. The thermocouple junction was surrounded by a tantalum sheet and filled with beryllium oxide as an insulator.

The performance of these thermocouples was quite varied and the resulting data has to be used judiciously in order to determine actual nozzle insert temperatures. Calculations were performed in order to attempt to correlate experimental data with theoretical values of temperature. Theoretical curves of time vs. temperature were established for the materials for which thermal properties were readily available, namely tantalum carbide and columbium carbide. No analytical temperature data was calculated for the Avco Corporation material because of the lack of the required properties for this composite structure.

The method used for calculating the temperature-time curves is described in detail in Appendix A. Calculations for both materials were performed using a throat diameter of 0.750" and a pressure of 500 psi. Since a certain amount of experimental data was recorded from tests using a smaller throat diameter and higher pressure, another set of calculations was performed for tantalum carbide at a throat diameter of 0.630" and a pressure of 800 psi, all other parameters remaining the same, to determine the combined effect of these parameters on the temperature-time curves.

Figures 15 through 20 show both the theoretical and test curves for tantalum carbide and columbium carbide at distances from the inner wall of 0.1, 0.18, and 0.3". The curves for tantalum carbide, Figures 15 through 17 also show the combined effect of pressure and throat diameter variations on the theoretical temperatures. The effect appears to be small at 0.1" from the inner wall, with the higher pressure and lower throat diameter resulting in somewhat higher temperatures. At 0.18" from the inner wall the temperature difference becomes more pronounced during the early stages of the firing, but tends to disappear at about 30 seconds. At 0.3" from the inner wall, this temperature difference is reduced again during the early stage of firing and by the end of 30 seconds actually results in a somewhat lower temperature.

The shape of the temperature-time curves as a function of throat diameter and pressure can be explained as follows:

A reduction in the throat diameter reduces the total heat flow because of the smaller flow area available. At the same time the heat flow per unit area is increased because of the higher heat transfer coefficient resulting from the higher pressure. Analysis shows that the effect of the diameter change is stronger than that of the pressure change and the total heat flow is reduced. The temperature at the inner wall is therefore increased due to the higher heat input per unit area while the temperature at the outer wall tends to decrease for two reasons: (1) the lower total heat input and, (2) the larger heat sink available due to the reduction in the I.D.

On the basis of the evaluation of the effect of throat diameter and pressure on the temperature-time curves, it is apparent that this effect is small enough to allow comparison of all test data to the theoretical curve based on a throat diameter of 0.750" and a pressure of 500 psi.

Figure 15 presents the theoretical and experimental data for tantalum carbide at a distance 0.1" from the inner wall. In this and all following curves only that experimental data recorded by thermocouples

whose operation appear normal is presented. Malfunction of thermocouples resulting in either no data or extremely erratic data occurred frequently in this series of tests, indicating a fairly low reliability. Test curves from two tests are indicated on Figure 15. These curves bracket the theoretical curves and vary by approximately 600°F at the 20 second mark. Figure 16 indicates test data 0.18" from the inner wall from three tests with a much closer correlation. The spread in the data at the 20 second mark is only about 200°F. Figure 17 at a distance 0.3" from the inner wall again has test curves from three tests and shows a maximum spread of approximately 400°F.

A general conclusion to be drawn from these three families of curves is that the experimental data tends to lie above the theoretical data at the early stages of firing and then drops below the theoretical data at the end of the firing. The highest temperature recorded for the series of tantalum carbide tests was about 4100°F at a distance 0.1" from the inner wall which closely approximates the theoretical temperature-time relationship indicated on Figure A-1 of Appendix A. Appendix A also shows the theoretical inner wall temperature at 30 seconds to be approximately 5000°F.

Figures 18 through 20 show both the theoretical and experimental temperature data for columbium carbide. Data from only one test is available at the 0.1" distance from the inner wall and this data checks very well with the theoretical. At the 0.18" distance from the inner wall, Figure 19, data from three tests bracket the theoretical with a maximum spread of about 800°F.

Figure 20 shows the experimental data from two tests at a distance of 0.3" from the inner wall to lie appreciably above the theoretical. The highest temperature recorded for this material was about 4000°F at a distance of 0.18" from the wall at 40 seconds, and 3820°F at 0.1" from the wall at about 29 seconds. Figure A-3 of Appendix A shows the theoretical wall temperature at the end of 30 seconds to be about 5140°F.

The general conclusions that can be drawn from this examination of the temperature data is that the reliability and accuracy of thermocouples in this temperature range leaves much to be desired. Variations in temperature, under supposedly similar conditions, of up to 20% were found to be not unusual. On the basis of the series of tests performed under this contract it must be concluded that the problem of accurately measuring these high temperatures by means of thermocouples has not been solved.

8.2.2 Radiation Pyrometers

It was recognized at the initiation of this work that the state of the art, insofar as thermocouples were concerned, limited their use to temperatures no higher than approximately 4000°F. Heat transfer analysis indicated that temperatures of over 5000°F would be reached in this program.

To provide a means for measuring higher temperatures, other methods of pyrometry were investigated. Two types of pyrometers other than the thermocouple are the optical and total radiation pyrometers, the operating principle of which are based upon the radiation emitted by a body.

The optical pyrometer utilizes the fact that the brightness of a radiating body increases as its temperature is raised and allows the observer to compare the brightness of the body at one given wave length with that of a calibrated tungsten filament. The wave length to be used is established by a narrow band pass filter. The radiant flux received is found to vary as the sixth power provided the source is near the anticipated test gas temperature of 6150°F.

The total radiation pyrometer makes use of the full spectrum emitted by a radiating source. The radiation is focused by a concave mirror upon a tiny disk of a thermopile. If the radiation is emitted from a black body, the radiant flux received upon the thermopile disk is found to vary as the fourth power of the absolute temperature.

Since the radiant flux "seen" by the total radiation pyrometer varies only with the fourth power of the absolute temperature as compared with the sixth power law of the optical pyrometer, the optical pyrometer is more sensitive to temperature changes and was chosen on this basis for this program.

The optical pyrometer was set up to view the bottom of the thermocouple well as shown in Figure B-1 of Appendix B. Because of the effect of reflections from the sides of the thermocouple well upon the bottom, an analysis was made, see Appendix B, to determine the effective emissivity. To approximate the actual temperature the apparent temperature can be corrected by use of the effective emissivity.

The analysis concluded that it should not be necessary to know the actual emissivity values better than ± 50% to obtain 10% accuracy, see Figure B-3.

For comparison purposes the same analysis was conducted for the total radiation pyrometer. Since the radiation from the sides of the thermocouple well varies as the fourth power of the temperature for the total radiation pyrometer, as opposed to the sixth power for the optical pyrometer, the thermocouple well bottom more closely approximates an ideal black body. The effective emissivity is higher at a given temperature for the total radiation pyrometer than the optical pyrometer, when a temperature gradient exists through the thermocouple well. When the temperature gradient is small the effective emissivity is unity for both the optical and total radiation pyrometer.

It was interesting to note that the difference in the power laws followed by the optical and total radiation pyrometers was compensated for by the reversed difference in the effective emissivities.

Similar to the optical pyrometer the analysis showed that it was not necessary to know the actual emissivity values of the total radiation pyrometer better than ± 50% to obtain 10% accuracy, see Figure B-4.

On the basis of this analysis, it can be concluded that temperature sensitivity is not the proper criteria

for choosing between an optical or total radiation pyrometer. However, at the initiation of this program an optical pyrometer was procured and was therefore used in attempting to measure nozzle insert wall temperatures.

Since safety precautions barred visual observation a camera was mounted behind the optical pyrometer to record the image and thereby allow the determination of the temperature. Initially a movie camera was used to record the image but this was later changed to a sequence camera which permitted taking pictures at the rate of 40 per minute during the test run.

The theory of operation was that the tungsten filament in the pyrometer was illuminated to some known temperature and its image superimposed on the image of the bottom of the thermocouple well on the photographic film. A comparison of the densities of the filament image and the thermocouple well image would then determine when both were at the same temperature. By this means it was expected that the actual temperature at some fixed time during the test could be determined. An improvement upon this procedure, used in later tests, was that pictures of the tungsten filament at various temperatures were recorded before the test and compared to pictures of the thermocouple well taken continuously during the test. Temperatures at various times during the test were expected to be established by this means.

Evaluation of the photographic data collected led to the conclusion that this means of measuring high temperature was not successful. In all instances the density of the image of the thermocouple well was appreciably below that of the minimum density of the tungsten filament. The minimum density of the tungsten filament that could be photographed corresponded to a temperature of approximately 3500°F. As both theoretical calculations and thermocouple data showed the temperature to be as high as 4000°F, the photographic data indicating temperatures appreciably below the 3500°F temperature of the tungsten filament, must therefore be considered to be erroneous.

The measuring of high temperatures existing in the walls of the rocket nozzle presents problems which

have not been solved in the course of the nozzle material test program carried out under this contract. Of the two methods used, thermocouples lacked both reliability and accuracy and the optical pyrometer method could not be made to work. It is felt that a total radiation pyrometer should be used in the future and with further development effort could be made to read high temperatures reliably. The distinct advantages of a total radiation pyrometer are its independence from a human observer or camera and its ability to continuously measure and record the temperature-time relationship during testing and over temperature ranges which overlap thermocouple capabilities.

9. RESULTS AND DISCUSSION

9.1 Electro-Thermal Industries' Materials

9.1.1 Titanium Carbide Bonded with Graphite

The initial material furnished by Electro-Thermal Industries was titanium carbide bonded with graphite. This material was selected not because of its expected performance, but because it was immediately available and could be used to evaluate the nozzle design and check out test operation and instrumentation reliability. The throat diameter of this insert was 0.677" and it was designed to operate at 500 psi for 30 seconds.

9.1.1.1 Test 1

Test results showed the burning time to be 41.7 seconds with a peak pressure of 604 psi and an average pressure of 338 psi over the burning time. The nozzle material, as expected, eroded extensively resulting in the long burning time. Figure 21 shows this extensive erosion. Subsequent to this test all nozzle throat diameters for the 500 psi tests were changed from 0.677" to 0.632" in order to more closely approach the nominal 500 psi pressure level.

9.1.2 Tantalum Carbide

The only other material received from Electro-Thermal Industries were two pieces of tantalum carbide which were made into a single nozzle insert.

9.1.2.1 Test 2

The test of this insert resulted in a firing time of 39 seconds with a peak pressure of 456 psi and an average pressure of 435 psi over the burning time. Examination of the insert after the test showed it to be cracked as indicated in Figure 22. This crack separated the inlet section of the insert completely from the throat section. The erosion was somewhat non-uniform and averaged out to 0.78 mils per second on the radius.

9.1.2.2 Conclusions

The conclusions drawn in testing this material are that it is subject to cracking due to thermal shock and its erosion rate is somewhat higher than that of other materials tested.

9.2 Raytheon Corporation Materials

9.2.1 Pyrolytic Graphite

A series of tests were performed using graphite nozzles coated with pyrolytic graphite by the Raytheon Corporation. A total of six nozzles were procured consisting of two identical sets of three nozzles each. Each set had the following throat diameters and pyrolytic graphite coating thicknesses and were to be tested at the indicated pressures. Figure 7 shows a sketch of these inserts.

Test Pressure	Throat Diameter	Coating Thickness
500 psi	0.710"	0.050"
750 psi	0.630"	0.045"
1000 psi	0.585"	0.040"

The thickness of the pyrolytic graphite coating was determined by the Raytheon Corporation with the objective of keeping the ratio of throat diameter to coating thickness within the range that was found to be most successful in previous tests.

Of the two inserts scheduled to be tested at a nominal chamber pressure of 500 psi, one insert was extensively damaged during the assembly of the nozzle and could not be tested.

9.2.1.1 Test 3

A detailed examination of the nozzle insert tested at 500 psi after an approximately 34 second firing indicated that the pyrolytic graphite was still attached to the nozzle insert and withstood the test exceedingly well. The peak pressure reached during the test was 576 psi and the average pressure over the burning

time was 542 psi. Erosion of the throat section of the insert was very uniform and at a rate of approximately 0.34 mils per second on the radius for most of the throat and approximately 0.43 mils per second at the exit. No evidence of flaking or spalling in the throat region could be seen. Maximum out-of-roundness after firing was 0.014".

Figures 23 and 24 show the nozzle assembly after the test. It is of interest to notice the buildup of aluminum oxide on the insulating liner and also on the graphite beyond this liner. The lack of aluminum oxide on the pyrolytic coating is due to the very high insulating properties of this coating which maintained its surface temperature above the condensation temperature of the aluminum oxide.

The circumferential cracking of the pyrolytic graphite coating at the junction of the conical and cylindrical section, Figure 24, resulted in the separation of the conical section of the pyrolytic graphite from the substrate and was found to be a characteristic phenomena of all pyrolytic graphite nozzles tested. Figure 25 shows this separated conical section and also a small piece of pyrolytic graphite that had flaked off. Examination of the crack revealed it to be exceedingly clean with no erosion pattern discernible. This led to the conclusion that the failure must have occurred after the firing and was probably due to thermal stresses occurring during the cooling of the nozzle.

An analysis showed that only a relatively small temperature difference in the pyrolytic graphite between the conical and cylindrical sections during cooling would cause a shear failure to occur at this location. A temperature difference of only 34°F is sufficient to cause this failure. Appendix E gives the detailed analysis indicating both the calculated temperature differences existing at the termination of the test and describing the method of analysis by which it was determined that a small temperature difference of 34° during cooling can result in

stresses beyond the capability of the material to withstand.

Two tests were performed with the pyrolytic graphite insert at a nominal pressure of 750 psi.

9.2.1.2 Test 4

The first test was only partially successful in that the pyrolytic graphite coating began to separate from the graphite substrate after approximately 17-1/2 seconds. The duration of the test was about 27 seconds and reached a peak pressure of 825 psi and an average pressure over the burning time of 799 psi. Examination of the nozzle insert after the test showed that the pyrolytic graphite had flaked off over a 270° segment from the exit of the throat section to within 1/4" of the inlet to the throat section. The pyrolytic graphite coating was intact for the remainder of the throat section and the conical inlet section with the exception of the characteristic circumferential crack just downstream of where the two sections meet. The pyrolytic graphite coating completely separated from the graphite substrate during nozzle disassembly.

Figures 26 through 28 show overall and closeup views of the nozzle and clearly indicate the condition of the pyrolytic graphite coating. Figure 29 shows the coating after separation from the substrate.

Erosion rates for this insert were determined from measurements taken at the section of the pyrolytic graphite that still formed a complete ring. This erosion rate was fairly uniform at 0.55 mils per second.

An examination of the pressure and temperature traces of this test very clearly indicate the exact time of the pyrolytic graphite coating failure. At about 17.5 seconds after ignition, two of the three temperature traces show a sudden increase with a simultaneous pressure

decreases, Figure 13. Temperature 1 was measured 0.136" from the nozzle wall, temperature 2 at 0.264" and temperature 3 at 0.500". The sudden rise of temperature 1 is due to the fact that as soon as the pyrolytic graphite coating failed, only 0.091" of graphite remained between the hot gas and the thermocouple. Under these conditions, calculations indicate that the temperature would rise at a rate of about 1200°F per second. This seems to be borne out by the temperature trace. Temperature 2 had much less of a rise while temperature 3 does not reflect any rise in temperature. It is interesting to note that the thermocouple reading temperature 3 was located radially behind the remaining section of pyrolytic graphite and the heat path to it was therefore much longer, requiring the heat to flow both radially and circumferentially. The timing of the initial failure of the pyrolytic graphite coating has also been substantiated by motion pictures which show a shower of sparks leaving the nozzle at approximately 17 seconds.

9.2.1.3 Test 5

The second test of a pyrolytic graphite insert at a nominal pressure of 750 showed excellent results. The coating did not fail, with the exception of the characteristic crack separating the conical section from the cylindrical section, during a firing of 30.7 second duration. The peak pressure during this test was 827 psi and the average pressure over the burning time was 782 psi.

Figures 30 through 32 show the condition of the insert after the test. The erosion rate at the throat was 0.65 mils per second on the radius with very little out-of-roundness evident.

Temperature data indicates that a temperature of 2290°F was reached at a point 0.091" from the nozzle wall at the end of the test. It is interesting to note that due to erosion this distance was reduced to 0.063" at the end of the

test. As the original thickness of pyrolytic graphite was only 0.045", only 0.017" of the coating remained which still provided sufficient insulation to keep the temperature at a reasonable limit.

9.2.1.4 Test 6

The first test of the pyrolytic graphite nozzle inserts at 1000 psi resulted in a nozzle failure 1.7 seconds after ignition. This failure was due to the over-pressure caused by irregularities in the propellant as described in Section 7. Figure 10 shows the rapid rise of the pressure trace during this test.

9.2.1.5 Test 7

The second test of a pyrolytic graphite nozzle insert at 1000 psi was only partially successful. The duration of the firing was 28.2 seconds with a maximum pressure of 935 psi and an average pressure over the burning time of 873 psi.

Figures 33 through 35 show that the pyrolytic graphite coating has almost completely disappeared in the throat section leaving only the conical section behind. This loss of the pyrolytic graphite coating resulted in a fairly high erosion rate of 2.1 mils per second on the radius. Examination of the temperature and pressure traces indicated that the failure occurred approximately 12.5 seconds after ignition, Figure 14.

9.2.1.6 Conclusions

A number of conclusions can be drawn from this series of tests of pyrolytic graphite coatings:

9.2.1.6.1 The excellent insulating properties of pyrolytic graphite has been substantiated.

9.2.1.6.2 The characteristic cracks found in all tests are not detrimental because they occurred after the tests.

9.2.1.6.3 The ability of pyrolytic graphite to withstand these test conditions is markedly effected by the pressure level.

9.2.1.6.4 Failure, when it does occur, appears to be due to delamination of the pyrolytic graphite.

9.2.1.6.5 Erosion rates are relatively low when delamination does not occur.

9.2.1.6.6 It appears from this series of tests that complete success can not be expected from pyrolytic graphite at pressures above 500 psi.

9.3 Avco Corporation Materials

9.3.1 Tungsten Honeycomb Filled with Columbium Carbide

A series of three tests were performed using a material developed by Avco Corporation as a nozzle insert. A detailed description of this material can be found under Section 5. Briefly this material consists of a tungsten honeycomb filled with sintered columbium carbide. These tests were to be of 30 seconds duration at nominal pressures of 500 psi, 750 psi and 1000 psi. The throat diameters of these inserts were respectively 0.713", 0.632" and 0.575".

9.3.1.1 Test 8

The initial test of this series at a nominal pressure of 500 psi, resulted in an actual burning time of 28.5 seconds with a pressure profile reaching a peak pressure of 760 psi and an average pressure over the burning time of 590 psi.

The condition of this insert after the test was very good as can be seen from the several views of Figure 36. Erosion appeared to be relatively uniform and at a rate of 0.49 mils per second on the radius with very little out-of-roundness evident.

9.3.1.2 Test 9

The second of these inserts which was to be tested at a nominal pressure of 750 psi was exposed to pressures appreciably above that value due to apparent propellant irregularities explained in Section 7. Burning time for this test was 25.7 seconds and the pressure profile showed a sharp climb after ignition to a peak pressure of 1180 psi at the two second mark. The pressure then declined slowly to about 680 psi after 19 seconds and remained at this level until tailoff. This unusual pressure profile shown in Figure 11 resulted in an average pressure of 807 psi and was responsible for the relative short burning time.

Examination of this insert after firing indicated that it had experienced heavy erosion. Undoubtedly the unusual pressure trace with the initial high peak contributed to this extensive erosion. Figure 37, showing four views of this insert, clearly indicates the heavy erosion pattern. The throat section of the insert is very badly out-of-round. Measurements taken indicate that at its minimum diameter, the erosion rate was approximately 1.3 mils per second on the radius.

9.3.1.3 Test 10

The final test of this series of nozzle inserts was performed at a nominal pressure of 1000 psi. The burning time was 29.4 seconds with a peak pressure of 1040 psi and an average pressure over the burning time of 812 psi. This somewhat low average pressure is readily explainable by an examination of the pressure profile which indicates a continuous steady reduction of pressure after the peak pressure was reached. This reduction in pressure correlates with the fairly high erosion of the insert found upon examination after the test. Figure 38 indicates the heavy erosion experienced by this insert. Non-uniform erosion was again present and measurements found the erosion rate to be an average of 1.1 mils per second on the radius.

9.3.1.4 Examination of these three inserts after firing also indicated certain phenomena which were common to all. The most important of these is that there appeared to be no cracks in any of the inserts. The section on materials in this report points out that one of the objectives of the construction of this material was to prevent the cracking usually associated with refractory materials due to thermal stress. It appears that this objective was met successfully. Another characteristic common to all three inserts is that the tungsten honeycomb structure is clearly visible in the throat section. Apparently the columbium carbide filler eroded more readily than the tungsten structure, thereby leaving a raised diamond shaped pattern of tungsten clearly visible. The height of this pattern is estimated to be about 0.010" to 0.015" and is clearly visible in Figures 36 through 38.

9.3.1.5 Conclusions

9.3.1.5.1 The material meets one of its prime objectives of resisting cracking due to thermal stress.

9.3.1.5.2 The columbium carbide filler erodes more readily than the tungsten honeycomb.

9.3.1.5.3 The material performed satisfactorily at a pressure of 500 psi for a duration of about 30 seconds.

9.3.1.5.4 The material erodes appreciably at pressures above 500 psi.

9.4 Firth Sterling Inc. Materials

9.4.1 Columbium Carbide

Three sintered columbium carbide inserts were tested respectively for 30 seconds at 500 and 750 psi, and for 60 seconds at 500 psi. The throat diameters of these inserts were 0.710" for the 500 psi tests and 0.630" for the 750 psi test.

9.4.1.1 Test 11

The initial test in this series at a nominal pressure of 500 psi resulted in a burning time of 35.1 seconds, the pressure profile having a peak of 502 psi and an average of 484 psi over the burning time. The smoothness of the pressure trace and relatively long firing duration would normally be indicative of a nozzle material with a low erosion rate. Unfortunately the characteristics of the propellant used vary enough, as indicated in the Section 7, so that the above conclusion does not necessarily hold true. In this particular test though, the erosion rate was relatively low, amounting to 0.56 mils per second on the radius. Several views of this insert are shown in Figure 39. The erosion was very uniform with almost no out-of-roundness noticable. Some local pitting at the inlet section of the throat can be seen, but in general, the condition of the throat surface is very good. A number of hairline cracks can be noticed which were probably caused by thermal shock. Many of these originate at the thermocouple holes and the stress concentration caused by these holes was probably a contributing factor. These cracks did not appear to affect the structural integrity of the insert in any way. The density of this insert was 91.2% of the theoretical.

9.4.1.2 Test 12

The testing of the insert at a nominal pressure of 750 psi did not appreciably change any results of the test at 500 psi. Burning time was 28.8 seconds and the pressure profile reached a maximum of 790 psi with an average pressure of 735 psi over the burning time. Erosion again was very uniform and the erosion rate was 0.67 mils per second on the radius. Figure 40 shows four views of this insert. The condition of the throat is nearly identical with that of the insert fired at the lower pressure. Hairline cracks are again visible and in this case resulted in several chips missing from the exit plane of the

insert. It is believed that these chips were broken off during the disassembly of the test nozzle. The density of this insert was 90.7% of the theoretical.

9.4.1.3 Test 13

The test of an insert at 500 psi for a duration of 60 seconds unfortunately resulted in a nozzle failure at the 45 second mark which was not caused by the test material, but rather by the failure of the shear plate of the nozzle assembly. An analysis indicated that the temperature of this plate was about 2500°F at the time of failure. The plate, being made of steel, could not support the pressure load at this temperature and failed. Based upon an examination of the pressure traces it can be concluded that the erosion rate up to the time of failure was similar to that experienced with the initial 500 psi test of this material (Test 11).

9.4.1.4 Conclusions

9.4.1.4.1 Erosion rates are reasonable.

9.4.1.4.2 The effect of pressure on the erosion rate is nominal.

9.4.1.4.3 Cracking due to thermal shock, while very much in evidence, does not appear to affect the structural integrity of the insert.

9.4.2 Tantalum Carbide

Four sintered tantalum carbide inserts were procured from Firth Sterling Inc. One of the tantalum carbide inserts included a certain amount of aluminum for the purpose of providing a coolant for the nozzle during the firing, thereby reducing the erosion rate. A more detailed description of these inserts is contained in Section 5.

The three tantalum carbide nozzles were fired at approximately 500 psi for 30 seconds, 750 psi for 30 seconds, and 500 psi for 60 seconds. The tantalum

carbide insert filled with aluminum was fired at 500 psi for 30 seconds. Throat diameters for the nozzles fired at 500 psi were 0.708" and for the nozzle fired at 750 psi was 0.632".

9.4.2.1 Test 14

The initial test in this series at a nominal pressure of 500 psi resulted in a burning time of 33 seconds. Pressure data from this test was not reliable, due to plugged pressure lines.

Examination of the insert after the test indicated that a number of simple hairline cracks had occurred during the test, Figure 41. It should be pointed out that while all the visible cracks did exist after disassembly, this insert was accidently dropped before being photographed, resulting in widening of the cracks and chipping of the edges of the cracks.

A study of these pictures leads to a theory for a mechanism of failure. It can be notes that the inner wall of the insert has no cracks. All cracks apparently initiate from the outside and travel inward until stopped by a circumferential crack. This type of failure is typical of a failure due to thermal stress. During the initial heating of the insert the inner section rapidly heats up and expands. The insert being supported by relatively elastic materials is therefore only partially restrained, allowing the O.D. to expand and causing tensile hoop stresses. The stress distribution pattern therefore consists of tensile stresses at the O.D. and compressive stresses at the I.D. Failure at the O.D. occurs because the material is weaker in tension than in compression. The cracks propagate radially inward until they reach a location at which the stress level has been reduced to the point where the material can support it.

The circumferential crack in the face of the insert is not fully understood but one possible explanation may be that it occurred during the cooling period. Due to the cracking on the O.D.,

the compression stresses on the I.D. relieve themselves while the insert is hot. After the test, the I.D. shrinks while cooling but the wedge shaped cracked pieces do not allow the O.D. to follow. Radial tensile stresses therefore develop causing the inner section to separate from the outer section.

Disassembly of a nozzle and detailed examination of the insert indicated the following erosion pattern. At the upstream section of the throat the diameter increased from its original value of 0.708" to an average value of 0.744" resulting in an erosion rate of approximately 0.5 mils per second on the radius. At the downstream end of the throat section the erosion rate increased to about 0.8 mils per second. The inner wall of the insert did not show signs of excessive erosion or pitting and showed very little out-of-roundness.

The density of this tantalum carbide insert was 66.3% of the theoretical density and therefore appreciably lower than the density of inserts used in subsequent tests.

9.4.2.2 Test 15

The throat insert with a diameter of 0.632" was successfully fired for a duration of 32.2 seconds. The maximum pressure during the firing was 720 psi and the average pressure over the burning time was 663 psi.

Upon disassembly, the insert was found to be in very good condition as indicated in Figure 42. There was very little out-of-roundness and the erosion rate at the throat was 0.72 mils per second on the radius. The insert was almost free from cracks, only some minor hairline cracks being visible. These cracks generally originate from the thermocouple holes and are probably due to the stress concentration caused by these holes.

A number of bubbles are visible on Figure 42 in the throat section of this insert. Chemical analysis showed these bubbles to be aluminum oxide. It is of interest to note that the appearance of aluminum oxide bubbles in the throat of the insert occurred only in this and the subsequent test of tantalum carbide filled with aluminum. The reason for the deposit of aluminum oxide only in these two tests could not be determined.

The density of this insert was 81.2% of the theoretical density.

9.4.2.3 Test 16

The test of a tantalum carbide insert at a pressure of 500 psi for a duration of 60 seconds unfortunately resulted in a failure. A previous test of columbium carbide for the same duration had shown that the steel shear plate failed due to over-heating. This steel shear plate was therefore replaced by a tungsten shear plate which would provide higher temperature capability. Two circumstances combined to cause failure of this tungsten shear plate. The first was the choice of sintered and pressed tungsten which turned out to be very weak in shear and the second was an error in machining which resulted in a 25% reduction of the available shear area.

The test failure occurred 20 seconds after ignition.

9.4.2.4 Test 17

A throat insert made from tantalum carbide filled with 3.5% of aluminum by weight, or 16% of aluminum by volume was fired successfully for 37.4 seconds. The peak pressure during the test was 516 psi and the average pressure over the burning time was 468 psi. Figure 43 shows four views of this insert after firing. A few hairline cracks are visible but they did not affect the structural integrity of the unit.

The erosion rate was extremely low being only 0.16 mils per second on the radius and very uniform.

It was expected that the heat absorbed by the aluminum in going through a phase change from solid to liquid to gas would lower the surface temperature of the insert enough to reduce the erosion rate. Undoubtedly this expectation was realized, shown by the low erosion rate of 0.16 mils per second on the radius, compared with the erosion rate of 0.5 mils per second on the radius, measured in a tantalum carbide insert subjected to approximately the same environment for a 10% shorter duration of firing.

One of the major problems that was to be explored by this test was whether the amount of aluminum present in the insert was sufficient to provide cooling for a long enough period of time to be effective. It was felt that the possibility existed that all the aluminum would leave within the first few seconds of the test and therefore would not provide sufficient protection. It is apparent from the test results that this did not occur. To further check this point the insert was sectioned and examined for any remaining aluminum. Figure 44 indicated that a certain amount of aluminum at the outside of the insert and near the exit section was still present, leading to the conclusion that some aluminum evaporated continuously throughout the test. This conclusion was also supported by the low erosion rate which, it is believed, could not be achieved unless the benefits of cooling were present for at least most of the firing duration.

9.4.2.5 Conclusions

9.4.2.5.1 The addition of aluminum drastically reduced the erosion rate.

9.4.2.5.2 Variations in density from 66.3% to 81.2% did not appear to affect the erosion rate.

9.4.2.5.3 The effect of pressure on the erosion rate is nominal.

9.4.2.5.4 Hairline cracks are evident in this material but do not appear to affect the structural integrity of the insert.

Test No.	Material	Vendor	Press. psi	Firing Duration Seconds	Throat Dia. inches	Erosion Rate - Mils per Second (0.2 | 0.4 | 0.6 | 0.8 | 1.0 | 1.2)
1	Titanium Carbide bonded w/graphite	Electro-Thermal	500	41.7	0.677	Severe Erosion
2	Tantalum Carbide	Electro-Thermal	500	39	0.710	
3	Pyrolytic Graphite	Raytheon	500	34	0.704	
4	Pyrolytic Graphite	Raytheon	750	27	0.626	
5	Pyrolytic Graphite	Raytheon	750	30.7	0.630	
6	Pyrolytic Graphite	Raytheon	1000	* 1.7	.0.578	Test Terminated due to rig failure
7	Pyrolytic Graphite	Raytheon	1000	28.2	0.585	Severe Erosion
8	Columbium Carbide Tungsten Honeycomb	Avco	500	28.5	0.713	
9	Columbium Carbide Tungsten Honeycomb	Avco	750	25.7	0.632	
10	Columbium Carbide Tungsten Honeycomb	Avco	1000	29.4	0.575	
11	Columbium Carbide	Firth Sterling	500	35	0.707	
12	Columbium Carbide	Firth Sterling	750	28.8	0.629	
13	Columbium Carbide	Firth Sterling	500	* 45.4	0.709	Test Terminated due to rig Failure
14	Tantalum Carbide	Firth Sterling	500	33	0.708	
15	Tantalum Carbide	Firth Sterling	750	32.2	0.632	
16	Tantalum Carbide	Firth Sterling	500	* 19.4	0.710	Test Terminated due to rig Failure
17	Tantalum Carbide filled w/aluminum	Firth Sterling	500	37.4	0.710	* Time to failure

COMPARISON OF EROSION RATES

Figure 1

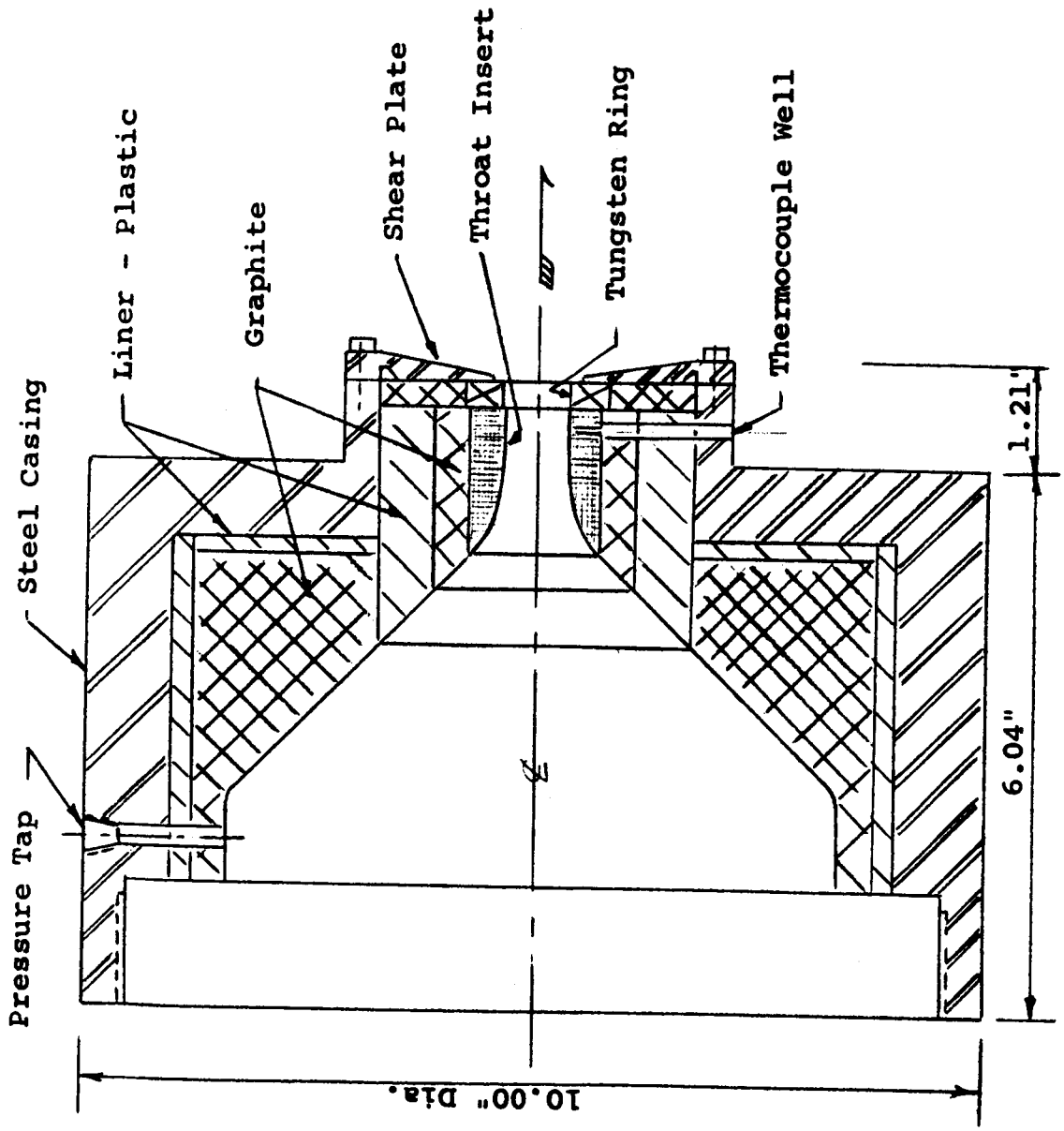

NOZZLE CROSS-SECTION

Figure 2

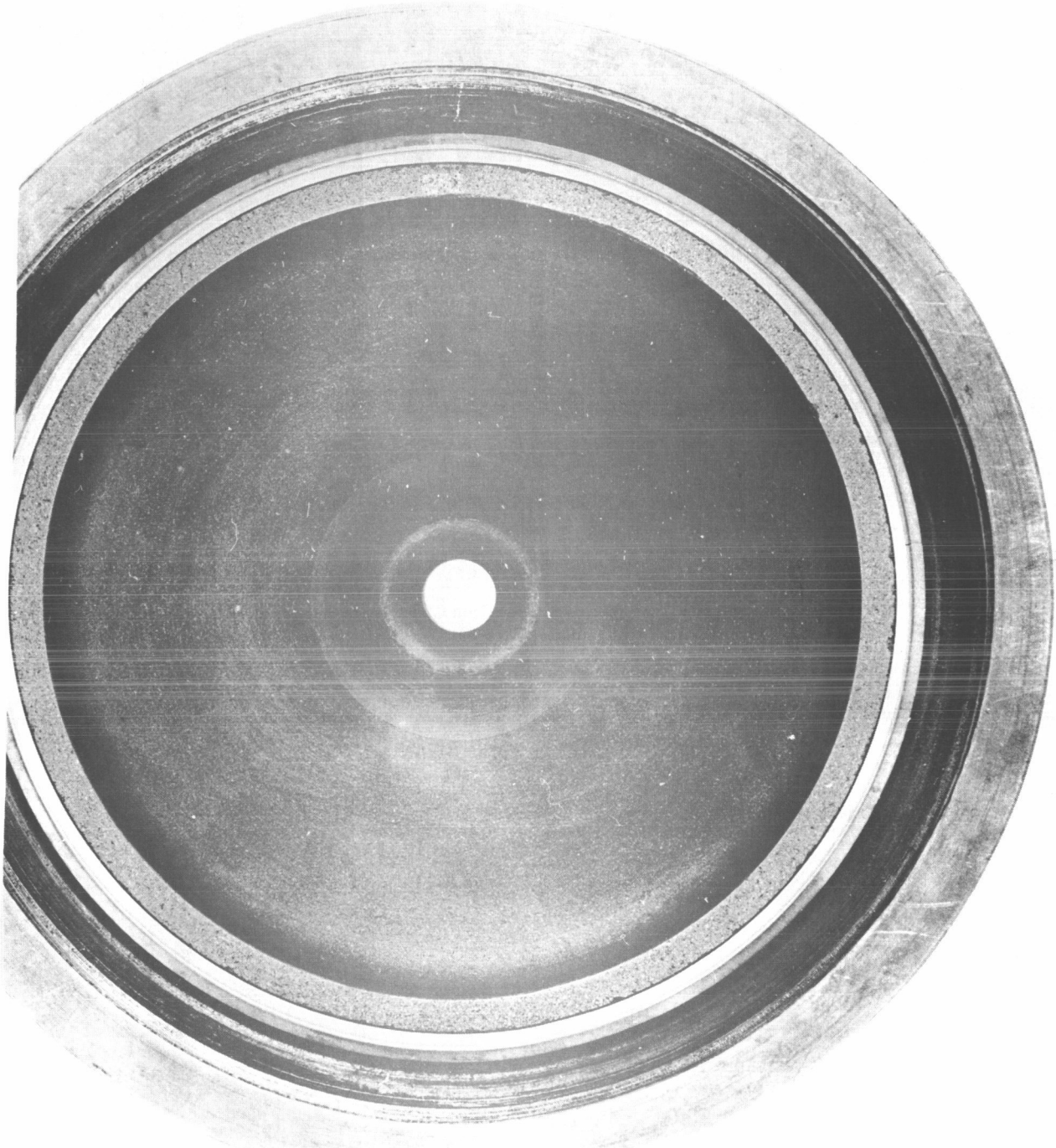

NOZZLE ASSEMBLY - INLET SIDE

Figure 3

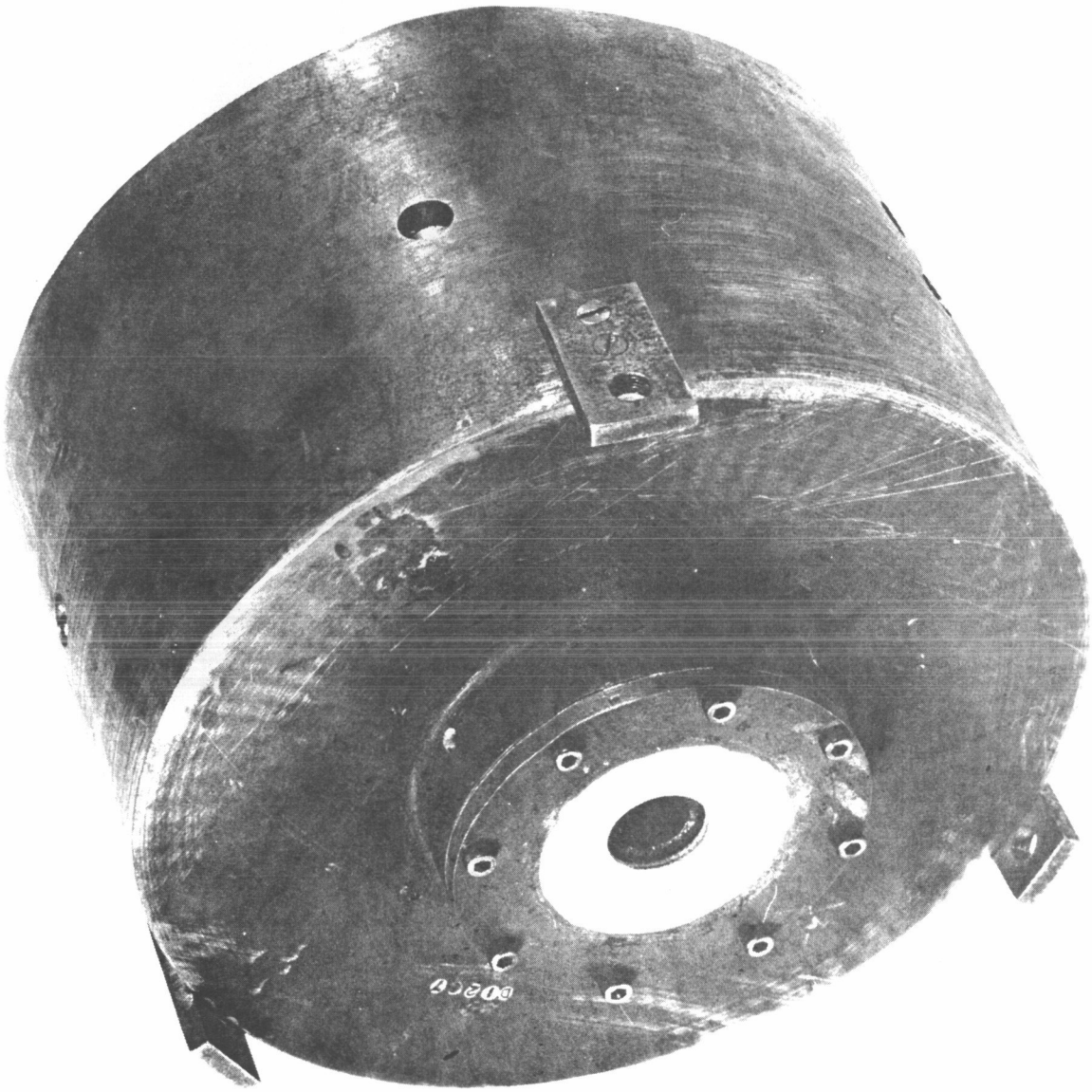

NOZZLE ASSEMBLY - EXIT SIDE

Figure 4

CONFIDENTIAL

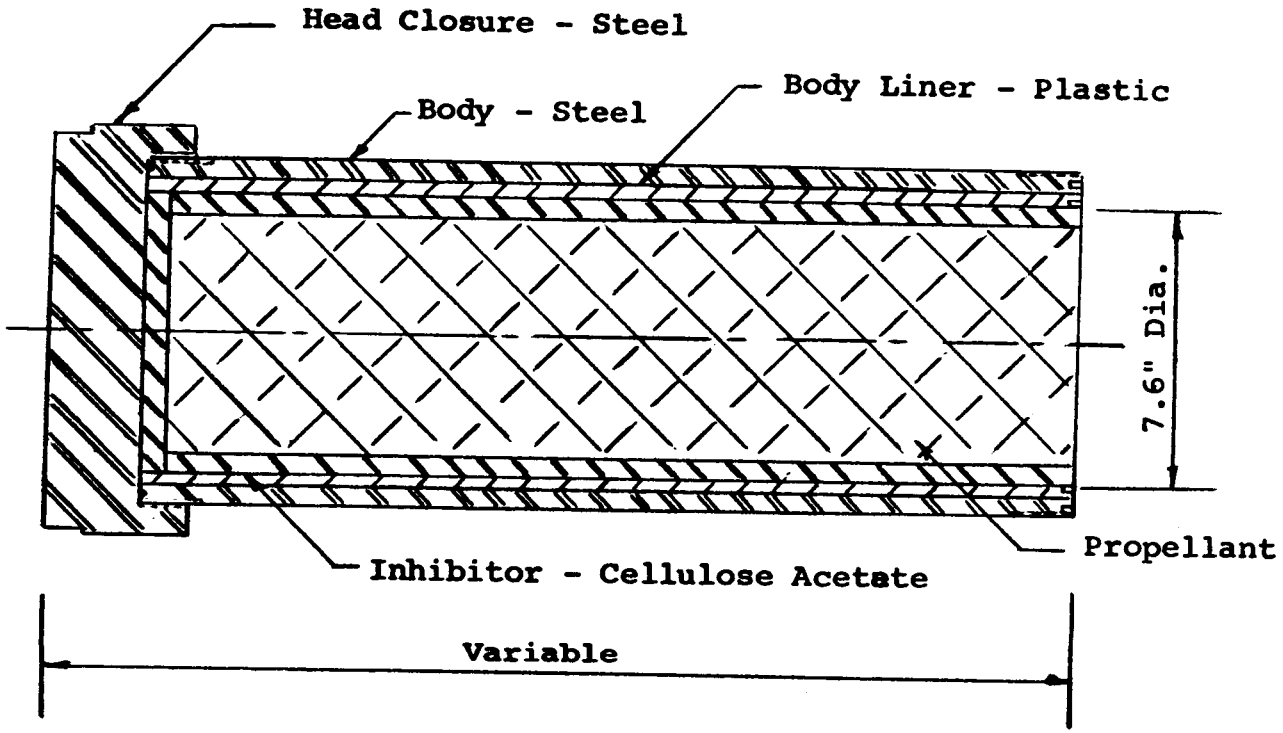

SCHEMATIC-TEST MOTOR

Figure 5

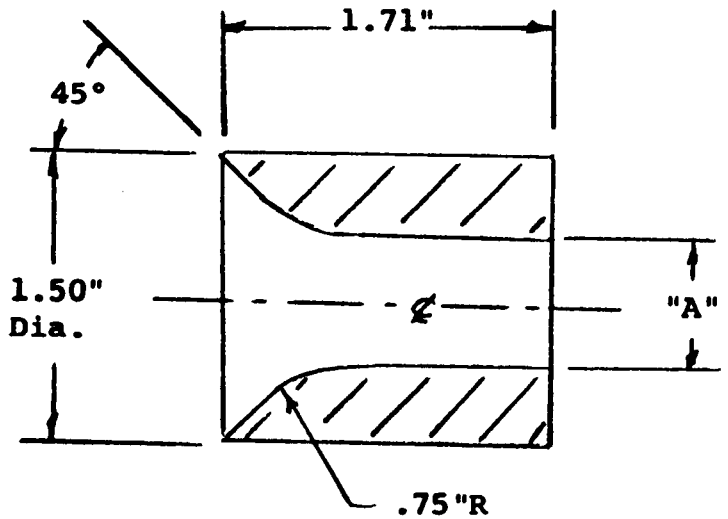

Press.lbs per sq in.	"A" Dia. in.
500	0.710
750	0.632
1000	0.578

TYPICAL TEST NOZZLE INSERT - REFRACTORY CARBIDE

Figure 6

CONFIDENTIAL

CONFIDENTIAL

Press. lbs per sq in.	Dia in	"t" in.
500	0.710	.050
750	0.632	.045
1000	0.578	.040

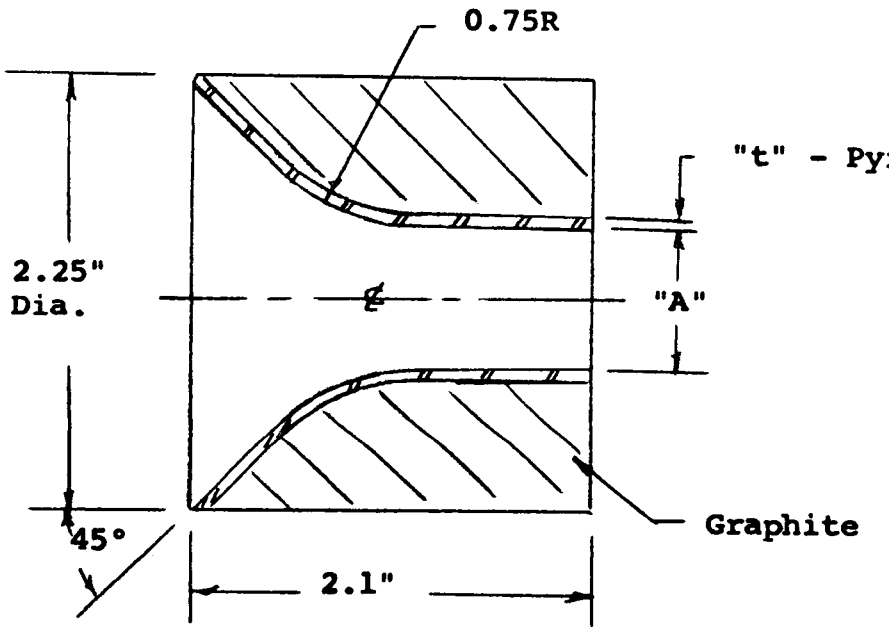

TEST NOZZLE INSERT - PYROLYTIC GRAPHITE

Figure 7

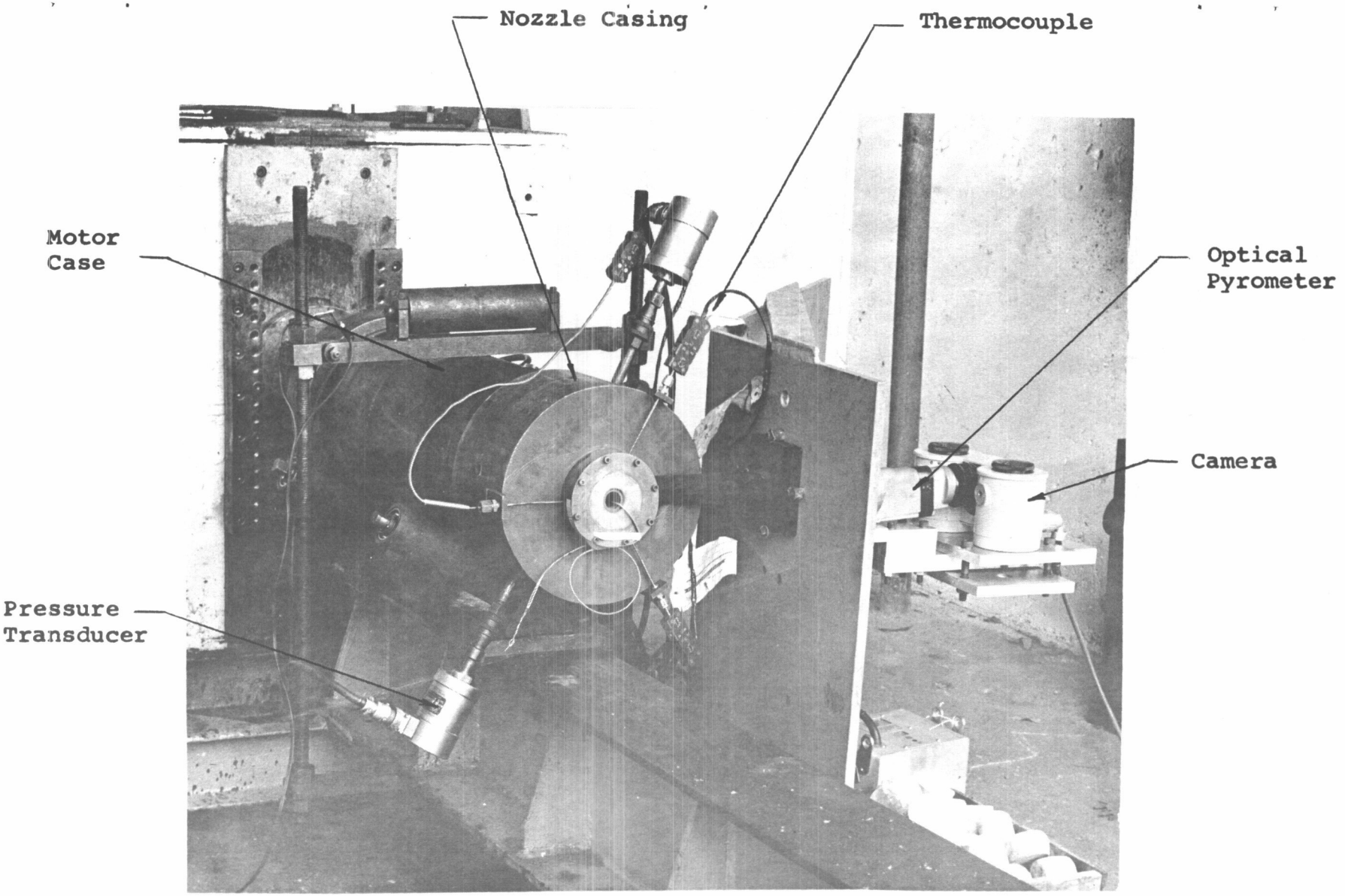

TEST STAND - HERCULES POWDER COMPANY

Figure 8

PRESSURE - TIME CURVE

Test - 15
Material - Tantalum Carbide
Vendor - Firth Sterling
Throat Dia. - 0.632 inches

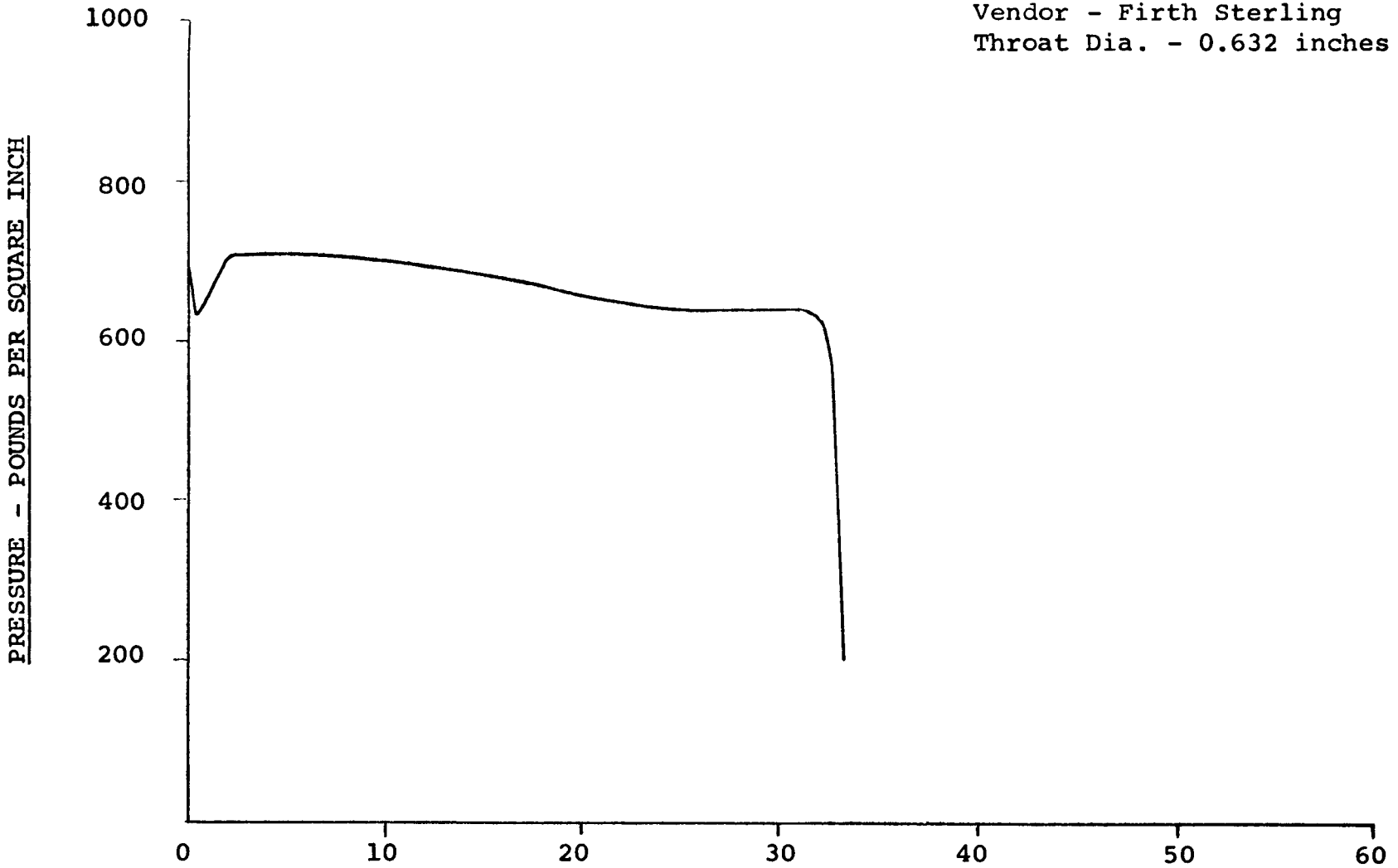

Figure 9

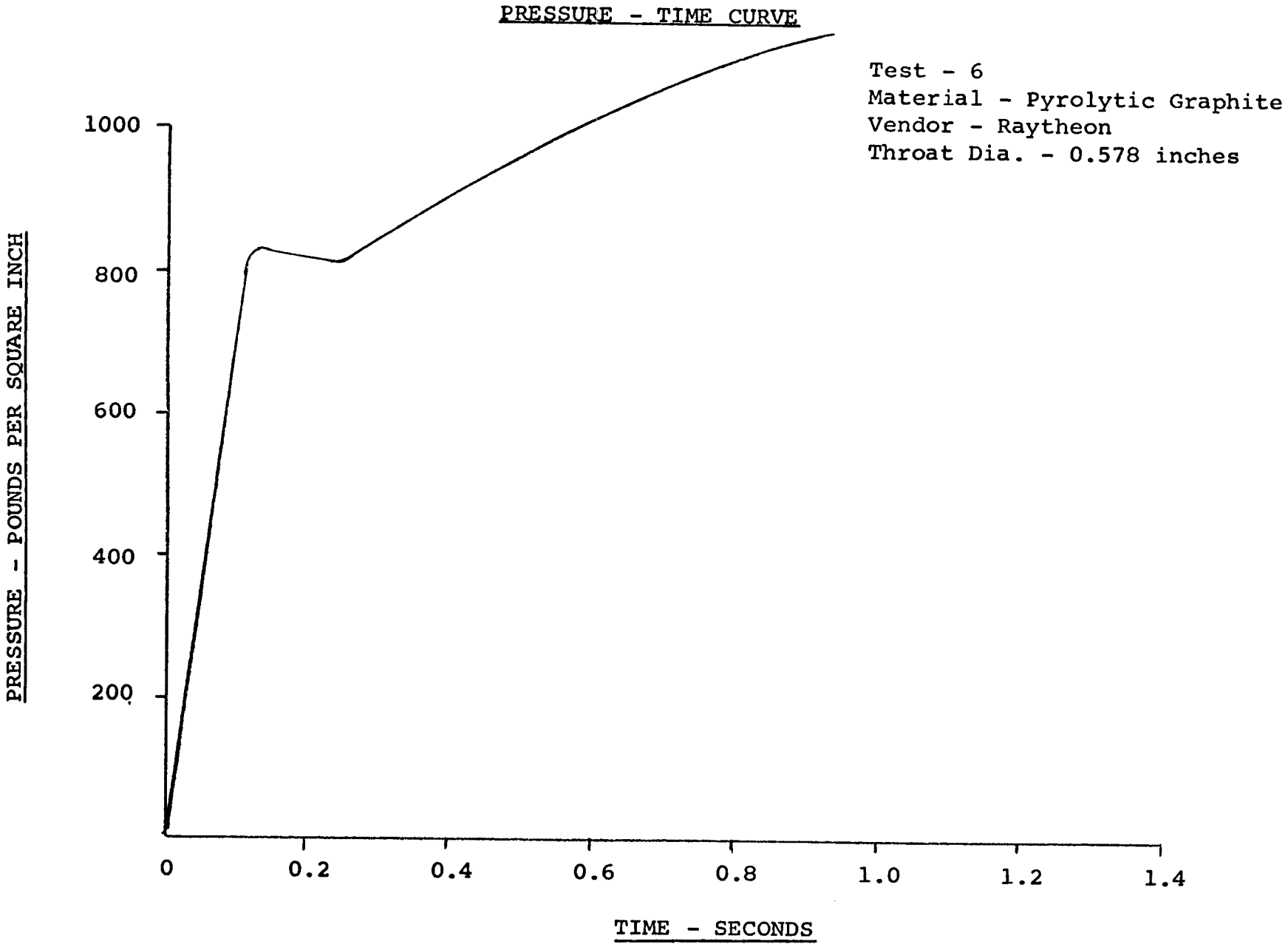
PRESSURE - TIME CURVE
Test - 6
Material - Pyrolytic Graphite
Vendor - Raytheon
Throat Dia. - 0.578 inches
PRESSURE - POUNDS PER SQUARE INCH
1000
800
600
400
200
0
0.2
0.4
0.6
0.8
1.0
1.2
1.4
TIME - SECONDS

Figure 10

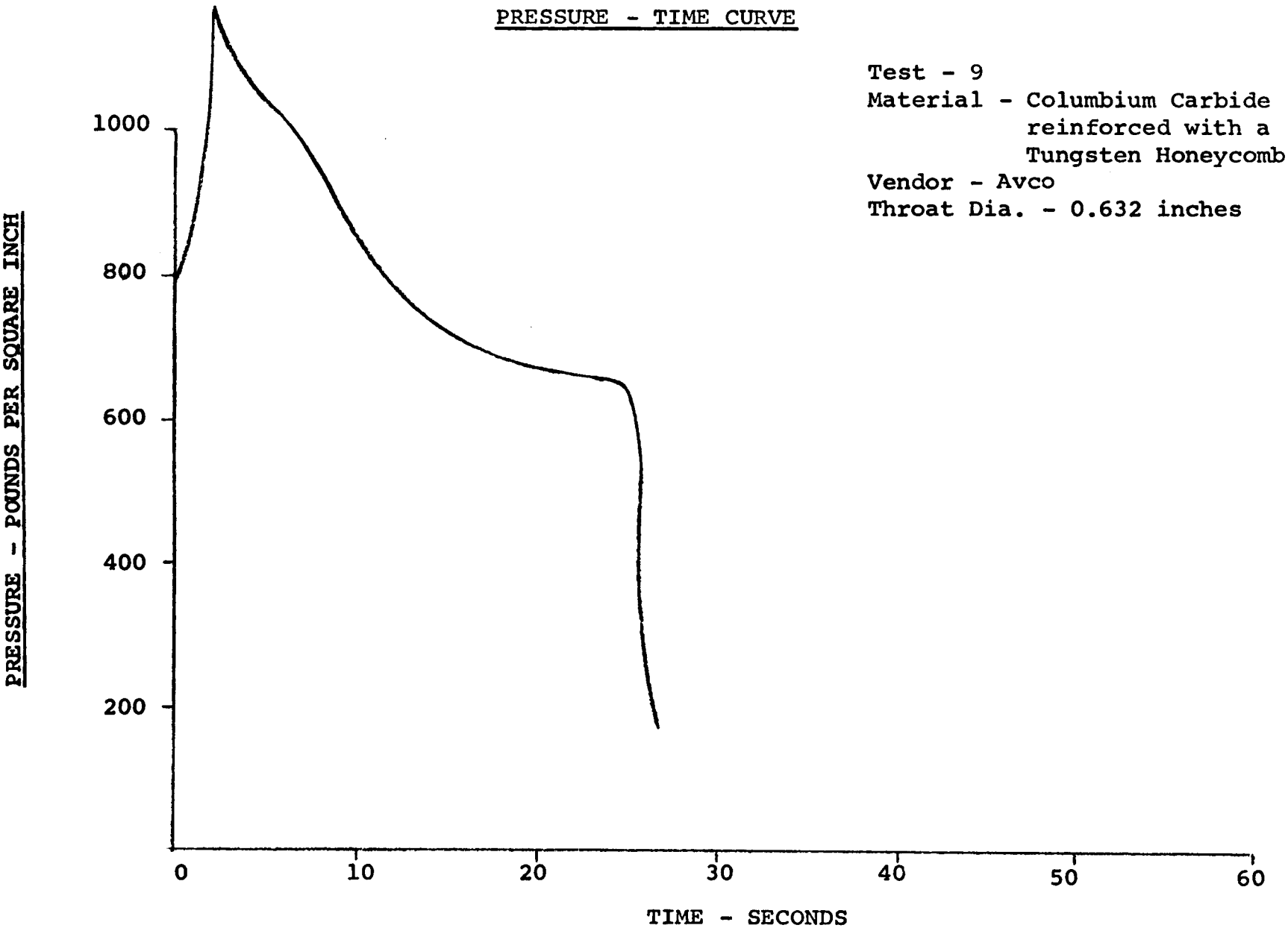

Figure 11

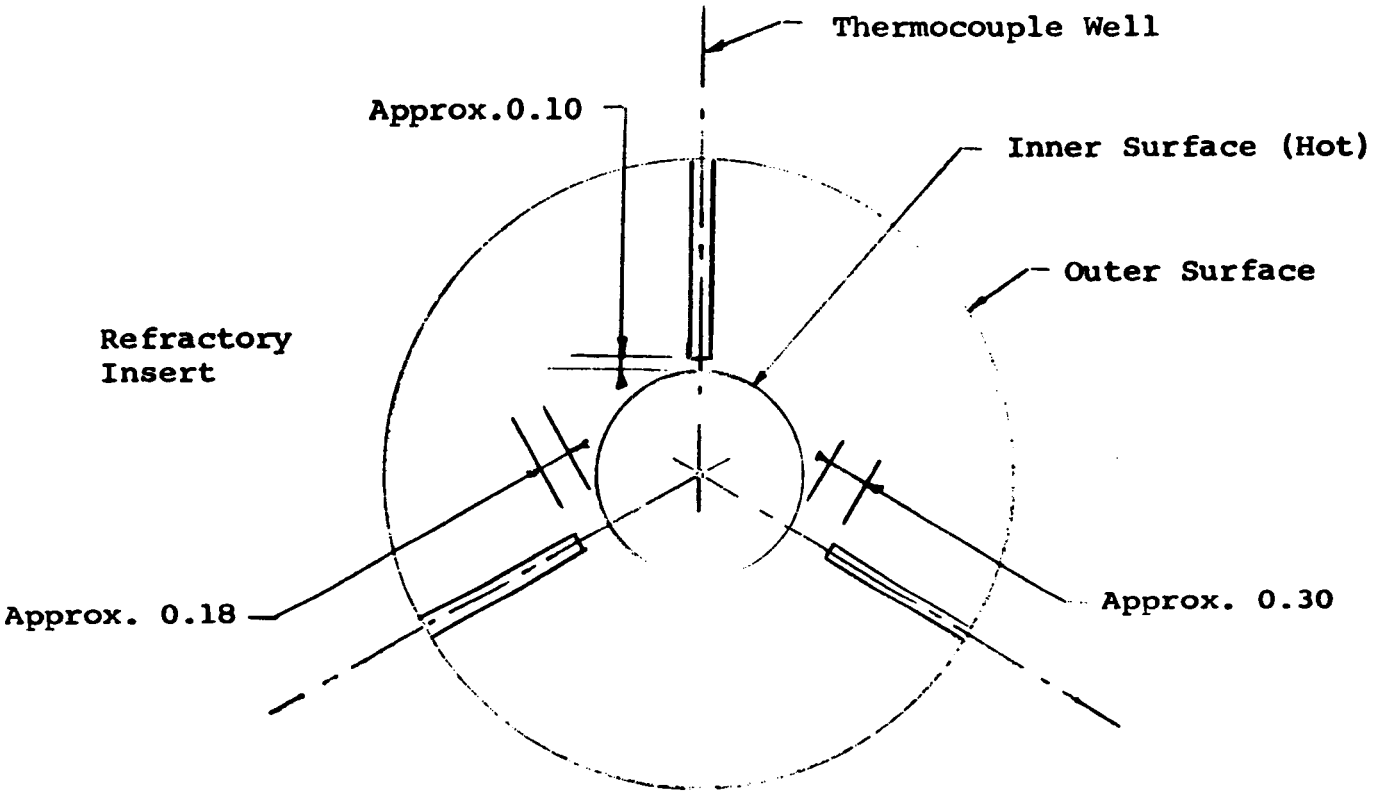

THERMOCOUPLE LOCATIONS

Figure 12

TEMPERATURE - TIME CURVES

for various distances from the inner wall

Test - 4
Material - Pyrolytic Graphite
Vendor - Raytheon
Throat Dia. - 0.626 inches
Pressure - 750 lbs. per sq. in.

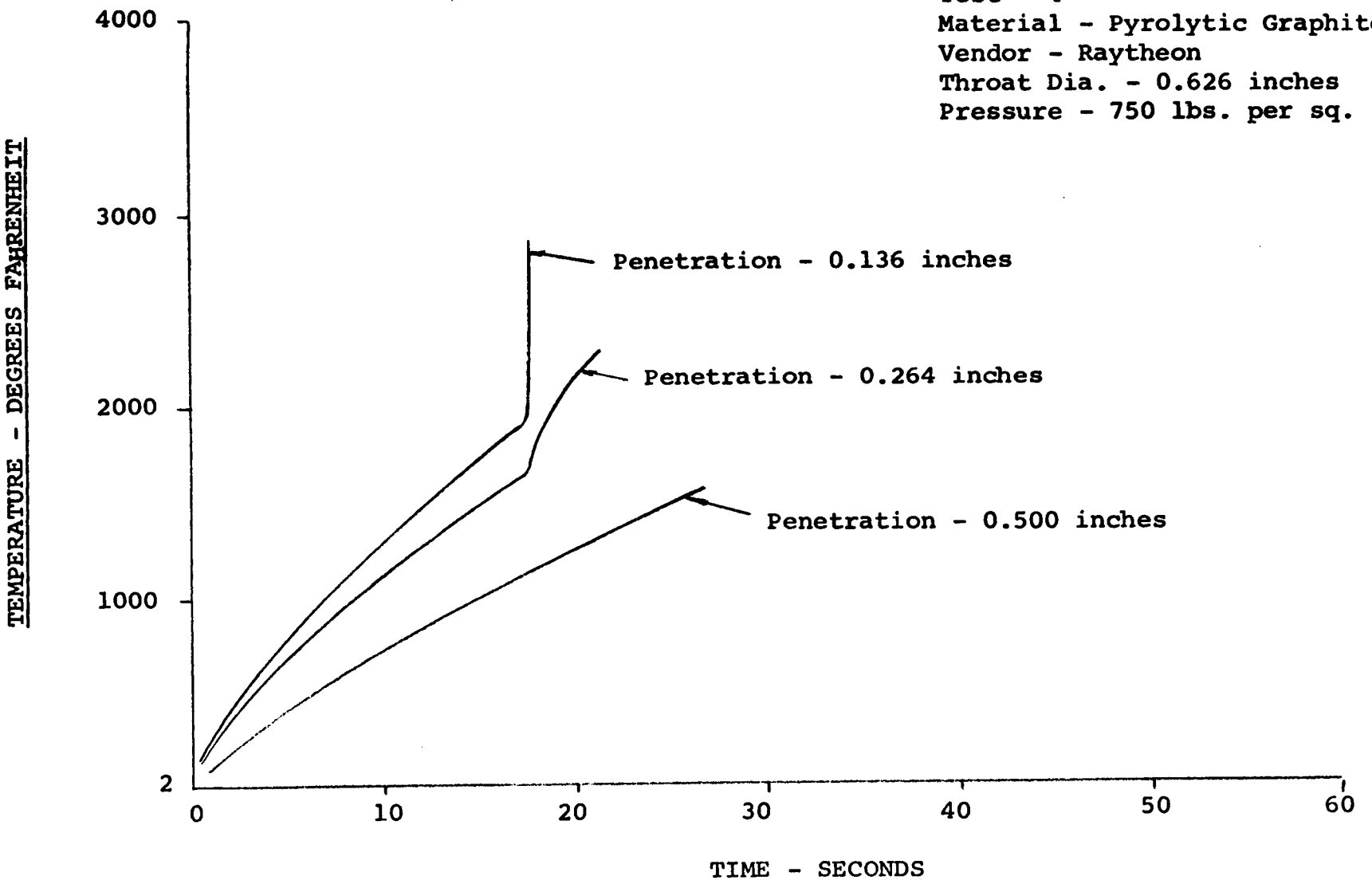

Figure 13

TEMPERATURE - TIME CURVES

for various distances from
the inner wall

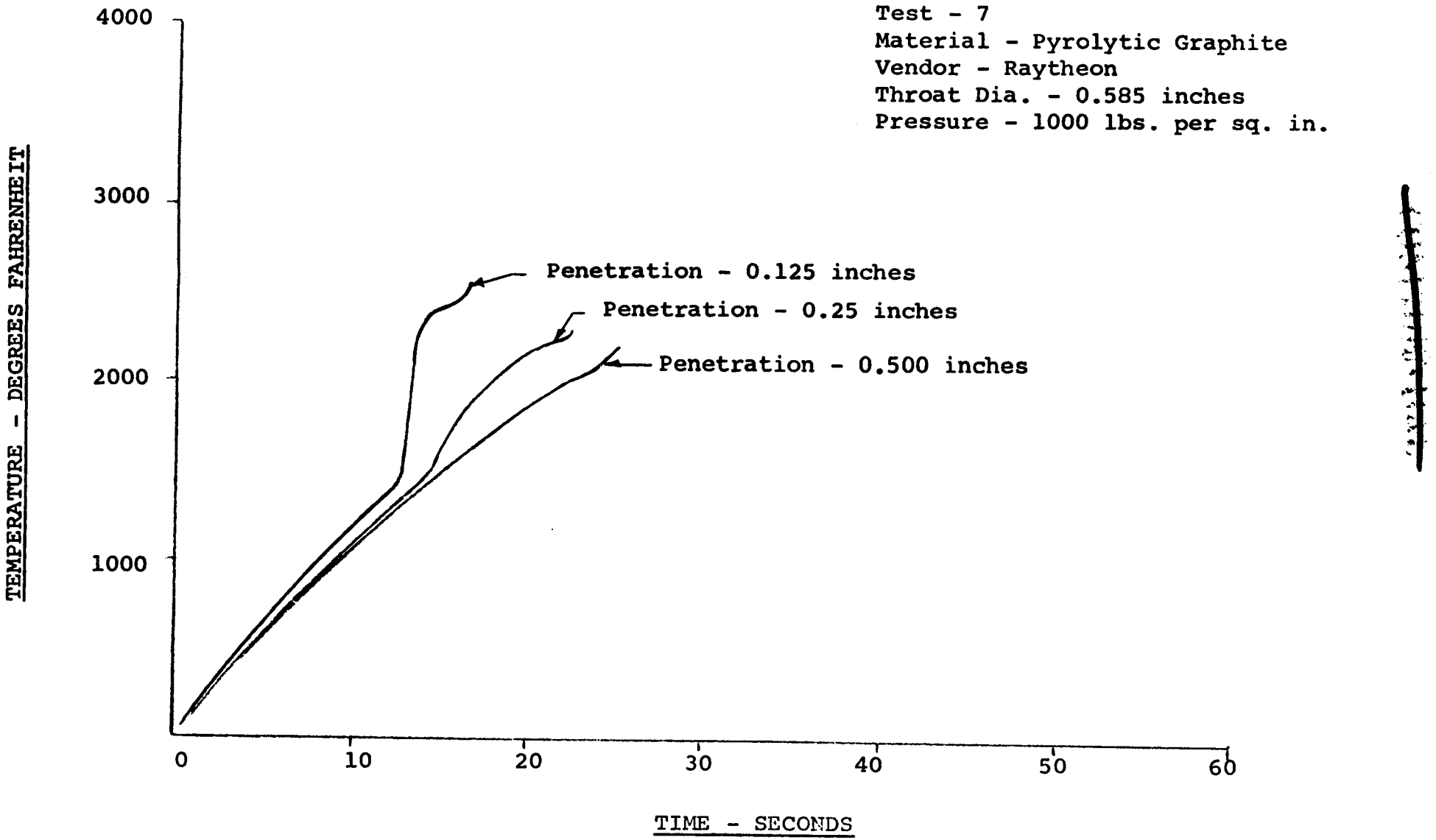

Figure 14

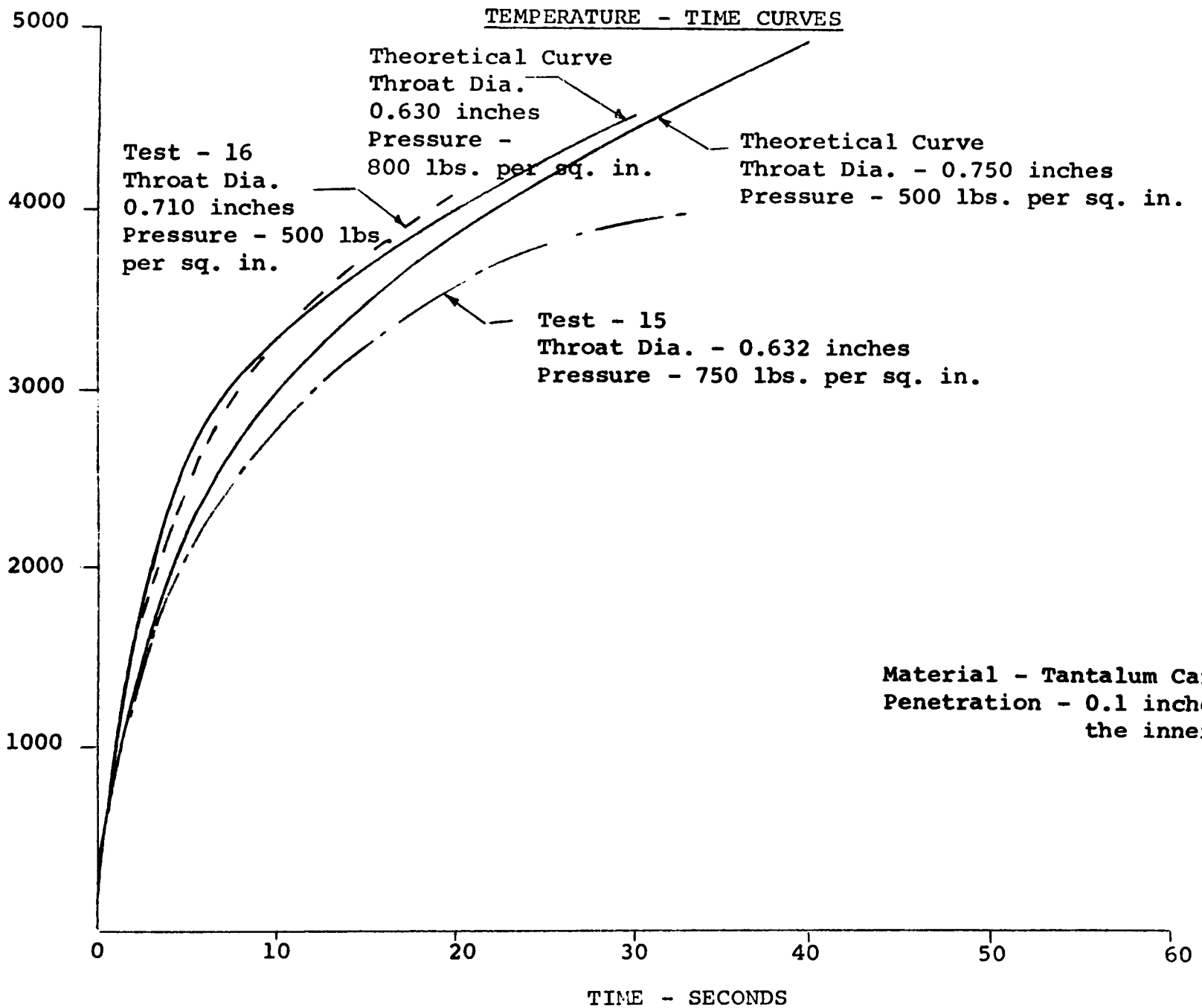
TEMPERATURE - TIME CURVES
Theoretical Curve
Throat Dia.
0.630 inches
Pressure -
800 lbs. per sq. in.
Test - 16
Throat Dia.
0.710 inches
Pressure - 500 lbs.
per sq. in.
Theoretical Curve
Throat Dia. - 0.750 inches
Pressure - 500 lbs. per sq. in.
Test - 15
Throat Dia. - 0.632 inches
Pressure - 750 lbs. per sq. in.
Material - Tantalum Carbide
Penetration - 0.1 inches from
the inner surface
5000
4000
3000
2000
1000
0
10
20
30
40
50
60
TEMPERATURE - DEGREES FAHRENHEIT
TIME - SECONDS

Figure 15

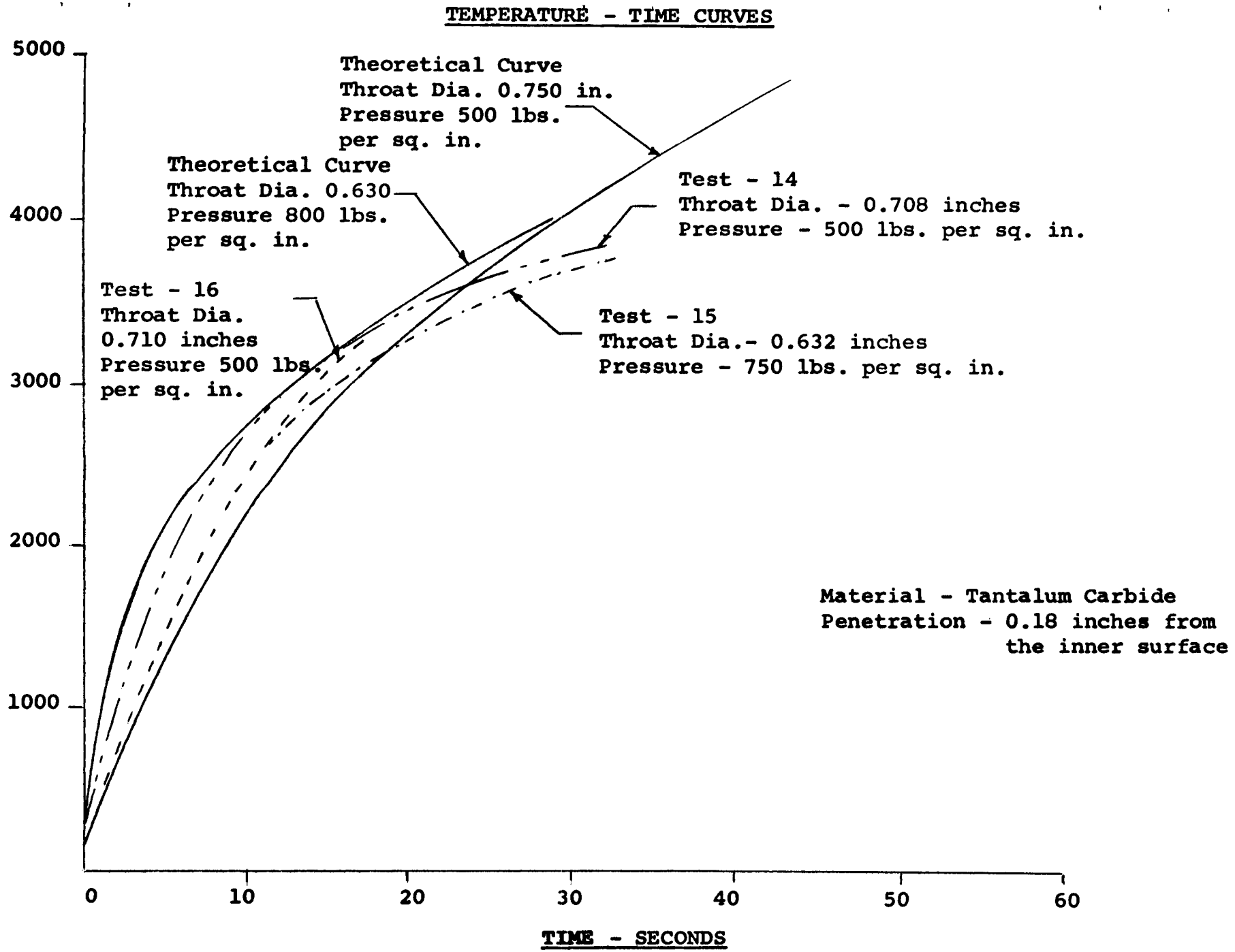

Figure 16

CONFIDENTIAL

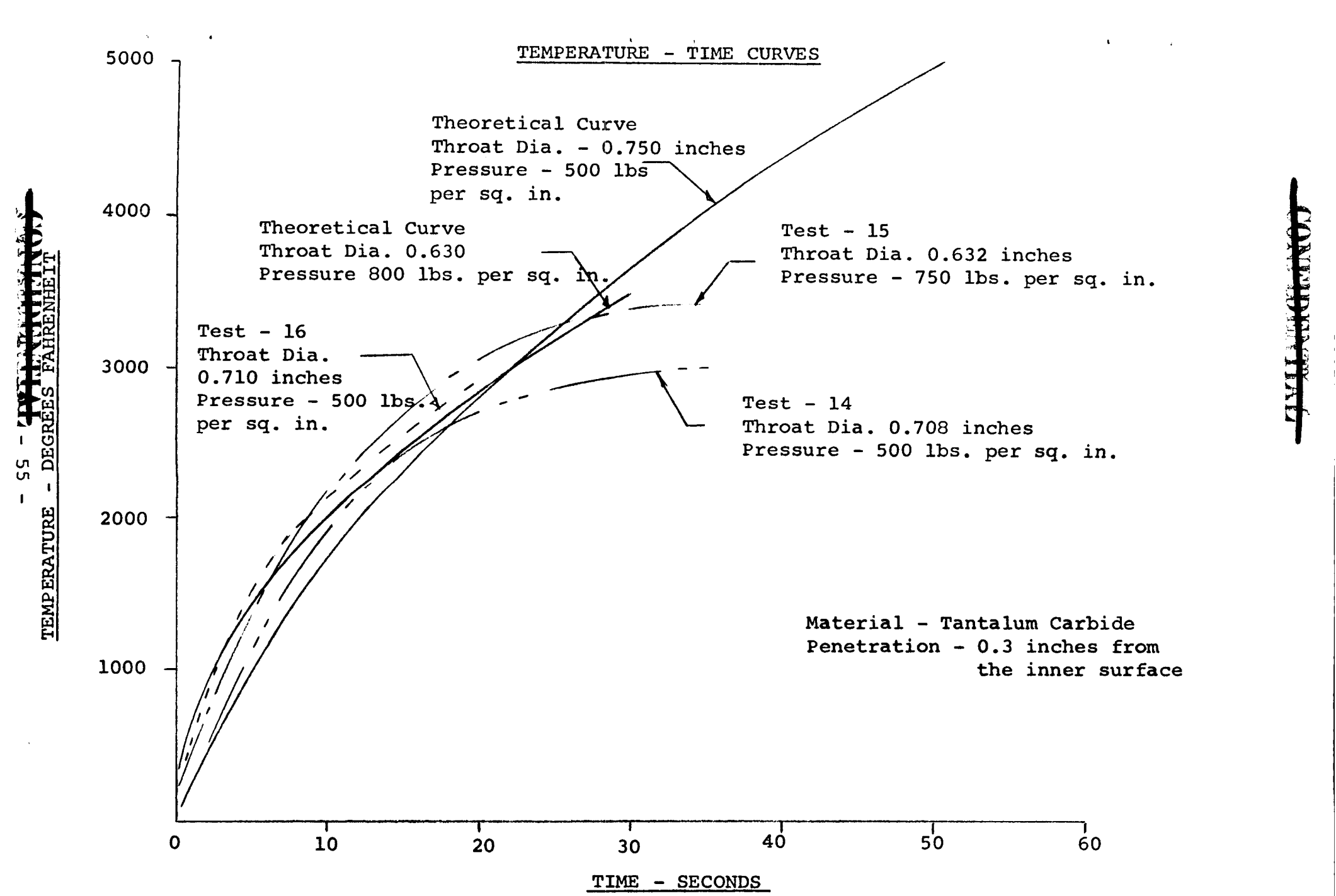
TEMPERATURE - TIME CURVES
5000
4000
3000
2000
1000
0
10
20
30
40
50
60
TEMPERATURE - DEGREES FAHRENHEIT
TIME - SECONDS
Theoretical Curve
Throat Dia. - 0.750 inches
Pressure - 500 lbs
per sq. in.
Theoretical Curve
Throat Dia. 0.630
Pressure 800 lbs. per sq. in.
Test - 15
Throat Dia. 0.632 inches
Pressure - 750 lbs. per sq. in.
Test - 16
Throat Dia.
0.710 inches
Pressure - 500 lbs.
per sq. in.
Test - 14
Throat Dia. 0.708 inches
Pressure - 500 lbs. per sq. in.
Material - Tantalum Carbide
Penetration - 0.3 inches from
the inner surface

Figure 17

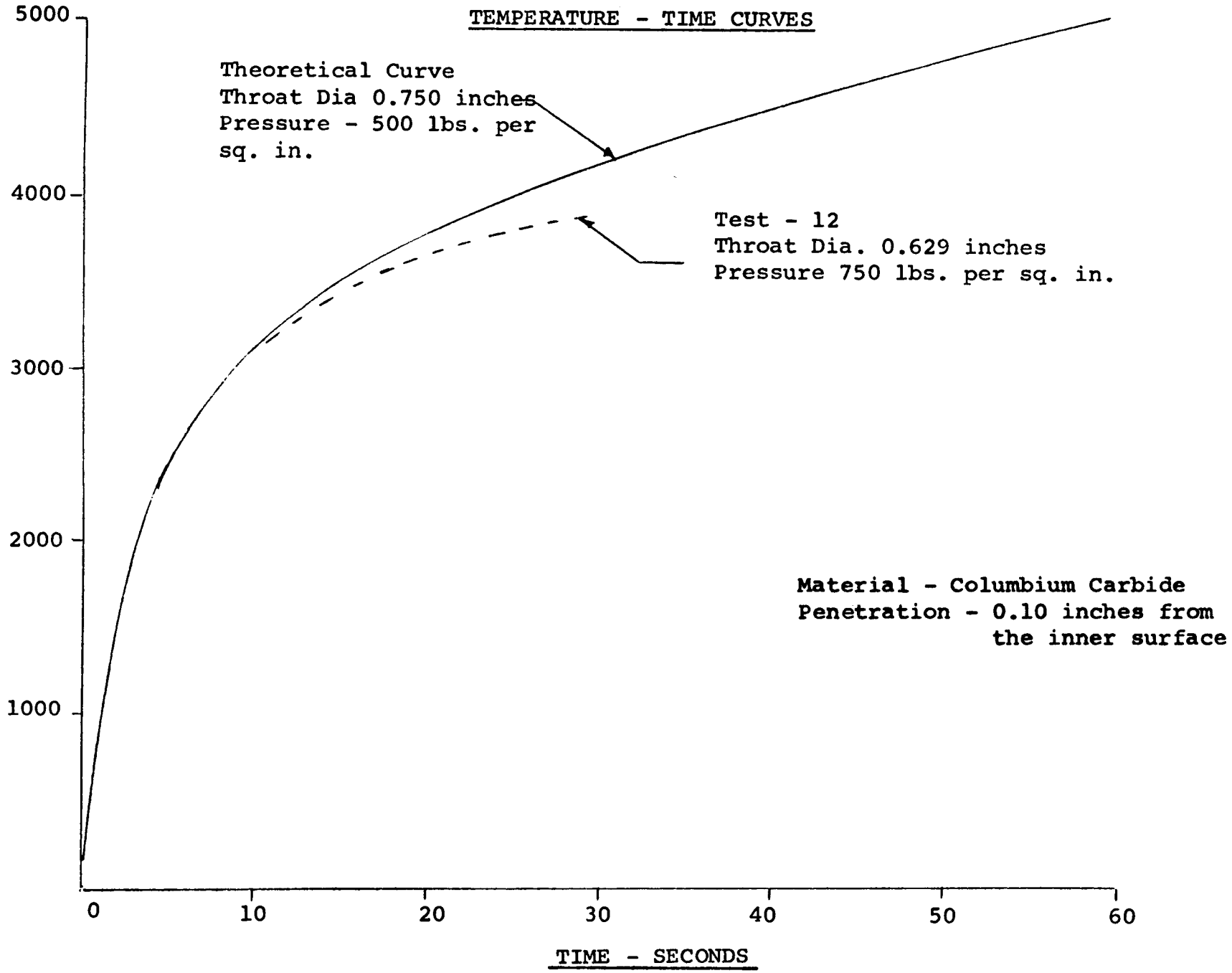
TEMPERATURE - TIME CURVES
Theoretical Curve
Throat Dia 0.750 inches
Pressure - 500 lbs. per sq. in.
Test - 12
Throat Dia. 0.629 inches
Pressure 750 lbs. per sq. in.
Material - Columbium Carbide
Penetration - 0.10 inches from the inner surface
TEMPERATURE - DEGREES FAHRENHEIT
5000
4000
3000
2000
1000
0
10
20
30
40
50
60
TIME - SECONDS

Figure 18

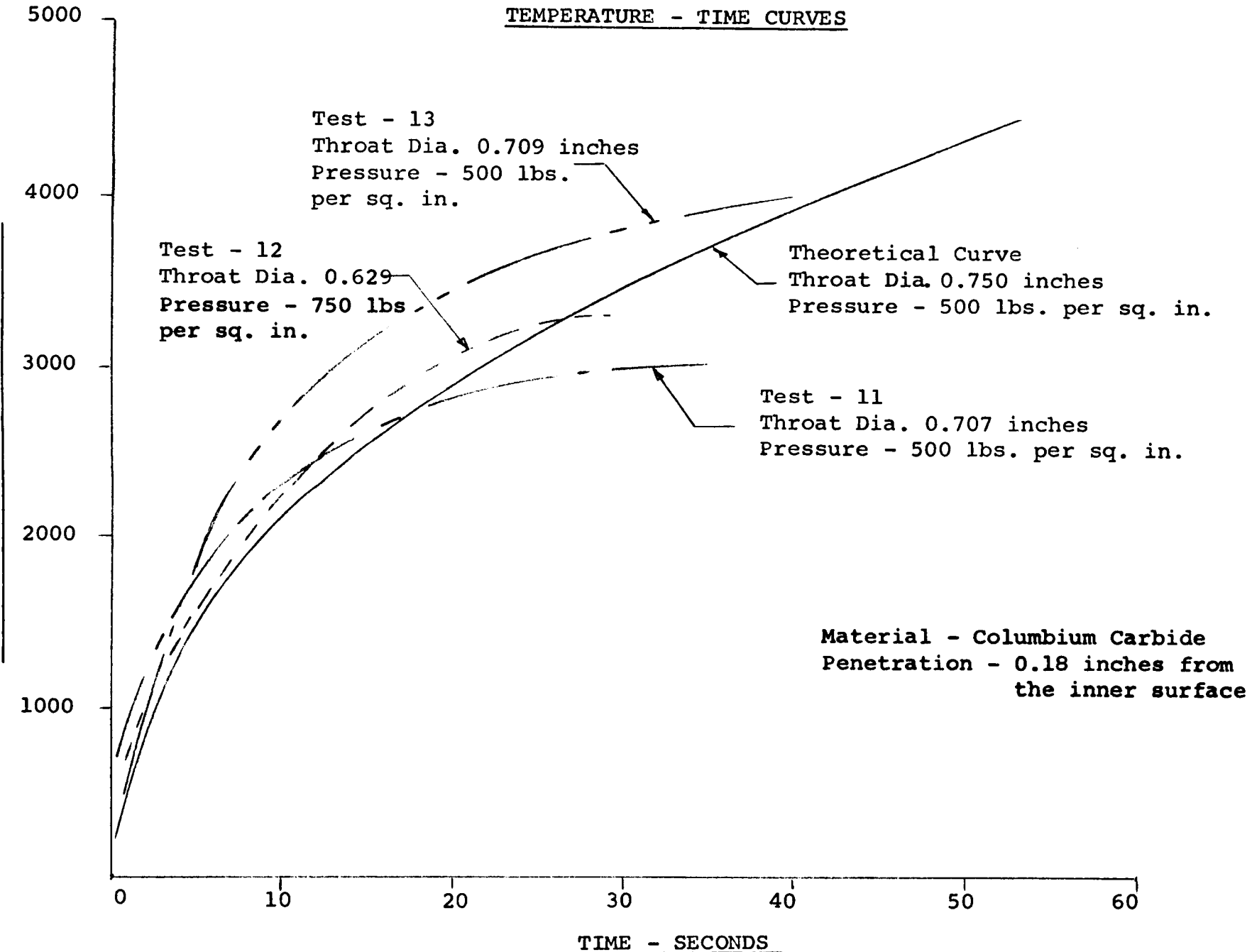

Figure 19

CONFIDENTIAL

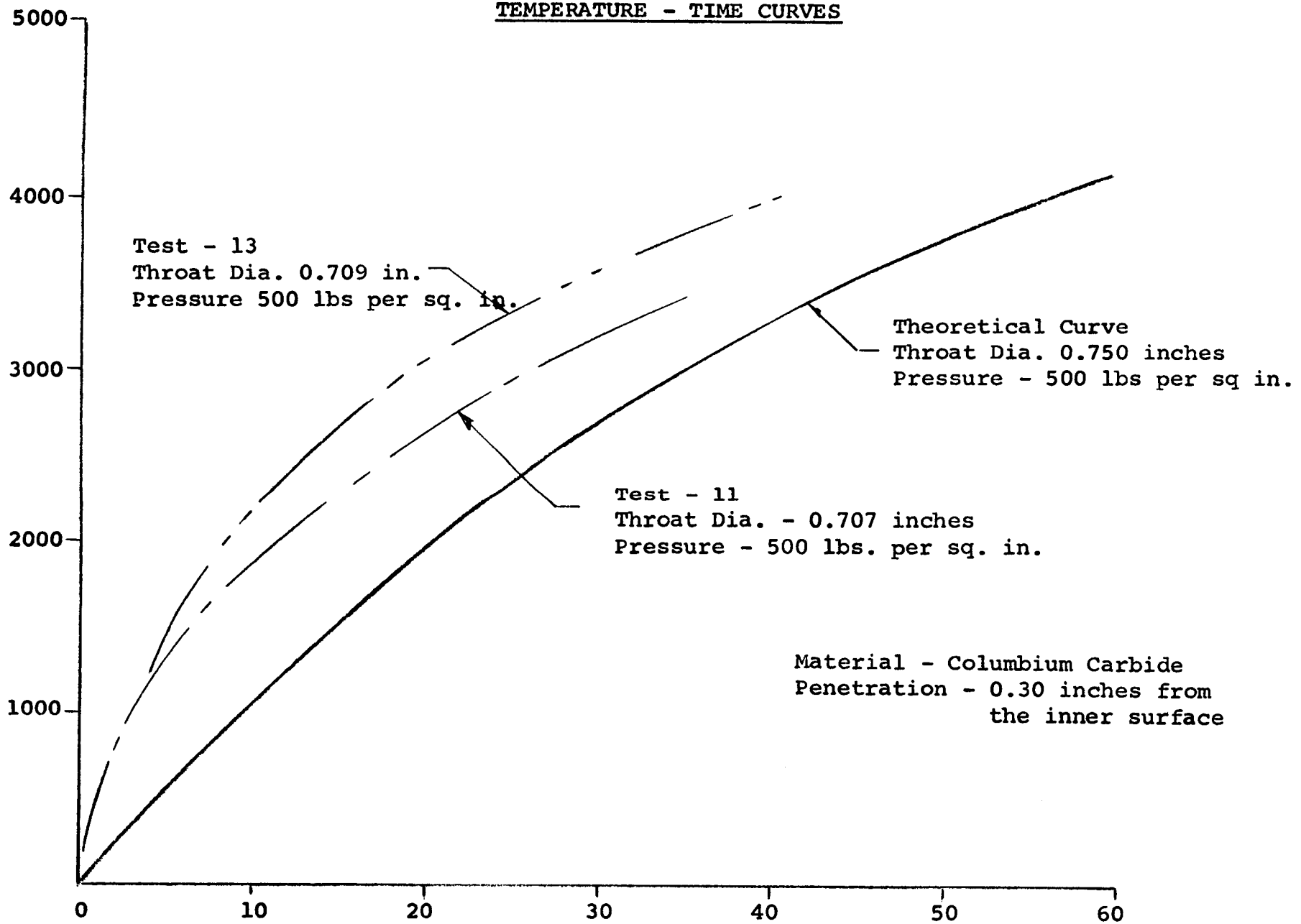

Figure 20

CONFIDENTIAL

TEST 1 - TITANIUM CARBIDE BONDED WITH GRAPHITE - NOZZLE EXIT

Figure 21

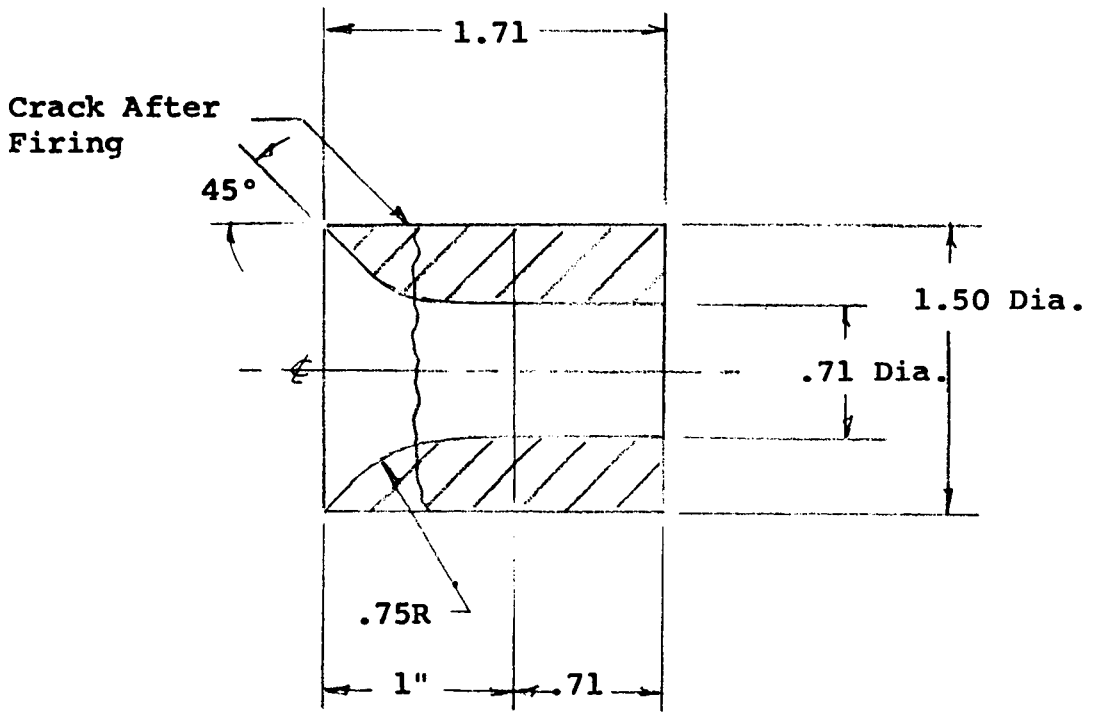

TEST 2 - TANTALUM CARBIDE INSERT (TWO PIECES)

Figure 22

ARDE-PORTLAND

PYROGRAPHITE NOZZLE INSERT—

THROAT DIAMETER- .710

— TEST DATE·6/30/60

TEST 3 - PYROLYTIC GRAPHITE - NOZZLE INLET

Figure 23

CONFIDENTIAL

TEST 3 - PYROLYTIC GRAPHITE - NOZZLE INLET - CLOSE-UP

Figure 24

TEST 3 - PYROLYTIC GRAPHITE - GRAPHITE SUBSTRATE AND CONICAL SHELL

Figure 25

ARDE-PORTLAND

PYROGRAPHITE NOZZLE INSERT

THROAT DIAMETER - .632

TEST DATE - 7/7/60

TEST 4 - PYROLYTIC GRAPHITE - NOZZLE INLET

Figure 26

CONFIDENTIAL

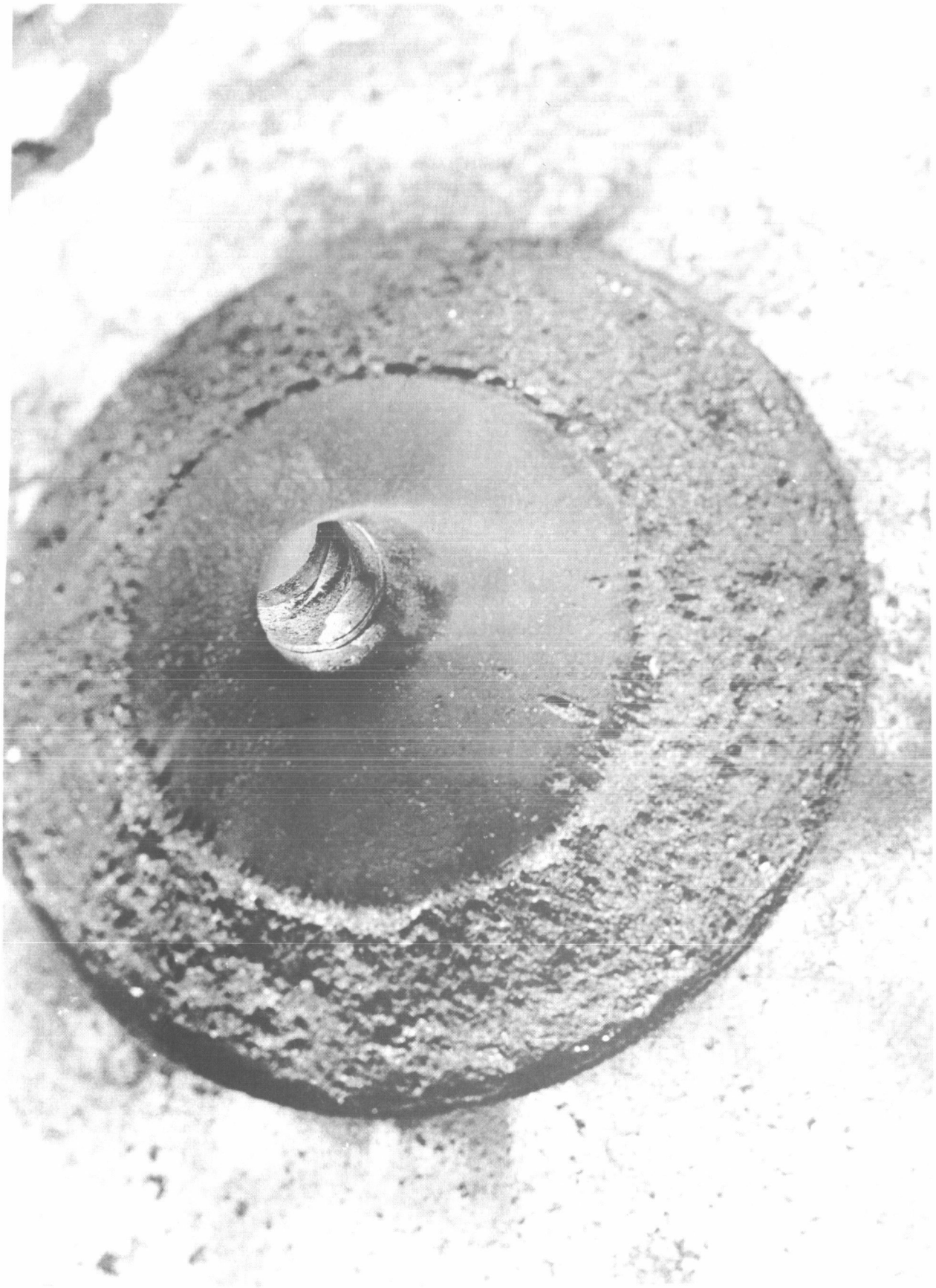

TEST 4 - PYROLYTIC GRAPHITE - NOZZLE INLET - CLOSE-UP

Figure 27

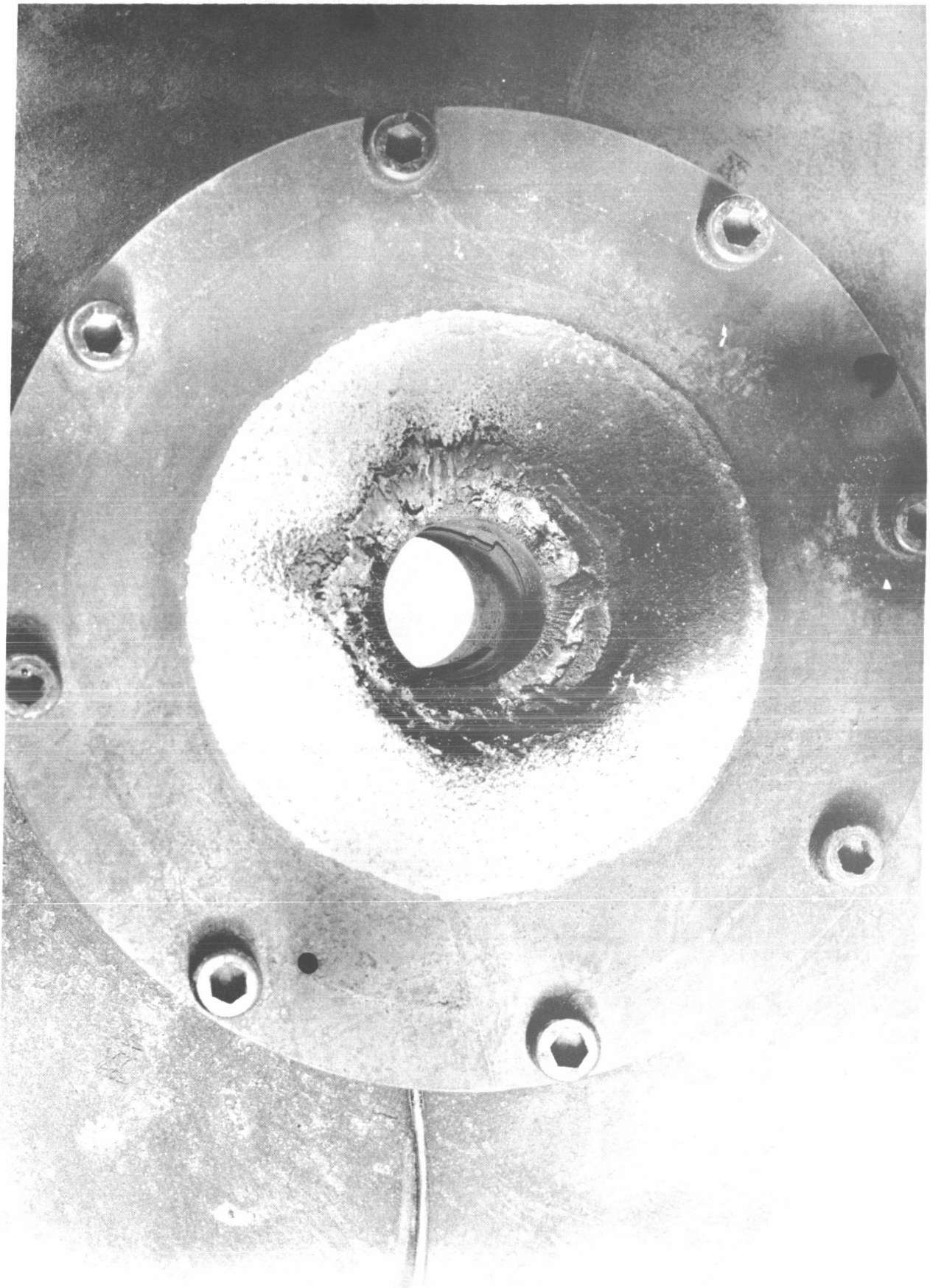

TEST 4 - PYROLYTIC GRAPHITE - NOZZLE EXIT

Figure 28

TEST 4 - PYROLYTIC GRAPHITE - CONICAL AND CYLINDRICAL SHELL

Figure 29

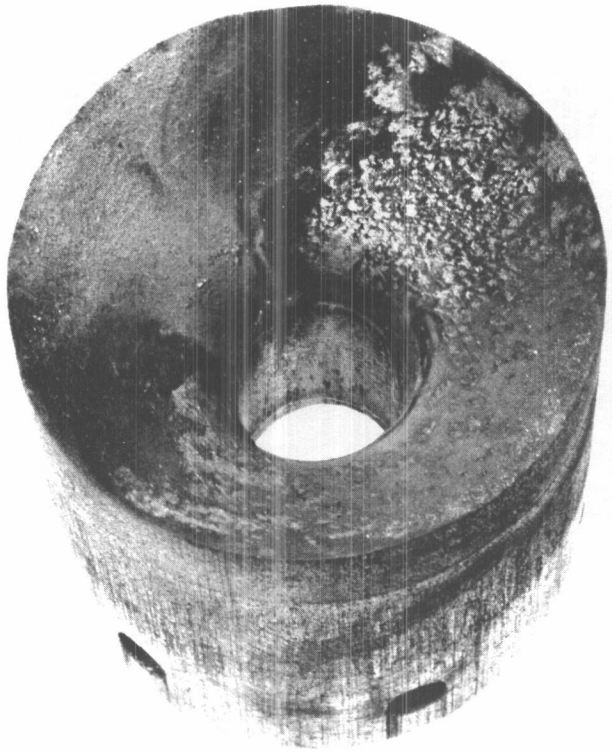

TEST 5 - PYROLYTIC GRAPHITE - INLET SECTION GRAPHITE SUBSTRATE WITH PYROLYTIC GRAPHITE CYLINDER ATTACHED

Figure 30

CONFIDENTIAL

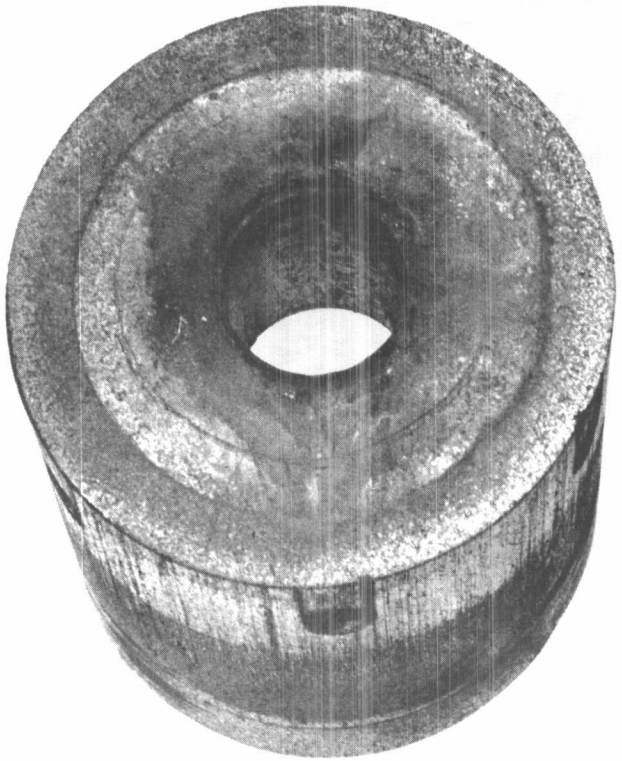

TEST 5 - PYROLYTIC GRAPHITE - EXIT SECTION GRAPHITE SUBSTRATE WITH PYROLYTIC GRAPHITE CYLINDER ATTACHED

Figure 31

CONFIDENTIAL

TEST 5 - PYROLYTIC GRAPHITE - EXIT SECTION GRAPHITE SUBSTRATE AND CONICAL SHELL

Figure 32

TEST 7 - PYROLYTIC GRAPHITE - INLET SECTION GRAPHITE SUBSTRATE

Figure 33

TEST 7 - PYROLYTIC GRAPHITE - EXIT SECTION GRAPHITE SUBSTRATE

Figure 34

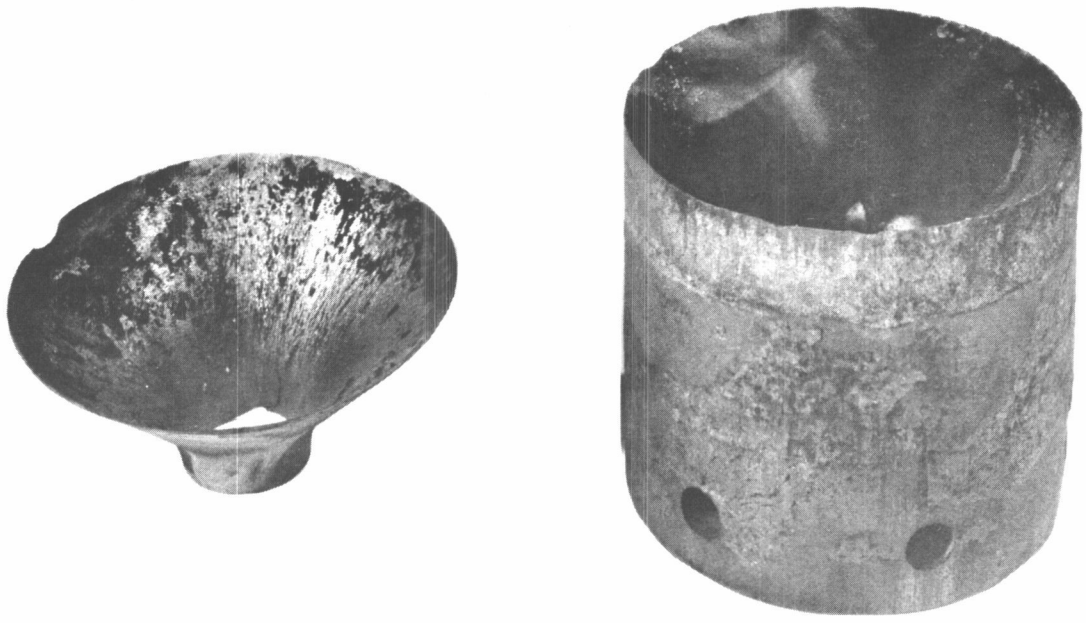

TEST 7 - PYROLYTIC GRAPHITE - GRAPHITE SUBSTRATE AND CONICAL SHELL

Figure 35

CONFIDENTIAL

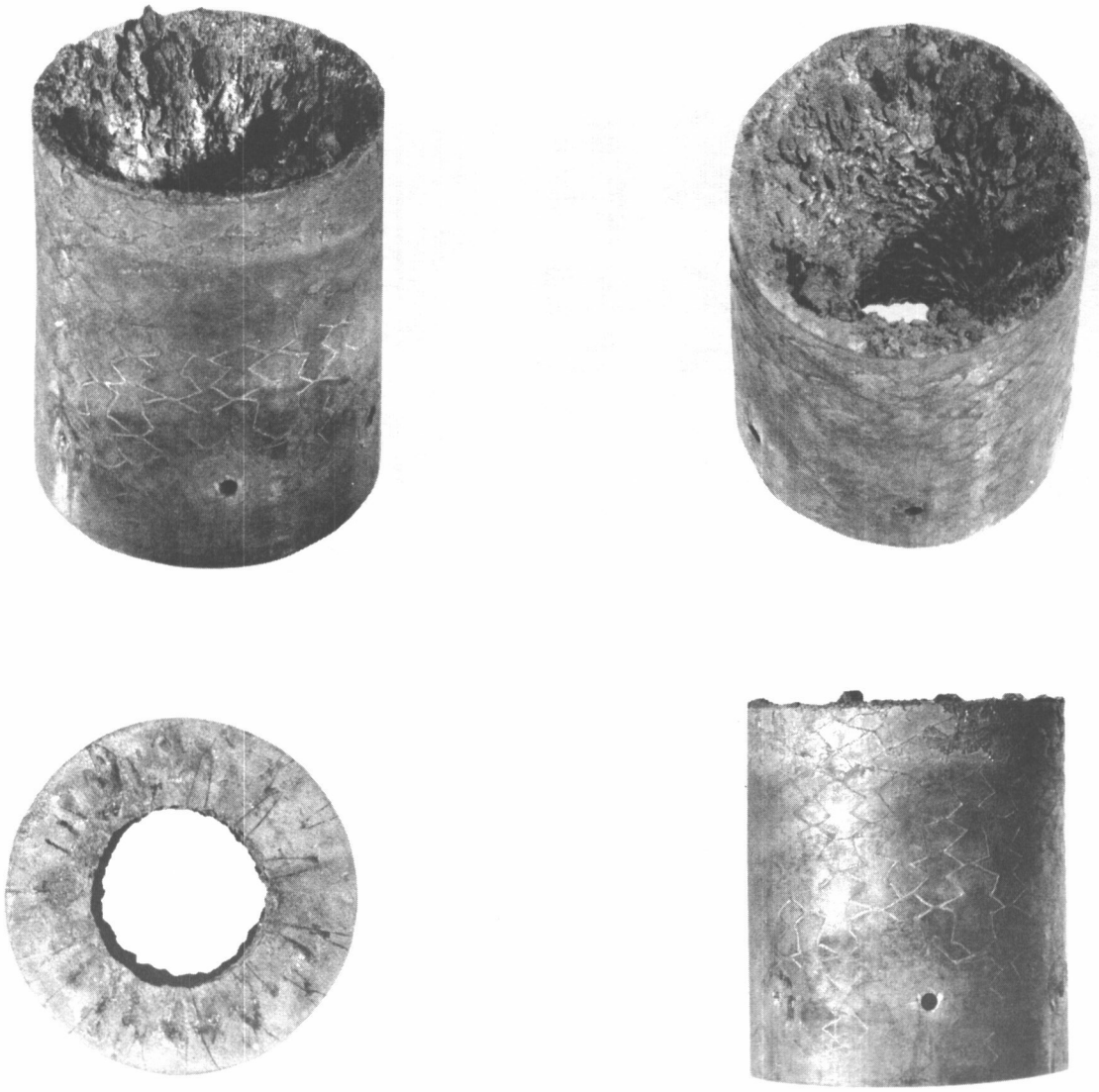

TEST 8 - COLUMBIUM CARBIDE WITH TUNGSTEN HONEYCOMB - NOZZLE INSERT

Figure 36

CONFIDENTIAL

TEST 9 - COLUMBIUM CARBIDE WITH TUNGSTEN HONEYCOMB - NOZZLE INSERT

Figure 37

TEST 10 - COLUMBIUM CARBIDE WITH TUNGSTEN HONEYCOMB - NOZZLE INSERT

Figure 38

CONFIDENTIAL

TEST 11 - COLUMBIUM CARBIDE - NOZZLE INSERT

Figure 39

CONFIDENTIAL

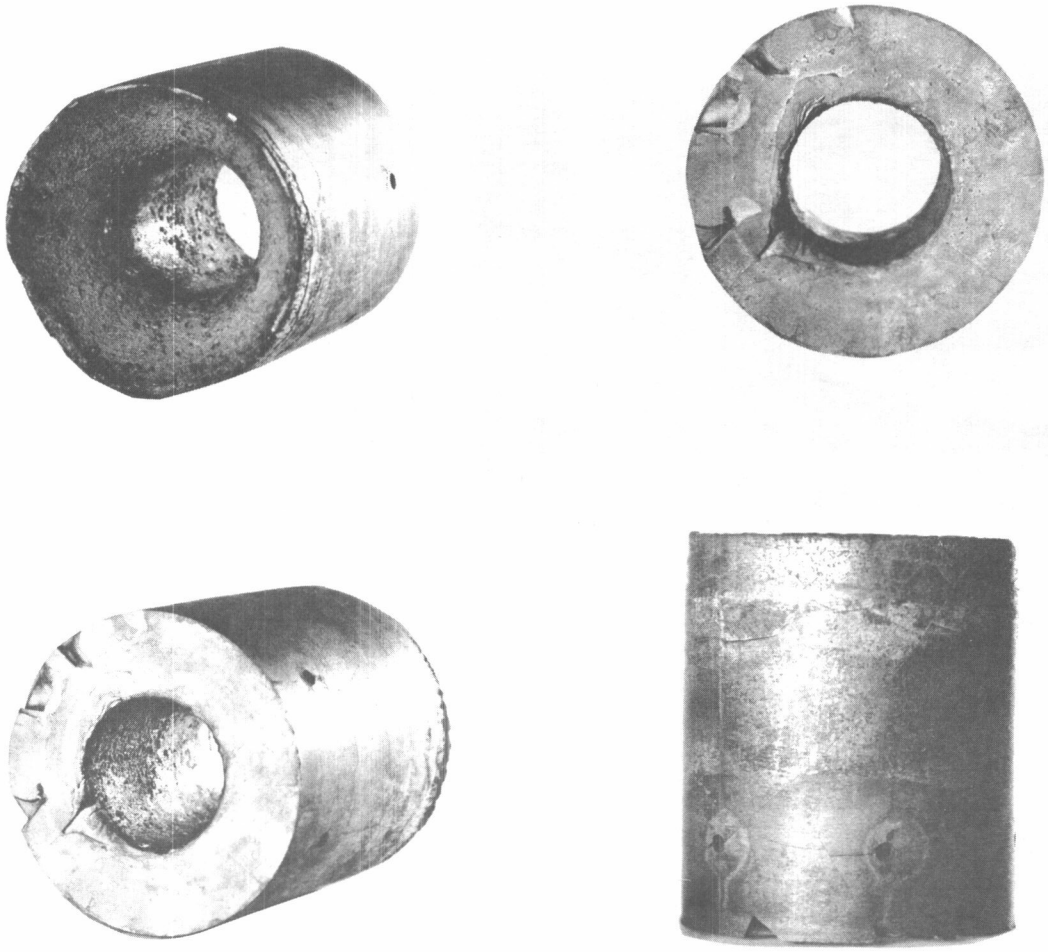

TEST 12 - COLUMBIUM CARBIDE - NOZZLE INSERT

Figure 40

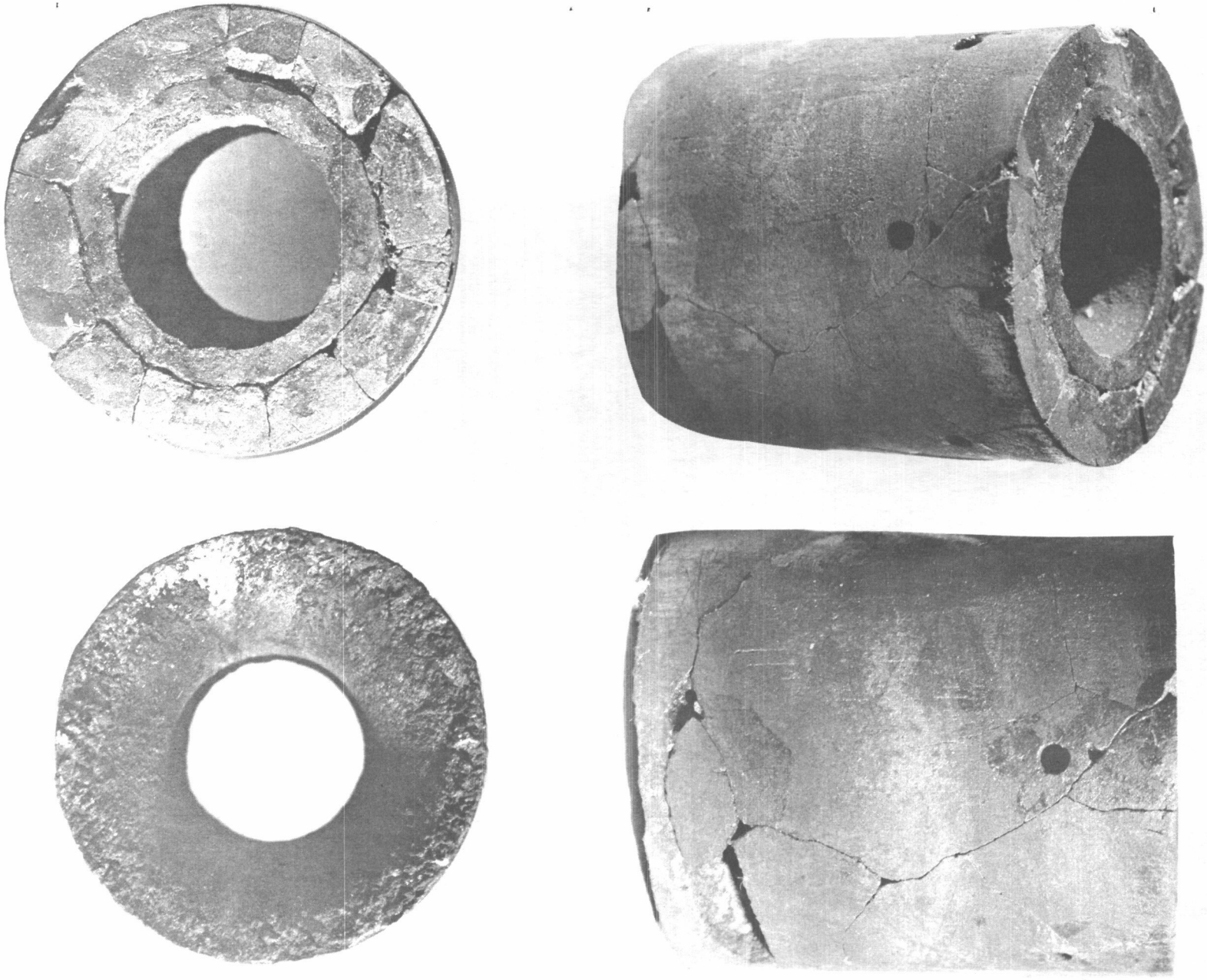

TEST 14 - TANTALUM CARBIDE - NOZZLE INSERT

Figure 41

CONFIDENTIAL

TEST 15 - TANTALUM CARBIDE - NOZZLE INSERT

Figure 42

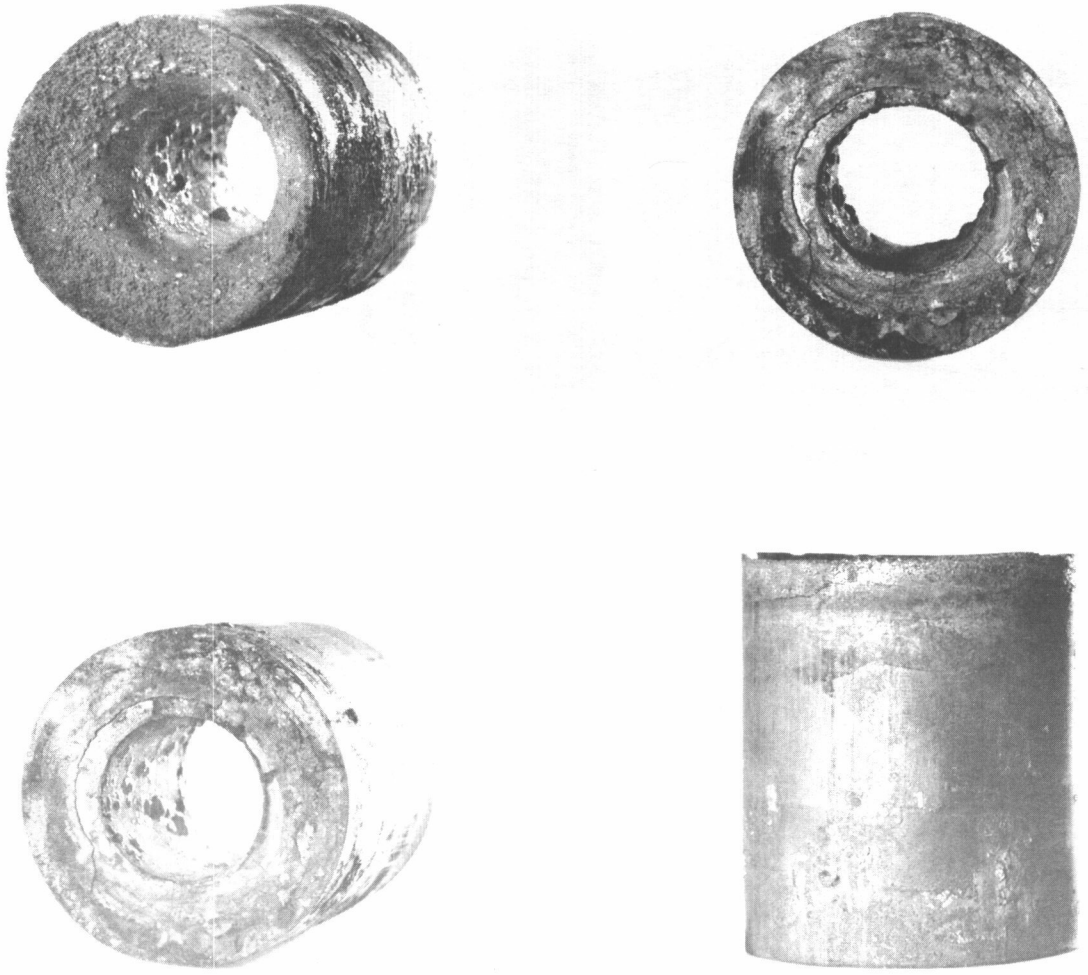

TEST 17 - TANTALUM CARBIDE FILLED WITH ALUMINUM - NOZZLE INSERT

Figure 43

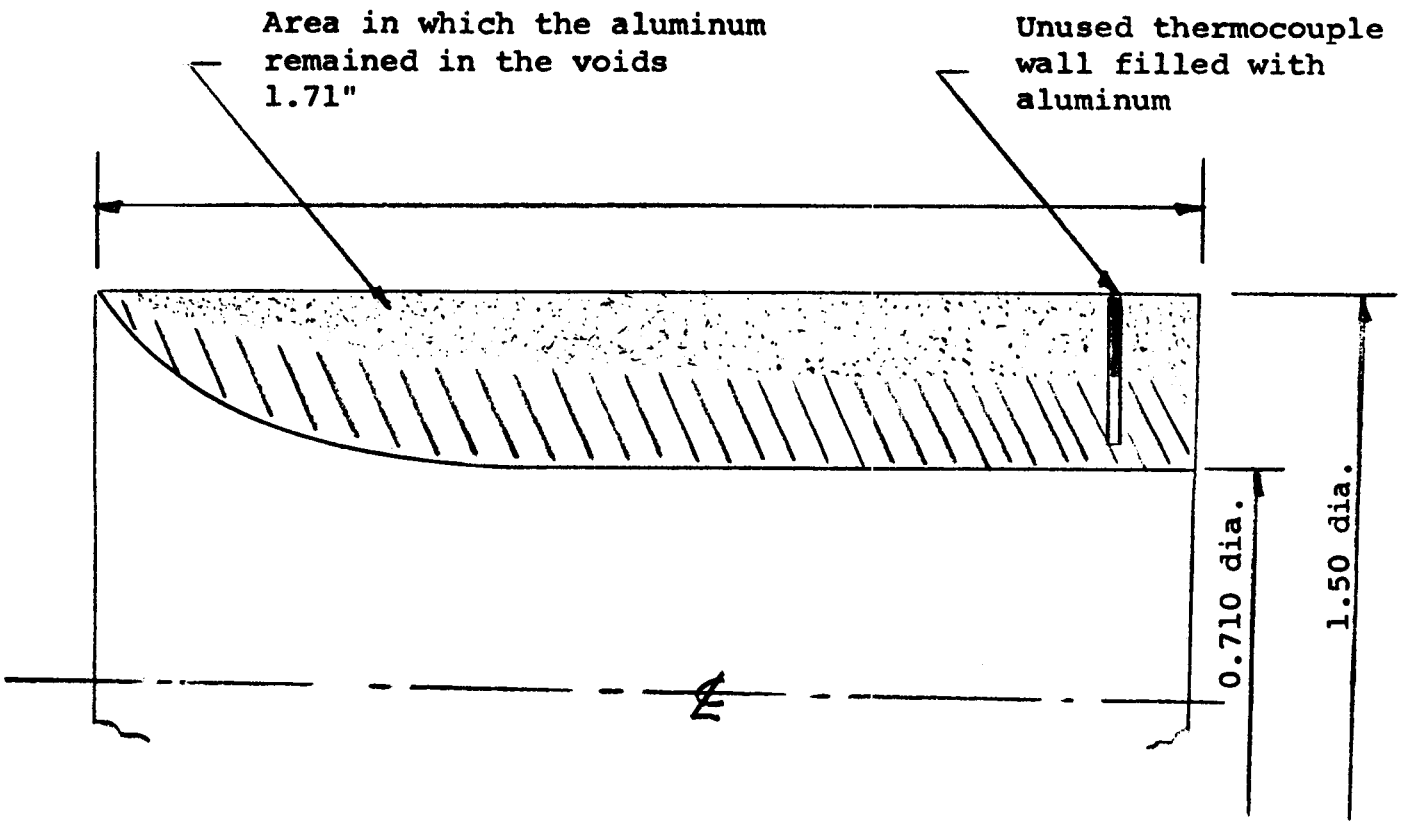

TANTALUM CARBIDE FILLED WITH ALUMINUM
CROSS-SECTION SHOWING REMAINING ALUMINUM AFTER TEST

Figure 44

CONFIDENTIAL

APPENDIX A

TEMPERATURE CALCULATIONS

Temperatures were calculated by one dimensional numerical methods for various time intervals at certain points within the refractory carbide inserts. The purpose of these calculations was to compare the experimental temperatures with the calculated temperature to determine the reliability of the instrumentation.

Because the ratio of the radius to the wall thickness of the inserts is less than four, the usual flat plate equations are not satisfactory. To take into consideration the constantly increasing area from the inside to the outside surface, a numerical technique developed by Arde Associates was utilized. See Figure A-1 of this appendix for a typical insert cross-section.

Four equations were developed to determine the temperatures at; (1) the inside surface of the insert; (2) the radial center of the insert; (3) the outer surface of the insert; (4) the outer surface of the graphite. Heat loss to the atmosphere was neglected and the outer surface of the graphite was considered perfectly insulated. The temperatures of each of the four points were determined for time intervals of 10, 20, 30, 40, 50, and 60 seconds.

The operation conditions were; (1) a gas temperature of 6900°R; (2) an initial insert temperature of 500°R; and (3) a gas pressure of 500 psi. The inside diameter of the insert was 0.75 inches. Figures A-2 and A-3 of this appendix show temperature versus depth of penetration for tantalum carbide and columbium carbide at various time intervals.

To evaluate the effects of a decrease in the inside diameter and an increase in gas pressure on the temperature profile, an analysis was made of a tantalum carbide insert with an inside diameter of 0.63 and a pressure of 800 psi.

The increase in pressure was expected to increase the rate of heat flow because of the higher heat transfer coefficient. The decrease in diameter was expected to decrease the rate of heat flow because of the smaller inside wall area. A comparison of curves A-2 and A-4 of this appendix indicates that at any given time the insert with the smaller inside diameter has a hotter inner surface and a cooler outer surface.

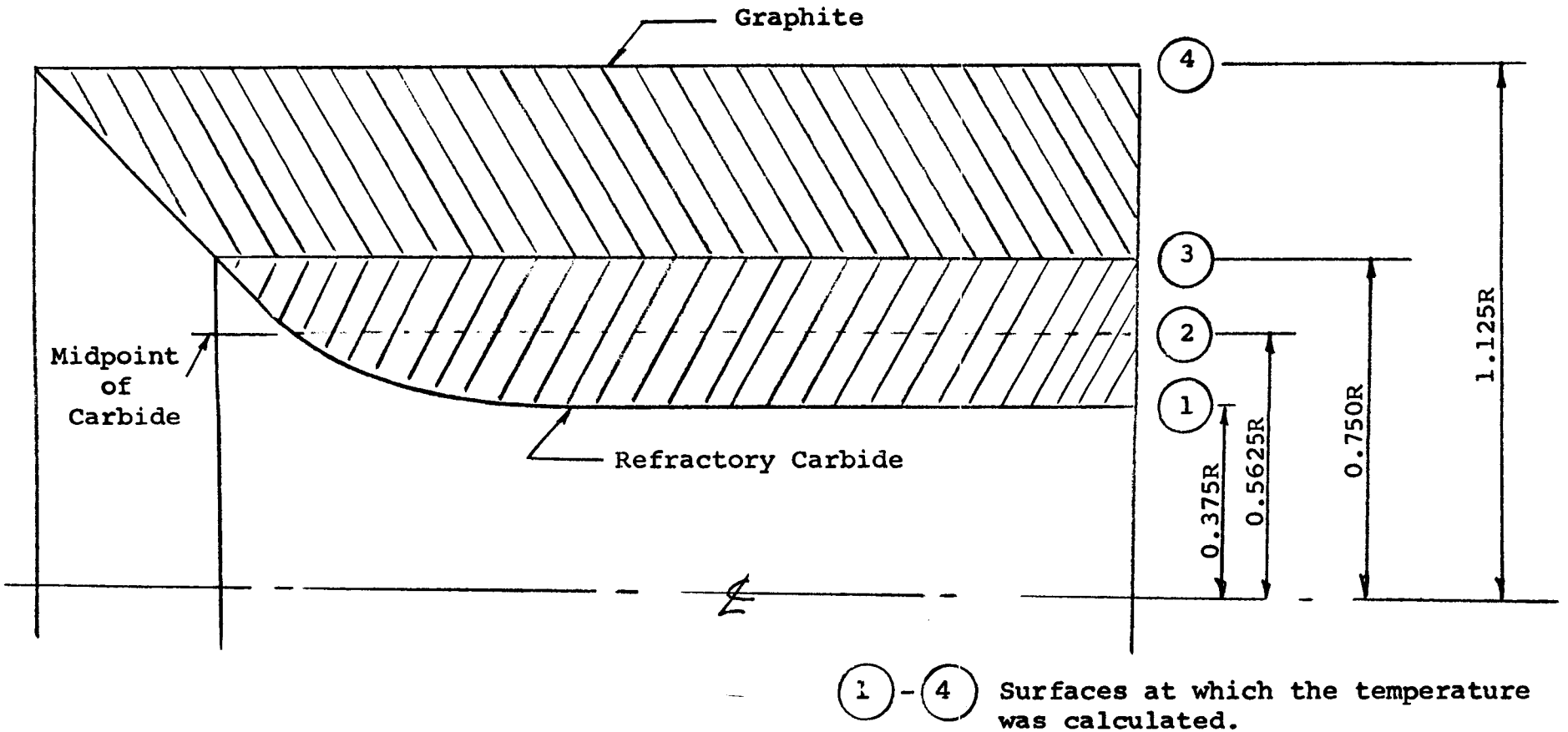

TYPICAL INSERT CROSS-SECTION

Figure A-1

TEMPERATURE DISTRIBUTION IN A TANTALUM CARBIDE INSERT
For Various Time Intervals

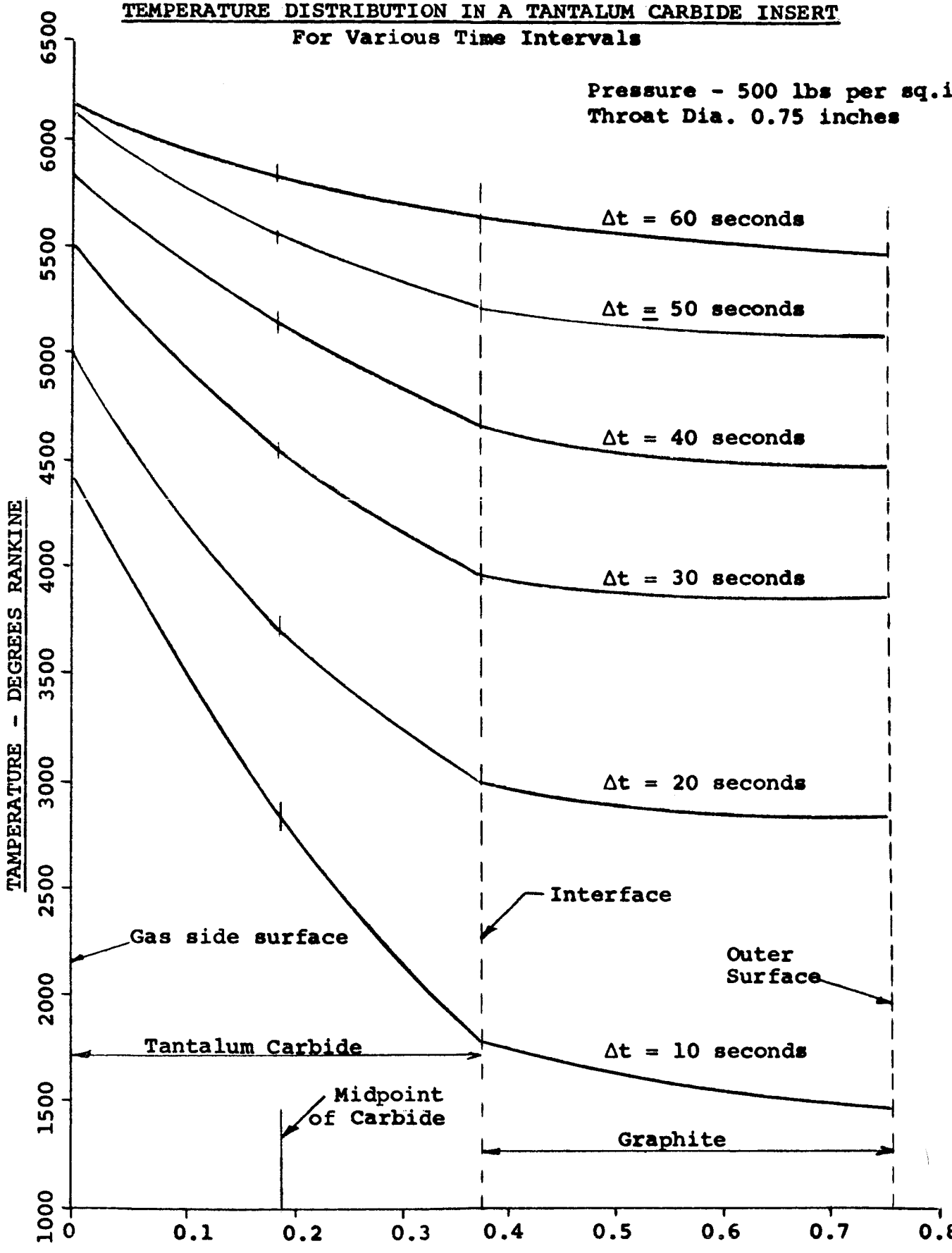

Figure A-2

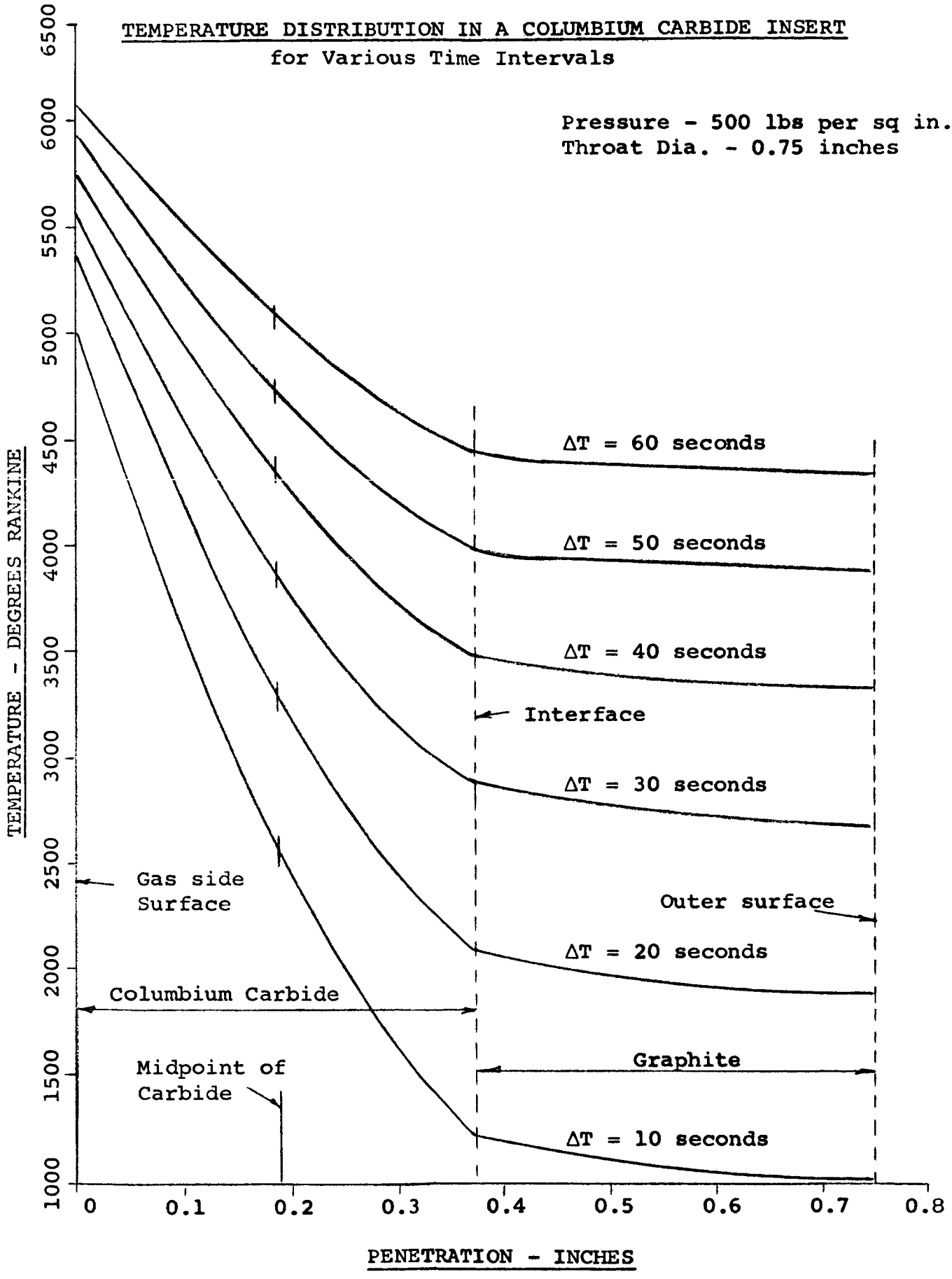
TEMPERATURE DISTRIBUTION IN A COLUMBIUM CARBIDE INSERT
for Various Time Intervals
Pressure - 500 lbs per sq in.
Throat Dia. - 0.75 inches
TEMPERATURE - DEGREES RANKINE
6500
6000
5500
5000
4500
4000
3500
3000
2500
2000
1500
1000
ΔT = 60 seconds
ΔT = 50 seconds
ΔT = 40 seconds
Interface
ΔT = 30 seconds
Gas side Surface
Outer surface
ΔT = 20 seconds
Columbium Carbide
Graphite
Midpoint of Carbide
ΔT = 10 seconds
0
0.1
0.2
0.3
0.4
0.5
0.6
0.7
0.8
PENETRATION - INCHES

Figure A-3

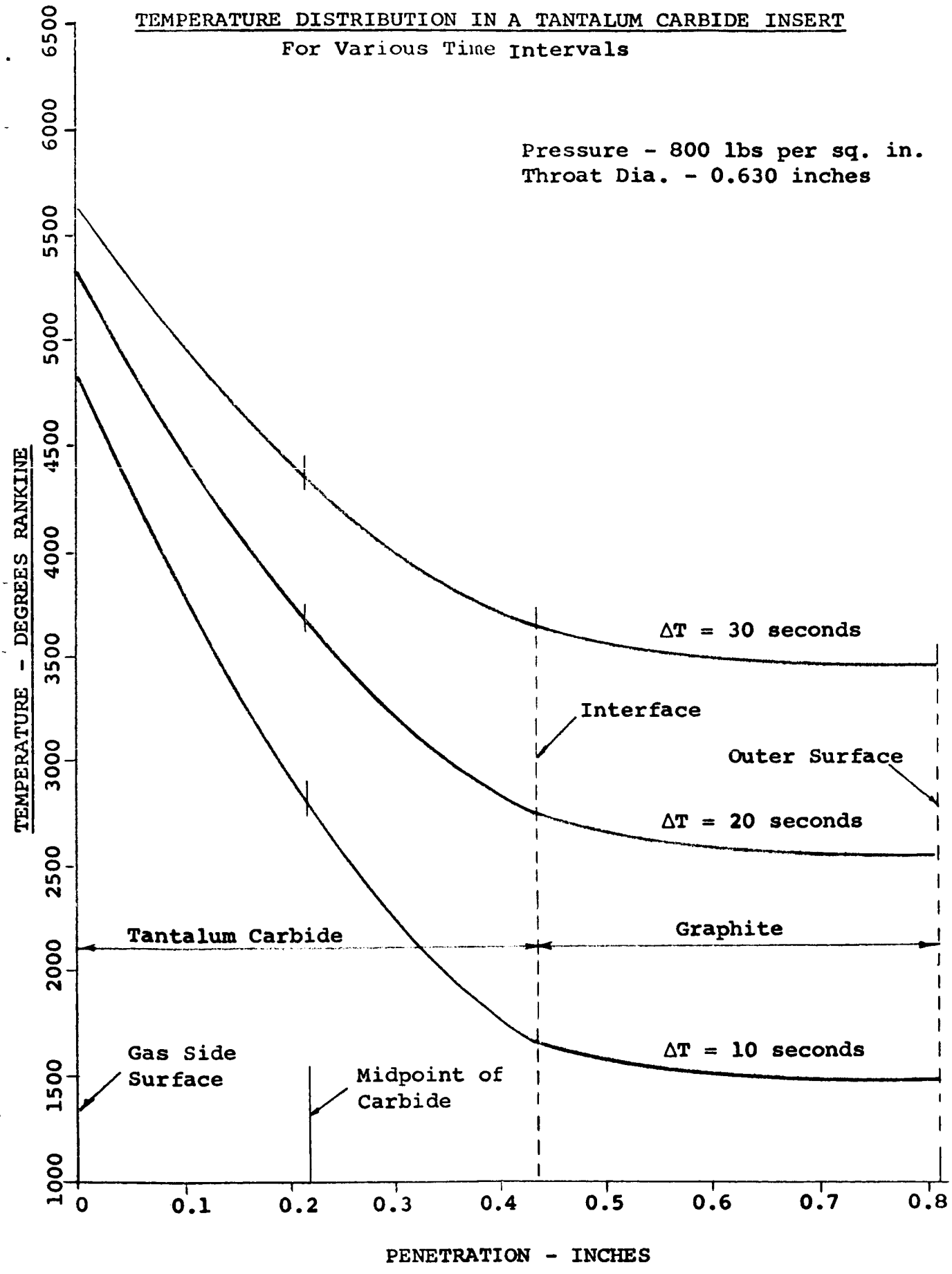
TEMPERATURE DISTRIBUTION IN A TANTALUM CARBIDE INSERT
For Various Time Intervals
Pressure - 800 lbs per sq. in.
Throat Dia. - 0.630 inches
TEMPERATURE - DEGREES RANKINE
6500
6000
5500
5000
4500
4000
3500
3000
2500
2000
1500
1000
ΔT = 30 seconds
Interface
Outer Surface
ΔT = 20 seconds
Tantalum Carbide
Graphite
ΔT = 10 seconds
Gas Side Surface
Midpoint of Carbide
0
0.1
0.2
0.3
0.4
0.5
0.6
0.7
0.8
PENETRATION - INCHES

Figure A-4

APPENDIX B

PYROMETER ANALYSIS

An analysis was made to determine the effective emissivity at the bottom of a thermocouple well for both an optical and total radiation pyrometer. This emissivity is needed to determine the actual temperature from the apparent temperature (assuming $\epsilon = 1$) measured by the instruments.

The effective emissivity depends on, (1) the depth of the cylinder into which the pyrometer is sighting, (2) the emissivity of the cylinder walls, (3) the emissivity of the flat surface at the closed end of the cylinder, and (4) the temperature distribution along the depth of the cylinder.

The problem undertaken is the determination of the radiation from a deep cylindrical hole in a plate. The reflecting surfaces are assumed to be radiating diffusively. The surface temperature increases as the closed end is approached. The emissivity ϵ and the reflection coefficient $(1-\epsilon)$ are considered everywhere constant.

Buckley's method of solution utilizing his one-term exponential expression for the kernel which appears in the integral equation will be used.

Consider a cylinder of length L closed at one end by a flat disk where the distances x and x_1 from the open end and L are expressed in terms of the radius, see Figure B-1. It is further assumed that the radiation emitted by the end disk, after inter-reflections are taken into account, is uniform over its surface. This is only approximately correct, but is closely approached for long cylinders. Then -

$$\phi(x_1) = \epsilon G\left[T(x)\right] + (1-\epsilon)\int_o^L \phi(x)\, K\left[x-x_1\right] dx + (1-\epsilon)\,\phi_o\, K_o\,(L-x_1) \quad \ldots\ldots\ldots\ldots\ldots\ldots\ldots\ldots\ldots (1)$$

$$\phi = \epsilon G\left[T(L)\right] + (1-\epsilon)\int_o^L \phi(x)\, K_o\,(L-x_1)\, dx \quad \ldots\ldots\ldots\ldots (2)$$

$$G_{max} = G\left[T(L)\right] \quad \ldots\ldots\ldots\ldots\ldots\ldots\ldots\ldots\ldots\ldots\ldots\ldots (3)$$

$$\epsilon_{eff} = \frac{\phi_o}{G_{max}} \quad \ldots\ldots\ldots\ldots\ldots\ldots\ldots\ldots \quad (4)$$

$$G(T) = G_{max}\left(\frac{T}{T_{max}}\right)^4, \text{ when sensing total radiation} \quad \ldots\ldots \quad (4a)$$

When the radiations of a single wave length are sensed,

$$G\ (T) \approx G_{max}\ e^{-25740\left(\frac{1}{\lambda T} - \frac{1}{\lambda T_{max}}\right)}$$

$$G\ (T) \approx G_{max}\left[\frac{T}{T_{max}}\right]^{\frac{25740}{\lambda T}} \quad \ldots\ldots\ldots\ldots\ldots\ldots \quad (4b)$$

The symbols used in this analysis are:

$\phi\ (x_1)$ = Total radiation per unit area emitted at x_1 on the side of the cylinder.

ϕ_o = Total radiation per unit area emitted by the end disk - assumed constant.

ϵ = Emissivity

$K(x-x_1)$ = Radiation received per unit area at x_1 from an annulus of the cylinder of unit width at x when the annulus at x is radiating unit radiation per unit area $\ldots\ldots\ldots\ldots$ (5)

$K_o(L-x_1)$ = Radiation received per unit area at x_1 from the end disk at L when the end disk is radiating unit radiation per unit area $\ldots$ (6)

$K'_o\ (L-x)$ = Radiation received per unit area by the end disk at L from an annulus at x is radiating unit radiation per unit area $\ldots\ldots\ldots$ (7)

$$K\ (x) = \frac{1}{4}\ \frac{d^2}{dx^2}\ F(x) \simeq e^{-\frac{x}{2}} \quad \ldots\ldots\ldots\ldots\ldots\ldots \quad (8)$$

$$K_o(x) = \frac{1}{4}\ \frac{d}{dx}\ F(x) \simeq e^{-\frac{x}{2}} \quad \ldots\ldots\ldots\ldots\ldots\ldots \quad (9)$$

$$K_o'(x) = 2K_o(x) \quad \ldots\ldots\ldots\ldots\ldots\ldots\ldots\ldots\ldots \quad (10)$$

$$\frac{\pi}{2} F(x) = \frac{\pi}{2} \left(x^2 + 2 - x\sqrt{x^2 + 4}\right) \quad \ldots\ldots\ldots\ldots\ldots \quad (11)$$

= Radiation received by a circular disk of unit radius from an equal co-axial disk at a distance x_1 radiating unit radiation per unit area.

ϵ_{eff} = Effective emissivity of the end disk.

G_{max} = Black body radiation at $T_{max} = T(L)$ (equations 4a and 4b)

$G(T)$ = Black body radiation (equations 4a and 4b)

T_{max} = Absolute temperature at the end disk.

T = Absolute temperature of the side of side of the cylinder.

= Wave length in u units (10^{-6} meters)

m = Exponential rate of temperature decay on the side of the cylinder.

n = Exponent of the temperature ratio which appears in equation 4a and 4b

T_a = Apparent temperature at the end disk as if black body conditions prevailed.

s = Dummy variable for x

The temperature profile, see Figure B-2, is approximated with adequate accuracy by -

$$T = T_{max}\ e^{-m\left(1 - \frac{x}{L}\right)} \quad \ldots\ldots\ldots\ldots\ldots\ldots\ldots \quad (12)$$

Combining this form with -

$$G = G_{max} \left(\frac{T}{T_{max}}\right)^n \quad \ldots\ldots\ldots\ldots\ldots\ldots\ldots\ldots \quad (13)$$

$$G = G_{max} \; e^{-mn\,(1 - \frac{x}{L})} \quad \ldots\ldots\ldots\ldots\ldots\ldots\ldots \quad (14)$$

Eliminating ϕ_o between equation (1) and equation (2) and using the approximate K values,

$$\phi(x_1) = \epsilon G\, T(x_1) + \frac{(1-\epsilon)}{2}\int_o^{x_1} \phi(x)\, e^{-(x-x_1)}\, dx$$

$$+ \frac{(-\epsilon)}{2}\int_{x_1}^{L} \phi(x)\, e^{-(x-x_1)}\, dx$$

$$+ \frac{(-\epsilon)}{2}\, e^{-(L-x_1)}\left[\epsilon\, G_{max} + (1-\epsilon)\int_o^{L}\right.$$

$$\left.\phi(x)\, e^{-(x-x_1)}\, dx\right] \quad \ldots\ldots\ldots\ldots\ldots\ldots \quad (15)$$

$$\frac{d\phi(x_1)}{dx_1} = \frac{\epsilon dG(x_1)}{dx_1} + \frac{(1-\epsilon)}{2}\left[-\int_o^{x} \phi(x)\, e^{-(x_1-x)}\, dx + \phi(x_1)\right]$$

$$+ \frac{(1-\epsilon)}{2}\left[\int_{x_1}^{L} \phi(x)\, e^{-(x-x_1)}\, dx - \phi(x_1)\right]$$

$$+ \frac{(1-\epsilon)}{2}\, e^{-(L-x_1)}\left[\epsilon\, G_{max} - (1-\epsilon)\int_o^{L} \phi(x)\, e^{-(L-x)}\, dx\right]$$

$$\frac{d^2\phi(x_1)}{dx_1^2} = \frac{\epsilon d^2 G_2(x_1)}{dx_1^2} + \frac{(1-\epsilon)}{2}\left[\int_o^{x_1} \phi(x)\, e^{-(x_1-x)}\, dx - \phi(x_1)\right]$$

$$+ \frac{(1-\epsilon)}{2}\left[\int_o^{L} \phi(x)\, e^{-(x-x_1)}\, dx - \phi(x_1)\right]$$

$$+ \frac{(1-\epsilon)}{2} e^{-(L-x_1)} \left[\epsilon G_{max} - (1-\epsilon) \int_o^L \right.$$

$$\left. \phi(x) \; e^{-(L-x)} \; dx \right] . . . . . (16)$$

Subtracting equation (15) from equation (16) one obtains -

$$\frac{d^2\phi(x_1)}{dx_1^2} - \epsilon \phi(x_1) = \epsilon \left[\frac{d^2G(x_1)}{dx_1^2} - G(x_1) \right] . . . . . (17)$$

The solution of this ordinary differential equation is:

$$\phi(x) = \frac{\sqrt{\epsilon}}{2} \left[e^{+\sqrt{\epsilon}x} \int_o^x e^{-\sqrt{\epsilon}s} f(s)ds - e^{-\sqrt{\epsilon}x} \int_o^x e^{+\sqrt{\epsilon}x} f(s)ds \right.$$

$$\left. + Ae^{-\sqrt{\epsilon}x} + B^{-\sqrt{\epsilon}(L-x)} \right] . . . . . (18)$$

Where $f(x) = \left[\frac{d^2 G}{dx^2} - G \right] . . . . . (19)$

To obtain A and B substitute in equation (18) and compare coefficients of like terms. If G is given by relation (14)

$$\phi(x) = A \; e^{-mn(1-\frac{x}{L})} + B \; e^{-\sqrt{\epsilon}(L-x)} + C \; e^{-\sqrt{\epsilon}x} . . . . . (20)$$

Where $A = \frac{\epsilon G_{max} (m^2n^2 - L^2)}{m^2n^2 - \epsilon L^2}$

$C_1 = N_{A_o}$

$C_2 = N_B$

$C_3 = -N_A$

$$B = A \left[\frac{C_1 + C_2 (1 - \epsilon) L e^{-mn}}{C_3 + \frac{e^{-\sqrt{\epsilon}L}}{1 - \sqrt{\epsilon}} (C_2) (1 - \sqrt{\epsilon})} \right] + \epsilon G_{max}$$

$$C = -(1 - \sqrt{\epsilon}) \frac{AL\, e^{-mn}}{L + mn} + \frac{B\, e^{-\sqrt{\epsilon}L}}{1 + \sqrt{\epsilon}}$$

$$C_1 = \frac{L}{mn-L} + \frac{(1-\epsilon)}{mn+L} \frac{L}{} (1-e^{-(mn+L)})$$

$$C_1 \approx \frac{L}{mn-L} + \frac{(1-\epsilon)\, L}{mn + L}$$

$$C_2 = \frac{1-\epsilon}{1-\sqrt{\epsilon}} (e^{-\sqrt{\epsilon}L} - e^{-L}) - \frac{e^{-\sqrt{\epsilon}L}}{1 + \sqrt{\epsilon}}$$

$$C_3 = + \frac{1}{1-\sqrt{\epsilon}} - \frac{(1-\epsilon)\ (1-e^{-(1+\sqrt{\epsilon})\ L})}{1 + \sqrt{\epsilon}}$$

Substituting in equation (20) -

$$\phi_o = \epsilon\, G_{max} + (1-\epsilon)\left[Ac_4 + Bc_5 + Cc_6 \right] \quad \ldots\ldots\ldots\ldots \quad (21)$$

Where - $C_4 = \dfrac{L\ (1-e^{-(1 + mn)}}{mn + L}$

$$C_5 = \frac{1 - e^{-L\ (1+\sqrt{\epsilon})}}{1 + \sqrt{\epsilon}}$$

$$C_6 = \frac{L}{mn + L} (1 - e^{-(L + mn)})$$

Finally - $\epsilon_{eff} = \dfrac{\phi_o}{G_{Max}}$ is used $\ldots\ldots\ldots\ldots\ldots\ldots\ldots$ (22)

The next problem is to approximate the actual temperature, T at L, when the apparent temperature, T_a, is known. T_a is the measured temperature assuming $\epsilon = 1$.

$$\epsilon_{eff}\, T^n = T_A{}^n \quad \ldots\ldots\ldots\ldots\ldots\ldots \quad (23)$$

$$T = \epsilon_{eff}\, T_A{}^{\frac{1}{n}} \quad \text{or} \quad \frac{T}{T_A} = \epsilon_{eff}{}^{\frac{1}{n}} \quad \ldots\ldots\ldots \quad (24)$$

Equations 21, 22, 24 were used with L = 16 radii and = 0.653 μ.

The selected values of n were:

n = 4, for a total radiation pyrometer

n = 6, for an optical pyrometer which corresponds to T_{max} = 6600°R

n = 8, for an optical pyrometer which corresponds to T_{max} = 4900°R

The values of m, which determine the temperature profile were 0, 2.3, 3.45, 4.6, 6.9, 9.2 and ∞. The corresponding temperature profiles and the curves of effective emissivity versus emissivity are shown on Figure B-2. Figure B-3 shows the computed values of T/T_A to be a function of m, n and ϵ for the optical pyrometer. Figure B-4 shows the computed values of T/T_A to be a function of m and ϵ for a total radiation pyrometer.

The important conclusion to be drawn from these curves is that ϵ need not be known better than ± 50% to obtain 10% accuracy while either a total radiation pyrometer or an optical pyrometer.

Figure B-5 is attached to show the good approximation of the ratio of energy emitted versus temperature when the simpler form,

$$\left(\frac{T}{T_{max}}\right)^{\frac{25740}{\lambda T}}$$ is used instead of the more complex form,

$$e^{-25740\left(\frac{1}{\lambda T} - \frac{1}{\lambda T_{max}}\right)}$$

REFERENCES

On the Radiation from the Inside of a Circular Cylinder
by: H. Buckley, Phil. Mag. Vol. 4 p.753 (1927)

On the Radiation from the Inside of a Circular Cylinder, Part III.
by: H. Buckley, Phil Mag. Vol. 17 p. 576 (1934)

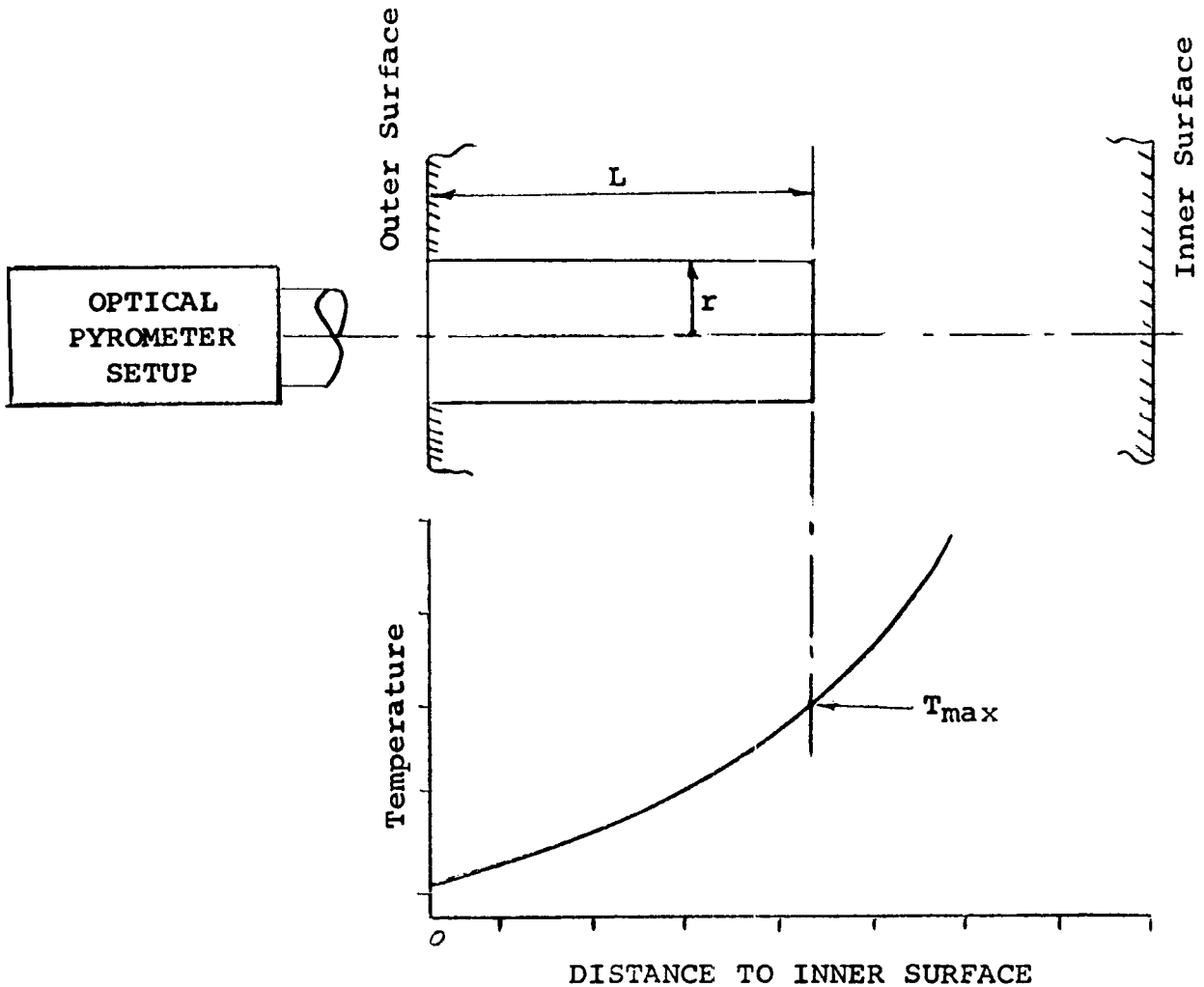

TYPICAL TEMPERATURE PROFILE
IN THE CYLINDER

Figure 3-1

TEMPERATURE RATIO VERSUS CYLINDER DEPTH

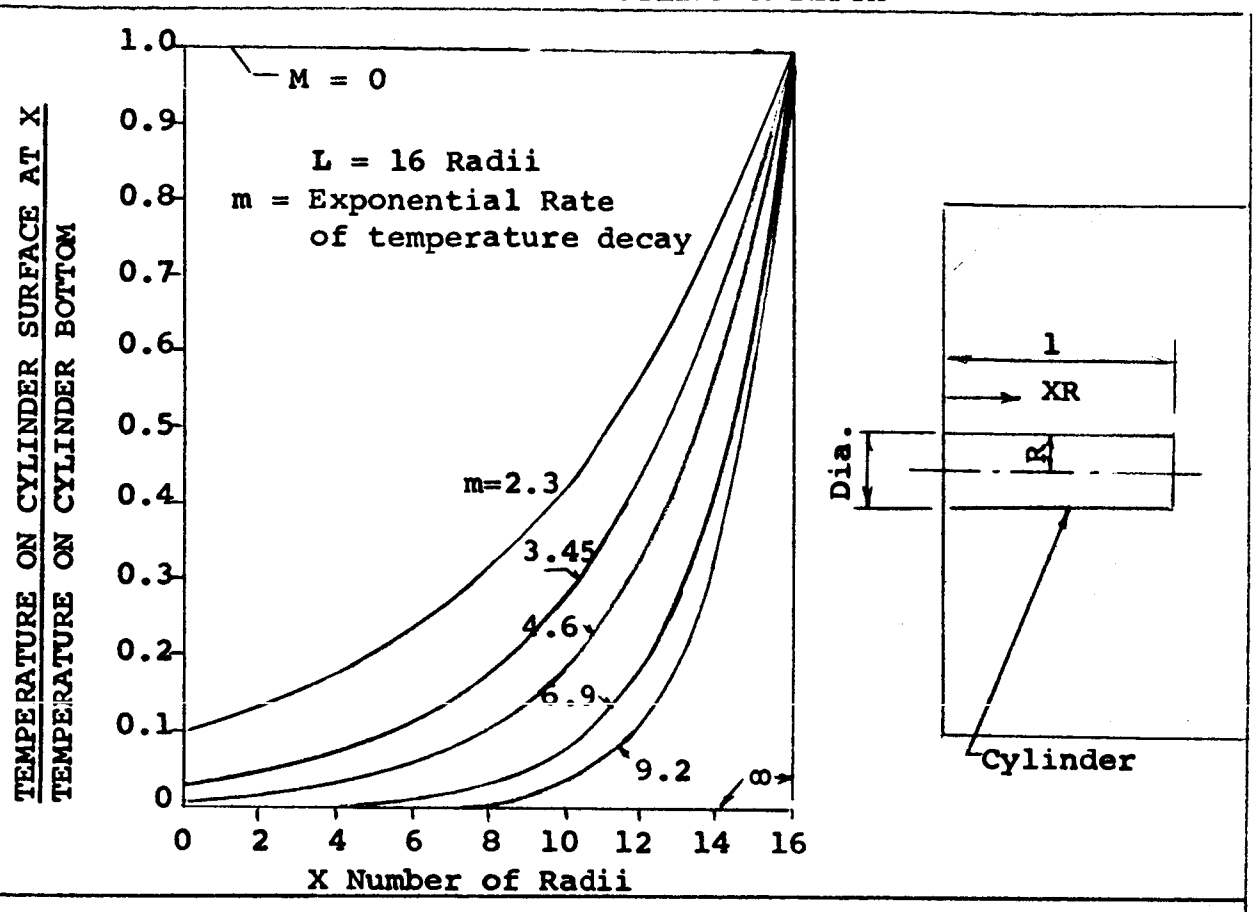

EFFECTIVE EMISSIVITY VERSUS EMISSIVITY

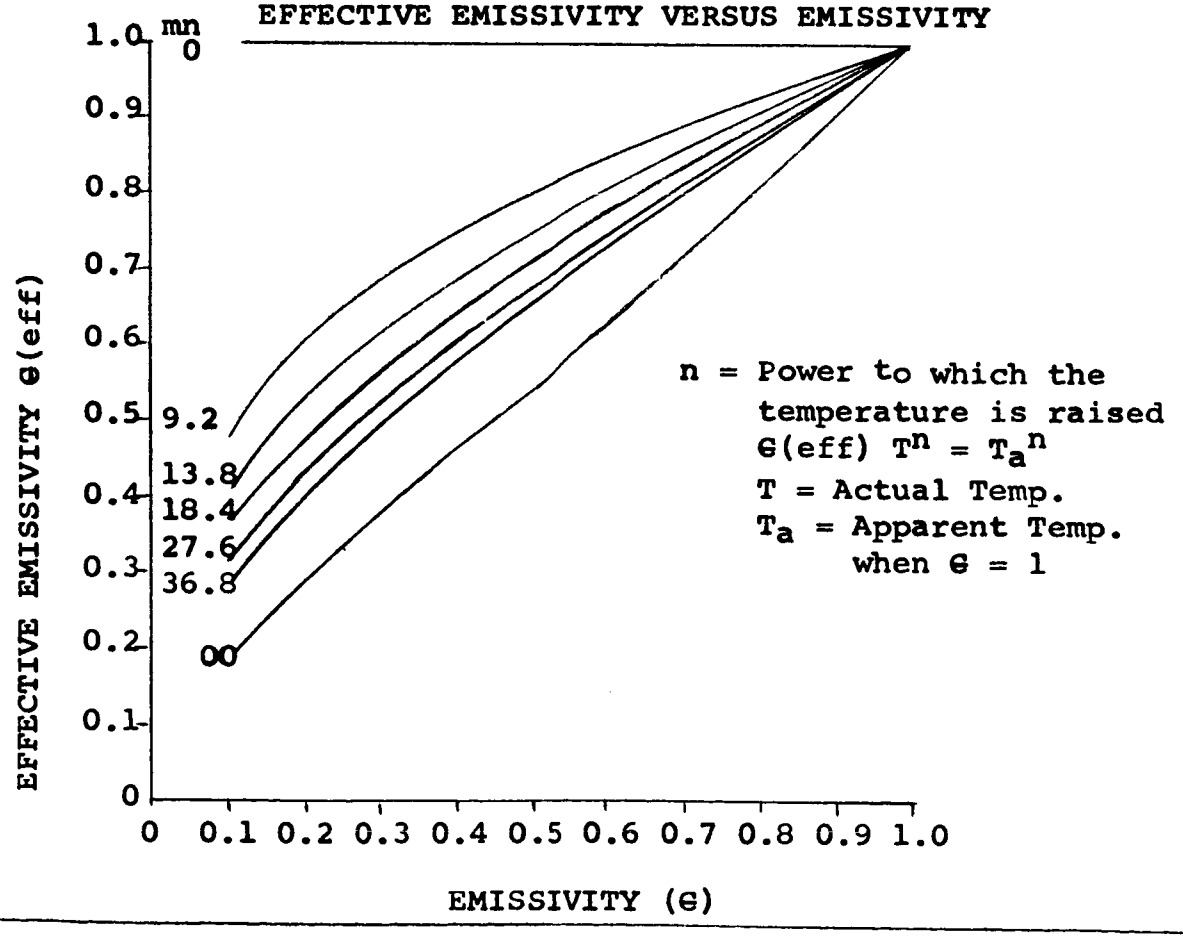

Figure B-2

TEMPERATURE RATIO VERSUS EMISSIVITY FOR A TOTAL RADIATION PYROMETER

Depth of Cylinder L = 16 Radii
m = Exponential Temp. Decay
n = Power to which temperature is raised $\epsilon(\text{eff})\ T^n = T_a{}^n$

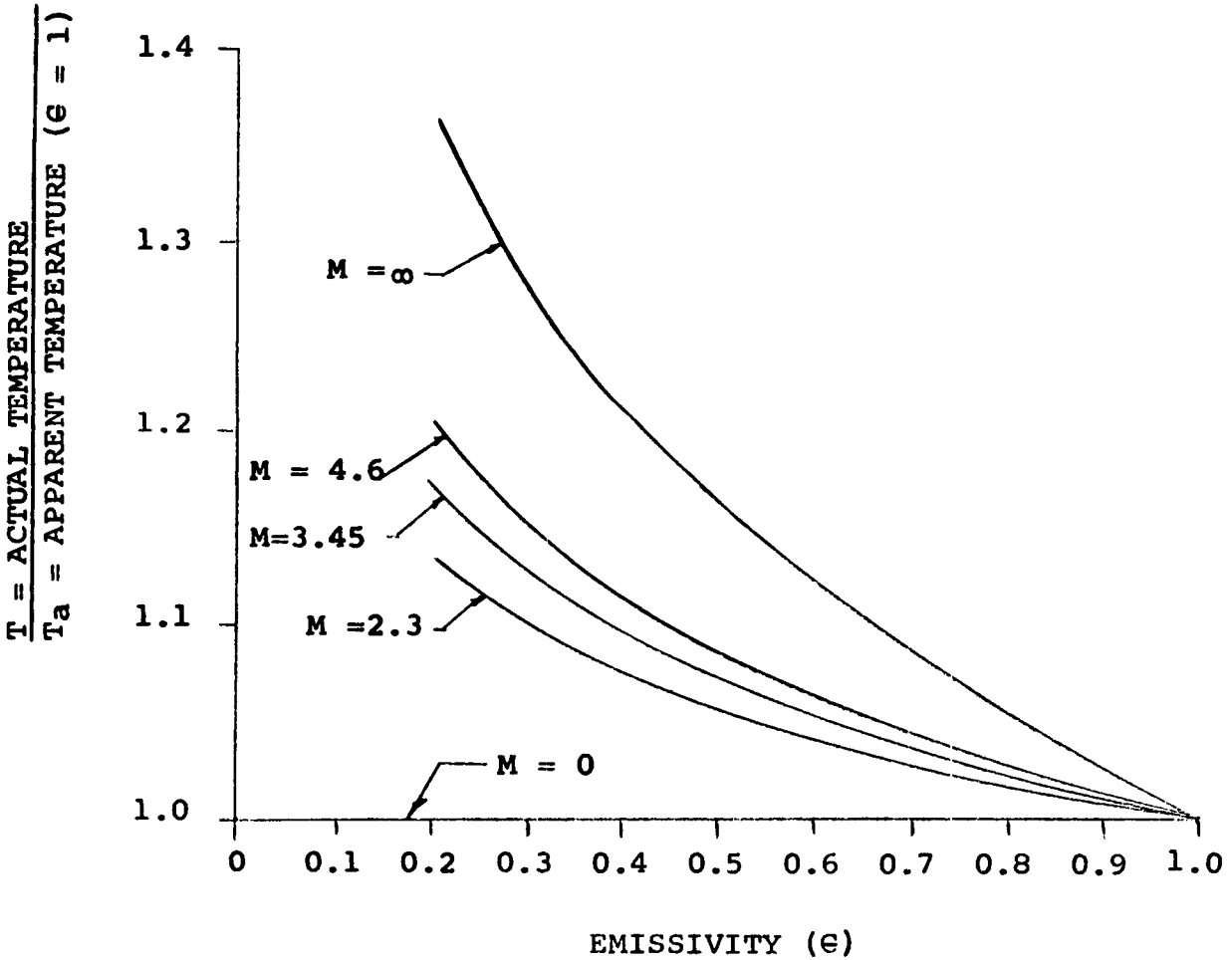

Figure B-3

TEMPERATURE RATIO VERSUS EMISSIVITY FOR THE OPTICAL PYROMETER

Depth of Cylinder L = 16 Radii
Wavelength, λ = 0.653 μ
m = Exponential Temp. Decay
n = Power to which the temperature is raised ϵ(eff)
$T^n = T_a^n$

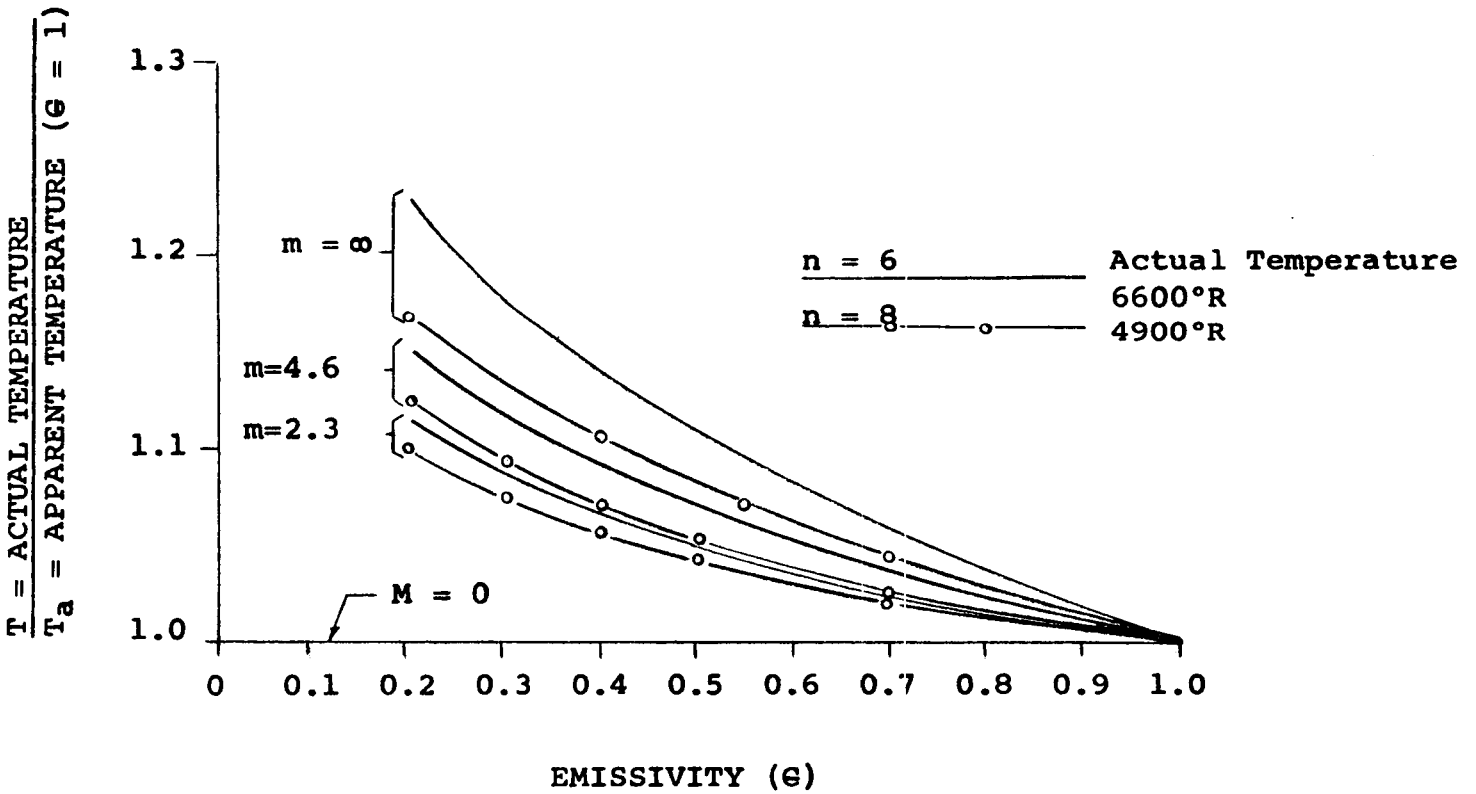

Figure B-4

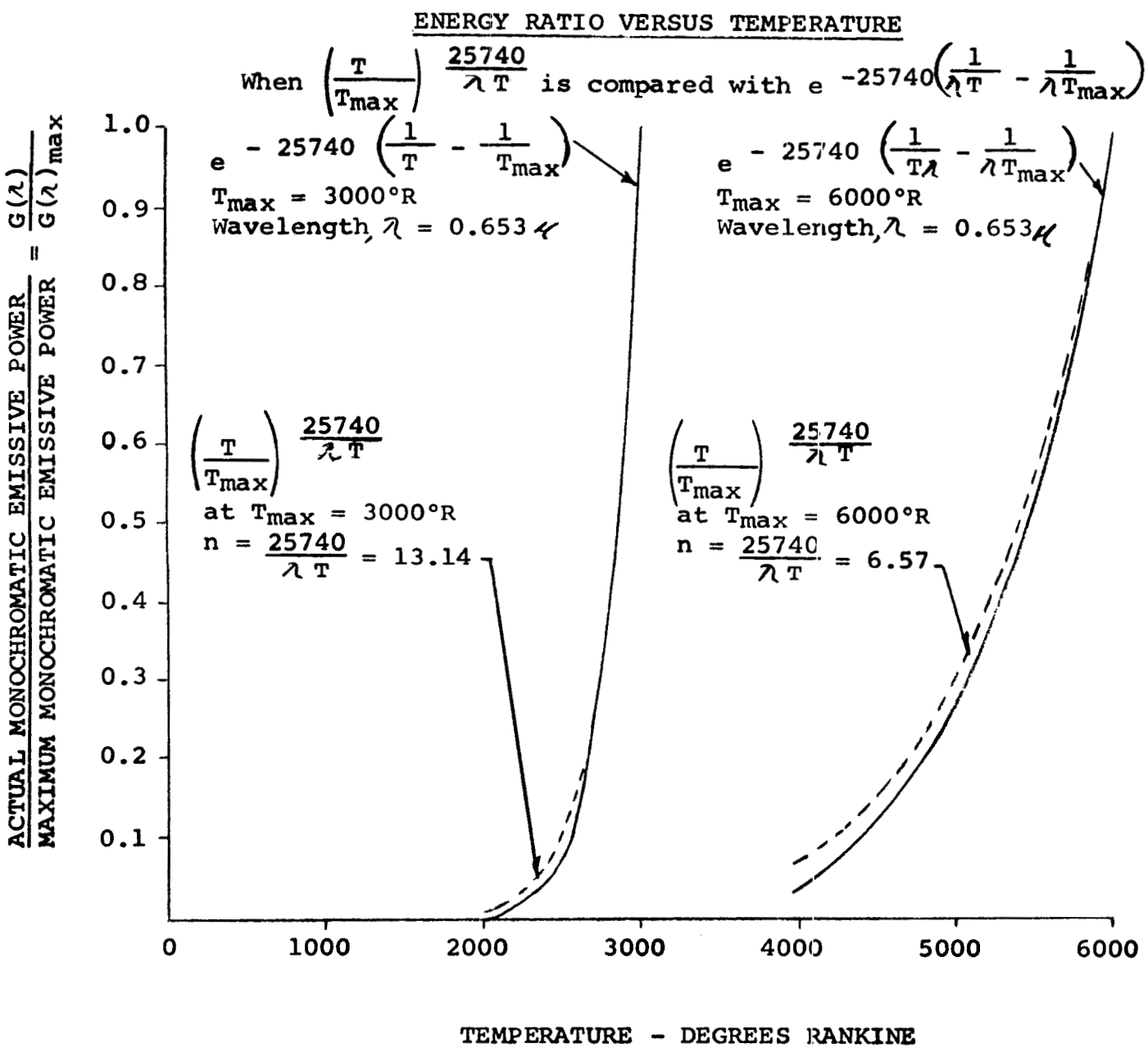
ENERGY RATIO VERSUS TEMPERATURE
When $\left(\frac{T}{T_{max}}\right)^{\frac{25740}{\lambda T}}$ is compared with $e^{-25740\left(\frac{1}{\lambda T} - \frac{1}{\lambda T_{max}}\right)}$
$e^{-25740\left(\frac{1}{T} - \frac{1}{T_{max}}\right)}$
T_{max} = 3000°R
Wavelength, λ = 0.653 μ
$e^{-25740\left(\frac{1}{T\lambda} - \frac{1}{\lambda T_{max}}\right)}$
T_{max} = 6000°R
Wavelength, λ = 0.653 μ
$\left(\frac{T}{T_{max}}\right)^{\frac{25740}{\lambda T}}$
at T_{max} = 3000°R
$n = \frac{25740}{\lambda T} = 13.14$
$\left(\frac{T}{T_{max}}\right)^{\frac{25740}{\lambda T}}$
at T_{max} = 6000°R
$n = \frac{25740}{\lambda T} = 6.57$
ACTUAL MONOCHROMATIC EMISSIVE POWER / MAXIMUM MONOCHROMATIC EMISSIVE POWER = $\frac{G(\lambda)}{G(\lambda)_{max}}$
1.0
0.9
0.8
0.7
0.6
0.5
0.4
0.3
0.2
0.1
0
1000
2000
3000
4000
5000
6000
TEMPERATURE - DEGREES RANKINE

Figure B-5

APPENDIX C

PROPELLANT DESCRIPTION

Table C-1 Description of Hercules Powder Co. CLW Propellant:

Number of grains - 1
Diameter - 7.6"
Length -
a. 20" for 30 second test
b. 48" for 60 second test
Weight -
a. 55 lbs for 30 second test
b. 132 lbs for 60 second test
Configuration - End Burning Restricted
Burning Characteristics - Neutral
Type - Cast double base
Inhibitor - 7/16" thick cellulose acetate

Table C-2 Formulation of Hercules Powder Co. CLW Propellant:

Ingredients			Percent
Nitrocellulose	-	NC	21.0
Nitroglycerine	-	NG	31.0
Aluminum	-	AL (Alcoa 123)	21.0
Amonium Perchlorate	-	AP (15 Micron)	19.3
Tri Acetone	-	TA	5.7
Magnesium Oxide	-	MgO	1.0
2-NDPA Nitro	-	Diphenylamine	1.0

Table C-3 Products of Combustion of Hercules Powder Co. CLW Propellant:

Ingredients			Percent
Carbon Monoxide	-	CO	38.9
Water Vapor	-	H_2O	14.6
Carbon Dioxide	-	CO_2	2.7
Hydrogen Chloride	-	HCL	5.8
Hydrogen	-	H_2	24.2
Nitrogen	-	N_2	13.8
Aluminum Oxide	-	AL_2O_3	liquid
Magnesium Oxide	-	MgO	liquid

APPENDIX D

PROPERTIES OF MATERIALS (ROOM TEMPERATURE)

Property	Tungsten	Graphite	Pyrolytic Graphite	Ti Carbide	Ta Carbide	Cb Carbide	Aluminum
Sublimation or Melting Point °F	6192	6602-6682	6602-6682	5682 ±200	6982	7052	1219
Boiling Point °F	10,642	7592	7592	7782	9932	-	3732
Specific Gravity	19.3	1.6-2.0	1.80-2.22	4.93	14.65	7.82	2.71
Tensile Strength psi	120,000	2-4000	15-20,000	-	-	-	9,000
Specific Heat	0.034	0.17	0.232	-	0.045	0.094	0.21
Thermal Cond. Btu Hr.-Ft.-°F	115 -85	109	*a=92-230 *c=1.1-2	9.9	16	8.2	118
Elect. Resist. Ohm-in x 10^{-6}	2.16	314	a = 79 c = .098	41.4	7.9	29	1.14
Hardness	-	0.5-1 (Moh)	a = 1 (Moh) c = 4.5	2460 (Knoop)	2050 (Knoop)	1880 (Knoop)	2 (Moh)
Spectral Emiss.	0.43	-	0.81-0.90	-	-	-	0.03
Thermal Exp. °F x 10^{-6}	2.2	1.5	0.37	4.1	4.6	-	12
$\frac{\text{Strength}}{\text{Density}} \times 10^3$	6.2	1.34	10	-	-	-	3.3

*a = with the planes

*c = across the planes

APPENDIX E

ANALYSIS OF THE PYROLYTIC GRAPHITE FRACTURE

A two dimensional analysis was made of the temperature differences longitudinally distributed along the inner and outer surfaces of the coating after 30 seconds of firing. The analysis was accomplished by the Finite Difference Technique.

The differential equation is replaced by a system of linear algebraic equations the solution of which give the values of the wanted functions at a finite number of points lying at the intersection of a gridwork. The equations were set up and programmed for the IBM 704 computer.

Figure E-1 shows the temperature profile in the pyrolytic graphite at the end of firing. Subsequent to this, as the material cools down, the conical section cools more rapidly than the cylindrical section because there is less graphite mass behind it. This analysis determines the average temperature differential between the conical and cylindrical sections which would cause failure due to the discontinuity stresses developed at the intersection of these sections.

To simplify the structural analysis the pyrolytic graphite coating was assumed to be a cone and cylinder as shown in Figure E-2. The stress equations for the junction between the cone and cylinder were resolved in terms of temperature differences.

The weakest strength property of the material is shear across the plane. Utilizing this stress as a limit and solving for the related change in temperature reveals that a 34°F temperature difference can result in failure. The method of solution is outlined on the following pages.

FREE BODY DIAGRAM OF NOZZLE SECTORS

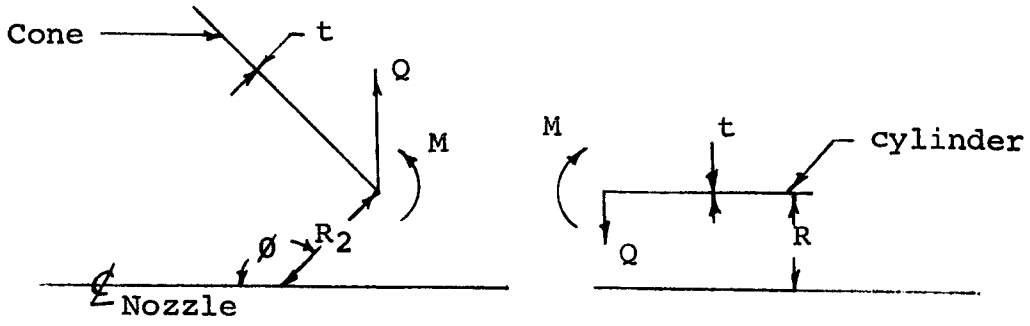

W_c = Deflection of cone at intersection.

$$W_c = R_2 (T_o - T_1) \sin \phi - \left(\frac{\sin^2 \phi}{2D\beta^3}\right) Q - \left(\frac{\sin \phi}{2D\beta^2}\right) M$$

θ_c = Rotation of cone intersection

$$\theta_c = \alpha (T_o - T_1) \cot \phi + \frac{\sin \phi}{2\beta^2 D} Q + \frac{M}{\beta D}$$

$W_{cyl.}$ = Deflection of cylinder at intersection

$$W_{cyl.} = \alpha R (T_o - T_2) + \frac{Q}{2D\beta^3} - \frac{M}{2D\beta^2}$$

$\theta_{cyl.}$ = Rotation of cylinder at intersection

$$\theta_{cyl.} = \frac{Q}{2D\beta^2} - \frac{M}{D\beta}$$

Where:

α = Thermal coefficient of expansion.

T_o = Temperature of cone and cylinder at a particular time during cool-down.

T_1 = Temperature of cone at failure.

T_2 = Temperature of cylinder at failure.

D = Flexural Rigidity = $\frac{Et^3}{12(1-\mu^2)}$

E = Modulus of elasticity = lbs/in^3

μ = Poisson's Ratio

β = Damping Parameter = $\sqrt[4]{\frac{3(1-\mu^2)}{R^2 t^2}}$

For Cylinder

$$B = \text{Damping Parameter} = \sqrt[4]{\frac{3(1-\mu^2)}{R_2^2 t^2}}$$

For Conical Sector

t = Thickness - inch
M = Unit moment $\frac{\text{in-\#}}{\text{in.}}$
Q = Unit load #/in.

Equating the deflections and rotations of the cone and cylinder and solving these equations, results in a value of Q which is a function of $(T_2 - T_1)$. Using the ultimate shearing strength of pyrolytic graphite as 1000 psi. (Across the plane) which is 2/3 of the tensile strength, the temperature differential $(T_2 - T_1)$ which would cause failure was found to be 34°F.

IDEALIZED NOZZLE CONFIGURATION

(Elimination of Blend Radius Between
Conical and Cylindrical Shells)

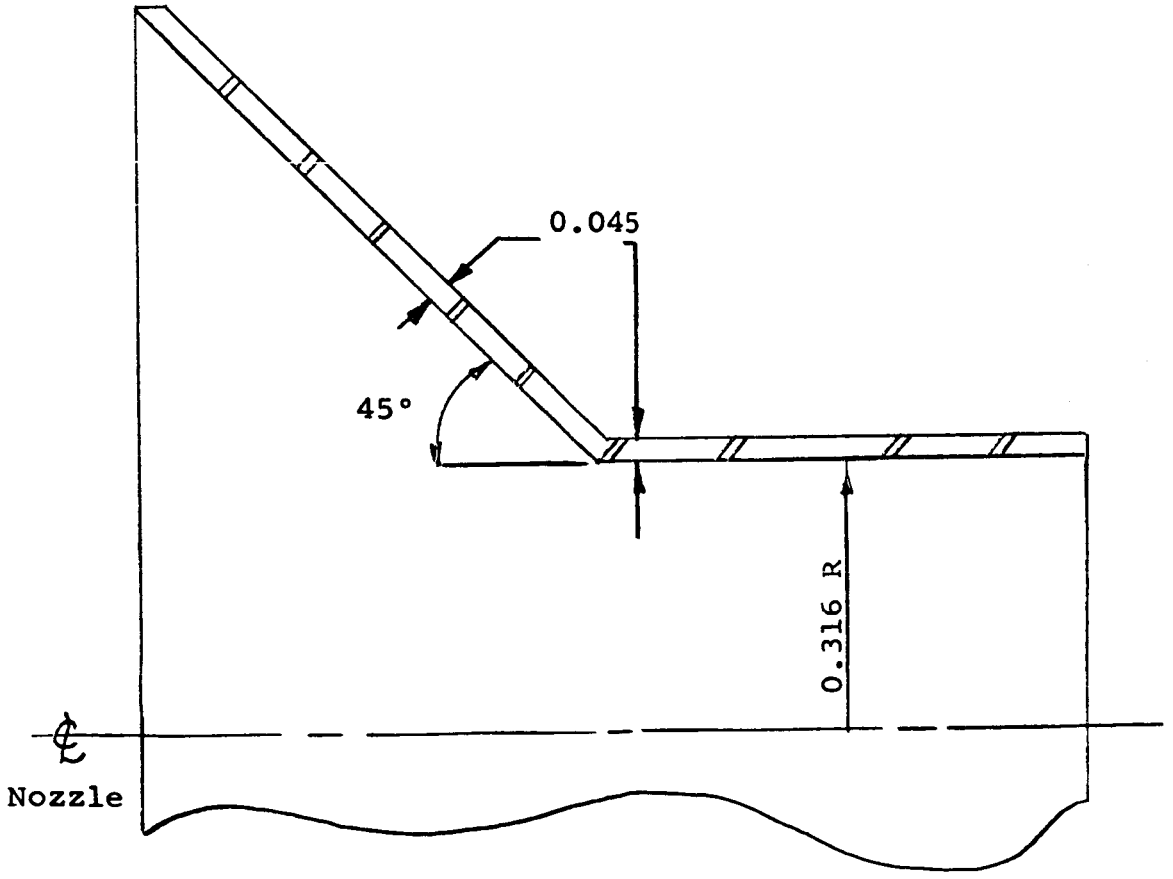

Figure E-1

TEMPERATURE PROFILE (°F) IN PYROLYTIC GRAPHITE
INSERT AFTER 30 SECONDS
(TERMINATION OF FIRING)

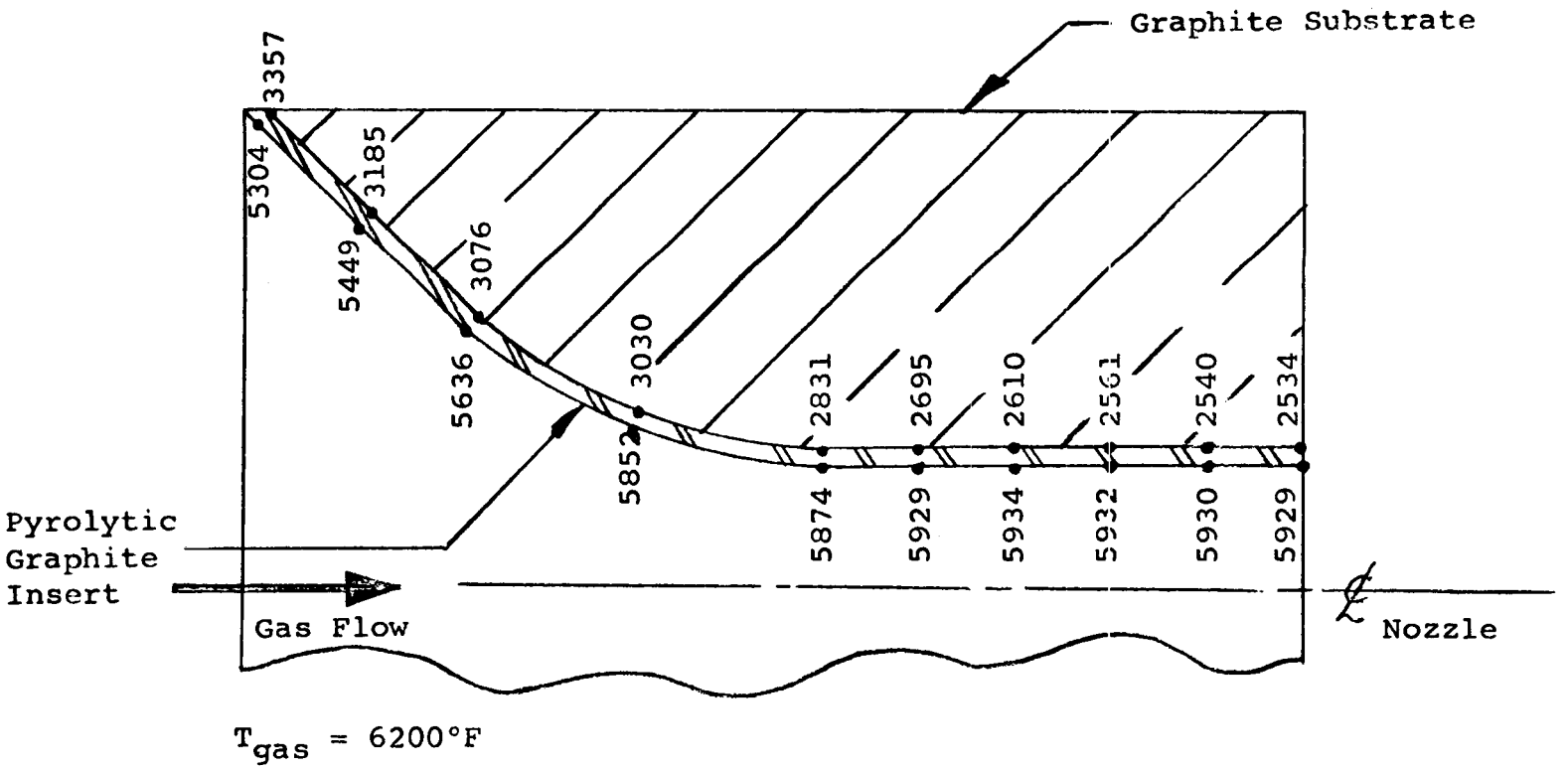

FIGURE E-2

APPENDIX F

INVESTIGATION OF THE PRODUCTION OF NEW COMPOUNDS WITH ULTRA HIGH PRESSURES

This report presents an analysis of, and possible approach towards the selection of materials suitable for synthesis into new crystalline forms upon the application of heat and extreme pressure. The design objective was taken to be a material which would:

a. have a melting point in excess of 7000°F
b. be stable under ambient conditions
c. have low density
d. have low thermal conductivity.

Properties a. and b. impose prime limitations on the selection whereas c. and d. were considered as secondary design factors.

In exploring the possibility of synthesizing new materials there are two broad approaches which could be followed:

1. Select combinations of elements on some statistical basis, subject them to the pressure and temperature treatment, and then evaluate their properties.

2. Assume a type of structure which should yield the desired design properties and determine if and how such a structure may be synthesized.

Both methods have been used in the past, and both have limitations. The "shotgun" approach of the first type requires extensive experimental analysis but could conceivably yield novel structures. While approach two seems safer, the success here is limited by (1) the theory presently available, and (2) the imagination of the inventor since the type of structure selected would be limited by current concepts. It appears, however, that approach two should be exhausted before attempting a broad experimental program. Therefore, in the succeeding sections the nature of the relations between bonding, structure, and properties of solids are discussed with an aim towards determining what type of structure may possibly be developed, within the scope of current theory and experimental practice, to satisfy the requirements stated above.

STRUCTURE VERSUS PROPERTIES

In this section the factors which influence melting point, stability, density, and thermal conductivity are discussed.

Melting Point

In order to obtain extremely high melting point materials, strong bonds must exist between the atoms. Four basic bond types exist: The homopolar covalent bond, metallic bond, the heterpolar ionic bond, and the Van der Waals bond.

A covalent single electron pair bond can form for each incompletely filled orbital of the reacting elements. The bond strength is due to the fact that the bonding electron exists in orbitals of both the atoms being held together. The covalent bond is the strongest type and should therefore be the primary bond in the high melting materials.

The metallic bond can be considered as a covalent bond in which the electron responsible for bonding is shared between several atoms. Since one electron is responsible for the bonding between several atoms, this bond is not as strong as the simple covalent bond.

The ionic bond is formed when an electron from one atom is transferred to an orbital of another atom, and the electrostatic forces between the two ions hold the pair together. This is the weakest form of direct atom bonding.

Van der Waals bonds are weak long range forces which exist between saturated molecules and are the result of polarization rather than direct electron - atom interactions. Van der Waals forces are generally not considered in the bonding of high melting point solids.

No single pure type exists. All bonds have mixed covalent, metallic, and ionic character. Evidence exists that additional stability is associated with a structure whose bond resonates between covalent and ionic.

The strength of the covalent bond varies with atomic position in the periodic table, being greatest for the low atomic number elements. As examples, if we consider the series carbon, silicon, germanium, the respective bond energies in kilocalories mole are 58.6, 42.5, and 42.5. In the series F, Cl, Br, I, the

covalent energies are 63.5, 57.8, 46.1, and 36.2 respectively. Therefore, one criterion for choosing elements for reaction to yield materials with high melting points is that low average mean atomic weights be used.

Let us next consider the ionic part of the bonding forces. The ionic bond strength varies as the difference in electronegativity of the two elements forming the bond. As a rough indication of the electronegativity, the sum of the ionization energy and electron affinity can be used. Again in the series F, Cl, Br, I, the electronegativities vary: 4, 3, 2.8, 2.5. However in the series Li, Na, K, Rb, Cs the electronegativity varies 1, 0.9, 0.8, 0.8, 0.7. Therefore if a strong ionic contribution to the bond is desired, anions of low atomic weight and cations of high atomic weight would be chosen. We see therefore, that to some extent these two requirements are not compatible, and the amount of ionic bond which can be added to the covalent bond for maximum bond strength is limited.

If high melting point is desired, the atoms should be held together with the largest number of bonds possible. A good approximation for the strength of one bond of a binary compound is one-half the sum of the covalent bond energies of the individual elements plus 23 times the square of the electronegativity difference of the bonding elements. Examination of the periodic table using this formuls indicates that elements situated near the center of the table near carbon are most suitable for supplying high bond strength. Due to the extremely stable standard state of oxygen and nitrogen, a correction must be made when these elements are used. In this case, the equation for the heat of formation of the compound would be:

$$1/2 \quad (A\text{-}A) + (B\text{-}B) + 23\ (x_a - x_b)^2 - 55\ N_N - 24\ N_O$$

where N_N and N_O are the number of atoms in the mol.

Stability

From the thermodynamic point of view, it is expected that the structures produced at high temperatures and high pressures would not be stable at room temperature. Thermodynamic calculations, if they could be extended to the range of temperatures and pressures proposed, and if they could predict the type of structure which would exist at the reacting temperature and pressure state, would still be unable to define the

stability of such a structure. In fact, thermodynamically, the transformation would generally be assumed reversible in that as the temperature and pressure are lowered, the structure would return to its original room temperature form. The best that can be hoped for is the production of a metastable structure, and therefore one which could not be predicted from a thermodynamic analysis. This is perhaps the strongest argument against using a direct theoretical approach.

Density

The density of a solid is determined by the atomic weight of the atoms in it, the crystal structure (coordination number), and the interatomic distance. Application of extreme pressure to structures must necessarily increase their density. As indicated in the previous discussion on bonding, a high coordination number would be desirable. However, this also leans in the direction of high density. On the basis of bonding, the lowest atomic number elements show the highest covalent contribution to bonding, which is in the right direction. It would appear that the probability of obtaining a low density structure with high bond strengths is good.

Thermal Conductivity

The thermal conductivity of a solid results from two contributions: electronic and lattice. The electronic condition is the result of the same electrons which conduct electrical current. Therefore, by using non-metals (non-metallic bonds), which is also indicated from bonding considerations, the thermal conductivity can be kept down. The lattice contribution to the thermal conductivity depends upon the atomic weight and the periodicity of the lattice. High atomic weight gives lower thermal conductivity. Deviations from periodicity also lower the thermal conductivity. The use of poly-component alloys in which the atoms are randomly distributed rather than monocomponent solids would yield lower thermal conductivity.

In summarizing the points raised in the above paragraphs, it would appear that the optimum properties would be obtained from a structure which was predominantly covalent with a partial ionic component, consisting of more than one atomic type, with the average atomic weight being low.

Review of Prior Related Work Including General Theory

The few theoretical calculations of the effect of pressure on solid structures have been limited to the transition from non-metal to metal, which is predicted by the band theory. These calculations indicate that hydrogen becomes metallic at 500,000 atmospheres [1], helium should become metallic at 30,000,000 atmospheres [2], ammonium at 250,000 atmospheres [3], and a more recent calculation predicts a metallic transition in lithium hydride at about 35,000,000 atmospheres [4]. In addition, most of the reported experimental work has been concerned with the appearance of metallic phases at ultra high pressures [5,6]. In fact, in many cases the drop in resistivity measured at elevated temperatures has been used as the criterion for the appearance of a transition structure. For reasons which will be pointed out in succeeding discussion, these calculations are not directly related to the problem of this investigation. Rather, the work of Hall[7] and the General Electric group concerned with the synthesis of diamond and boron-nitride are deemed to be more appropriate to the current problem. In these experiments it was demonstrated that graphite could be converted to diamond at extremely high temperatures and pressures and that also a diamond cubic crystalline form of boron-nitride could be synthesized at these temperatures and pressures.

It would be instructive to briefly review the band theory at this point. The band theory defines a metal as a solid having partially filled electron energy bands and an insulator as a solid having completely filled energy bands separated from an empty band by an energy gap. In the case of an insulator, increasing the pressure on the material will decrease the mean interatomic distance, causing greater interaction of electrons and resulting in a broadening of the bands. It then follows that if sufficient pressure is applied to an insulator the broadened empty band will overlap the broadened filled band producing a pybrid overlapped band which is incompletely filled. Thus the insulator becomes metallic. There is no basis for converting metallic structures into insulating structures by means of high pressure. From our previous discussion on bonding the conversion of a covalent insulating crystal to a metallic structure which would result upon the application of ultra high pressures is not desirable.

As can be seen from the paper by Behringer [4], theoretical calculations to determine the pressure at which lithium hydride converts to metallic form are quite complex and involve the

knowledge of a number of the physical properties of the material to be investigated. Such information is generally not available for more complex materials, that is the materials having large numbers of electrons. Thus again the direct theoretical approach does not seem feasible.

The production of metastable diamond and boron-nitride seems to provide the most fruitful direction for investigation and the possibility of producing additional structures of this type will be discussed in greater detail in the next section.

In addition to the creation of new structures, consideration could also be given to the densification and possible strengthening of existing structures. The most promising of these materials are the metallic carbides, borides, nitrides, sulphides, and silicides. These materials generally have high melting points and low vapor pressures [8]. The borides in particular are most attractive. They have low vapor pressures above 2500°C and are more stable than the carbides. A number of these compounds have relatively open structures (orthorombic, tetrahedral), which would lend themselves to high pressure densification and possible increase in bonding character. However, as discussed above, all of these materials should become more metallic at increased pressures.

Analysis of Materials for High Pressure Synthesization

In earlier sections it was pointed out that a material having the desired high temperature properties should be one which has:

1. a mixed covalent ionic bond.
2. maximum number of electrons per bond.
3. a large number of bonds (high coordination number).
4. low atomic weight.
5. more than one atom type (alloy)

Three possibilities may be considered:

1. The densification of open structures (elements). Essentially this is what was proposed in the previous section for magnesium, that is at ultra-high pressures (no estimate of the pressures necessary can be made), it may be possible to convert enough of the normally bound electrons available for bonding with neighboring atoms. The elements from hydrogen to fluorine have either 1s or 2 sp electrons. These electrons have no other shell

close in energy, and therefore it is doubtful that the application of pressure to these elements will result in appreciable changes in bonding. However, when we consider the second row from sodium to chlorine, the bonding electrons are the 3 sp electrons, and it is possible that the vacant 3d shell may contribute to bonding.

2. The densification of high melting compounds. This would be essentially the same as the above except that with the use of borides, silicides, nitrides, etc. the possibility of a coordination number of more than twelve is possible due to the large size differences between the metal and non-metal ions. In the case of a structure like titanium carbide each titanium atom can be considered as bonding with six carbon plus twelve titanium atoms for a total of eighteen bonds per unit cell. This high number of bonds will ordinarily produce a higher melting structure.

3. The production of metastable diamond type structures similar to the GE process seemed the most promising and a more detailed analysis of this follows.

Let us consider the two basic types of covalent bond, the σ- and the π bond. Nitrogen can be used to illustrate these two types of bonds. The N_2 molecule is bound by three p bonding orbitals. The three p orbitals of each nitrogen atom will be approximately at right angles to each other. Therefore, only one electron bonding pair can form with maximum overlap along the line of centers. Such a link is termed a σ-bond. The remaining electrons primarily exist in the two directions perpendicular to the line of centers. Overlapping will also occur between pairs of these orbitals forming two supplementary bonds, termed π bonds. However, since these bonding electrons cannot overlap as fully as in the σ- bond, they do not form as strong a bond. The π bond strength is a maximum if the two p orbitals from the different atoms are parallel, since such a configuration permits the maximum possible overlap of the bonding electrons. As the angle between the π- bonding electrons increases, the amount of exchange decreases and goes through a minimum when the bonding electrons are perpendicular to each other.

Summary and Conclusions

A qualitative theoretical approach was taken in investigating the possibility of producing new materials by subjecting them

to high pressures and temperatures. While such transitions could be produced, theoretically most of them would be metallic and not directly applicable to the present problem. There does exist however, a strong possibility that structures similar to diamond and boron-nitride can be produced by means of bond conversation in organic and inorganic type structures. It seems that this possibility should be investigated more thoroughly with both a theoretical and an experimental program. Although less time was devoted to the other possibilities, they still show some promise and should also be re-evaluated with more precision.

Bibliography

1. Wigner and Huntington, J. Chem. Phys. 3, 764 (1935)
2. Ten Seldam, Proc. Phys. Soc. (London) A 70, 97, 529 (1957)
3. Bernal and Massay, Monthly Nat. Roy. Astron. Sec. 114 No. 2, 172 (1954)
4. Behringer, Phys. Rev. 113 No. 3, 787 (1959)
5. Alder and Christian, Phys. Rev. 104, 550 (1956)
6. Griggs et al., Phys. Rev. 109, 1858 (1958)
7. Hall, Rev. Sci, Inst. 31 No. 2, 125 (1960)
8. Campbell, High Temperature Technology (Book), Wiley (1956)